Biofouling-resistant polymer hydrogel coating for desalination membranes

by

Jing Lei

From Hubei, China

Thesis submitted to the Department of Chemistry of

Universität Duisburg-Essen, in partial fulfillment of

the requirements of the degree of

Dr. rer. nat.

Essen, 2012

Approved by the examining committee on: 22.11.2012

Chair: Prof. Dr. Matthias Epple

Advisor: Prof. Dr. Mathias Ulbricht.

Reviewer: Prof. Dr. Christian Mayer

This work was performed during the period from February 2009 to October 2012 at the Institute of Technical Chemistry, Department of Chemistry, Universität Duisburg-Essen, under the supervision of Prof. Dr. Mathias Ulbricht.

I declare that this dissertation represents my own work, except where due acknowledgement is made.

Jing Lei

Abstract

Applying a hydrophilic coating to the membrane surface is an efficient and promising strategy to control membrane fouling. This work explored the use of a hydrogel coating with a high swelling as a means to reduce the propensity to biofouling.

Bulk poly(ethylene glycol) methyl ether methacrylate (PEGMEMA) hydrogels were prepared in water using macromonomers of three different molecular weights *via* redox free radical polymerization. To optimize gel composition, the effects of PEGMEMA, initiator and crosslinker concentrations on gel yield and swelling properties were studied. It was found that swelling of polyPEGMEMA gels in water decreases with increasing PEGMEMA concentration and increasing cross-linker content while the effect of these two parameters was opposite corresponding to gel yield. In addition, the chemical structure of the gels was characterized by FTIR and solid state NMR spectroscopy. It showed that the gels contain a small fraction of incompletely reacted cross-linker which increases with the length of the PEG side chain. Rheological measurements are employed to examine gelation time as well as the mechanical strength and mesh size of the gels as a function of synthesis conditions. Mesh sizes were also estimated using swelling data. Sorption experiments using proteins of three different sizes were performed to identify the relationship between the microstructure of the hydrogels and protein adsorption on the surface and its penetration into the hydrogel network. The swelling and rheological behaviors of hydrogels as well as protein partitioning into the gels are discussed in terms of the network mesh size. All results can be interpreted so that PEG side chains with the highest average molecular weight (1000 g/mol) have an additional effect onto physical cross-linking while the networks for the hydrogels with shorter PEG side chain are dominated by chemical cross-linking.

For the preparation of surface-anchored gel, the silanization of glass was used to introduce methacrylate groups and then performed via *in situ* cross-linking polymerizations in a mold. Contact angle measurement was employed to identify interfacial adaptation between surface

anchored hydrogels in water as function of preparation conditions. The bacterial deposition experiments were performed with *Pseudomonas fluorescens* strain under well-defined laminar flow conditions. The deposition results revealed an interesting non-monotonic dependence on swelling which at the same degree of crosslinking was lower with higher molecular weight of the PEG side chains. The highest efficiency of the gels comprising relatively long PEG chains was attributed to the complex effect of the side chain length. Accelerated biofilm development (biofouling) tests after bacterial attachment in the parallel plate setup also showed that the biofilm growth on polyPEGMEMA gels was strongly inhibited as compared to the hydrophilic glass surface used as reference, which was well correlated with deposition experiments.

The approach of using macroinitiator layer mediated anchored gel layer on membrane was explored to reduce/avoid homopolymerization in bulk solution and prevent delamination of gel layer from membrane surface. The cationic photoreactive macroinitiator based on poly(2-dimethylamino-ethyl methacrylate-*co*-2-hydroxyethyl methacrylate) comprising photoinitiator side groups was electrostatically adsorbed onto oppositely charged membrane surface. Subsequently hydrogel layers were prepared via surface initiated *in situ* graft and cross-linking photopolymerization from the membrane surface. Two commercial desalination membranes, NF270 composite membrane with the top layer of polyamide and NTR7450 membrane made from sulfonated polyethersulfone, were used as base membrane to evaluate the effect of surface chemistry of membrane in macroinitiator adsorption and subsequent photopolymerization. The protocols for grafted gel layers were based on procedures developed earlier for bulk gels. The modification degree and its effect on the membrane properties was characterized with respect to membrane chemistry by ATR-IR spectroscopy, surface charge by zeta potential, surface wettability by contact angle, and with respect to pure water permeability and salts rejection measurements as well as propensity to protein fouling. Zeta potential measurements showed an effective reduction in the net surface charge of gel modified membranes relative to pristine membranes. Water permeability decreased and salt rejection increased with degree of grafting.

Gel modified membranes demonstrated improved fouling resistance compared to pristine membranes.

In conclusion, this work developed the bulk polyPEGMEMA gels with the low protein sorption and low propensity to bacterial deposition and grafted these gel layers on NF membranes, to yield an efficient antibiofouling surface.

Acknowledgements

First of all, I would like to express the deepest gratitude to my supervisor, Prof. Dr. Mathias Ulbricht, for the patient guidance, valuable ideas and vast expertise he has offered throughout my PhD study. I have been extremely fortunate to have a supervisor who cared so much about my work, and who responded to my questions and queries so promptly.

I'm also grateful to Prof. Slava Freger, Dr. Roni Kasher, Inbal Eshet and Maria Bass for allowing fruitful collaboration and sharing their great knowledge and Dr. Moshe Herzberg for giving his experienced opinions.

I would like to thank my reviewer Prof. Dr. Christian Mayer for his precious advice and discussion as well as giving a good opportunity for pleasant cooperation and Manfred Zähres for his assistance and suggestions with solid state NMR measurement.

I would like to thank the German Israeli Foundation (GIF) for supporting this research.

Completing this work would have been all the more difficult without the support and friendship provided by Qianqian Jiang and the current and former members of our research group at Lehrstuhl für Technische Chemie II, Universität Duisburg-Essen. I am indebted to them for their help.

Finally, I would like to thank my family, especially my husband, Enfeng Song, for looking after me in difficult moments and continuing encouragement. Their love kept me going through it all.

Contents

List of Tables

List of Figures

Chapter 1 Introduction

1.1 Background and existing problems

Reverse osmosis (RO) or nanofiltration (NF) membranes employed in water purification and desalination of sea and brackish water suffer from biofouling, caused by formation of a biofilm on the membrane surface [1-3]. Sudden outbreaks of biofilm growth cause a severe loss of membrane performance (decreased flux and rejection) [4, 5], require more frequent cleaning and, ultimately, shorten membrane lifetime, then adding to the cost of the process.

Several potentially viable engineering approaches are being examined, such as depletion of the feed from nutrients [6], development of early warning methods [7, 8] and cleaning protocols [9], and the use of biocides [6]. None of these offers a robust, affordable and environment- and membrane material-friendly solution. Another promising approach is to apply a non-toxic and fouling-resistant coating to the membrane surface, which imposes only a minimal change in the existing desalination or water treatment technologies. This requires a detailed understanding of how the physical and chemical characteristics of a surface affect its propensity to fouling.

Concerning the effect of chemistry on biofouling, biofilm formation proceeds as succession of phenomena initiated by initial adsorption of organic species (i.e., proteins and other organic molecules) and attachment of microorganisms [3]. Therefore, a non-fouling surface should show protein-resistant properties to prevent biofilm formation. A large number of studies which focus on optimizing the chemical composition of solid surfaces and identifying chemical motifs responsible for low protein adsorption have been described in the literature. This led, for instance, to the formulation of the “four rules” that confer “protein resistance”, namely, surface moieties must be hydrophilic, hydrogen-bond acceptors but not hydrogen-bond donors and bear zero net charge [10-12]. Poly(ethylene glycol) (PEG) and PEG-based materials are the best known and most important examples of materials with such combination of properties, and they also have

already been shown to increase the fouling resistance of commercial membranes during water purification [13-15].

On the other hand, highly water-swollen materials fulfill the general requirements for "bioinert" surfaces, i.e., they provide an interface at which water has a structure similar to bulk water, so that its replacement by other molecules is not thermodynamically beneficial. Also importantly, the interfacial tension of such materials is very low due to the dilution of the interacting moieties; therefore the actual driving force for adhesion is largely reduced. A correlation had been found between the degree of swelling of polymethacrylate-based hydrogels and the resistance of ultrafiltration membranes to fouling by proteins for thin surface-grafted layers of such hydrogels [14]. Highly swollen hydrogels can also have a reduced propensity to cell adhesion to their surface [16-18]. Composites of membranes and hydrogels have become an active and diverse field of research with many applications, including those which depend on controlling the interactions of synthetic membranes with biomolecules and cells [19]. With respect to the "design" of antifouling coatings, one should note that highly swollen hydrogels ("bioinert" with respect to large bioparticles) will be prone to the uptake of small enough biofoulants (e.g., proteins); therefore an optimization of the degree of swelling will probably be necessary.

1.2 Objectives of the research

Generally, the objectives of this research work are:

(i) synthesis of bulk PEG based hydrogels with systematically varied structure.

(ii) physical and chemical characterization of bulk hydrogels.

(iii) optimal design of the grafted layer and surface grafting procedures suitable for desalination membranes.

(iv) obtaining systematic insight into the relationship between protein and bacteria fouling and the characteristics of the swollen gel (bulk and grafted thin layer) and the relative importance of physical and chemical structural factors.

1.3 Scope of this dissertation

A series of poly(ethylene glycol) methyl ether methacrylate (PEGMEMA) hydrogels was synthesized using macromonomers of three different molecular weight. The synthesis conditions for *in situ* polymerization were studied and optimized by varying the concentrations of PEGMEMA, initiator and cross-linkers. Typically, the properties of hydrogels are correlated with the composition of the reaction mixture, and monomer concentration and cross-linker content are considered the key parameters. However, only at quantitative monomer conversion to a polymer network and for isotropic, homogeneous gels, direct and quantitative correlations between synthesis parameters, and polymer volume fraction and cross-linking density of the network can be obtained. In many previous studies, this was actually not known; an attempt was made here to obtain more detailed insights suing established synthesis protocols based on redox initiation [20]. To analyze the degree of monomer conversion and the residual content of double bonds in the network IR and NMR spectroscopy were used. Furthermore, the hydrogels with three different PEG side chain lengths were characterized by their swelling and rheological behavior. Average mesh sizes as function of preparation conditions were estimated and discussed. Sorption tests with three different proteins were performed with bulk gels to estimate the partitioning coefficients. These data were also discussed with respect to network structure.

For the preparation of surface-anchored gel, the silanization of glass was used to introduce methacrylate groups and then performed in situ cross-linking polymerizations in a mold. Contact angle measurement was employed to identify interfacial adaptation between surface-anchored hydrogels in water as function of preparation conditions. The bacterial deposition kinetics was examined also included assessment of gravity effects on bacterial deposition and accelerated biofouling was investigated, in which sterile nutrient-containing medium was pumped along gels after initial bacterial attachment.

The tightly anchored hydrogel coatings on membranes were prepared via *in situ* graft and cross-linking photopolymerization. Therefore, adsorbed cationic photoreactive macroinitiators based on

poly(2-dimethylamino-ethyl methacrylate-co-2-hydroxyethyl methacrylate) and comprising photoinitiator side groups were used. The structure of the macroinitiators was analyzed by ATR-FTIR spectroscopy, NMR, and GPC techniques. Two NF membranes, NF270 composite which is composed of polyamide containing weakly acidic groups as active layer on top of a polysulfone support, and NTR7450 which is composed of sulfonated polyether-sulfone containing strongly acidic groups on the active layer, were used as the base membrane to investigate the effects of cationic photoreactive macroinitiator adsorption on membrane surface chemistry. The mechanism of modification has been analyzed based on the effect of UV irradiation time and premodification condition (varied macroinitiator) as well as modification condition (varied monomer molar masses and crosslinker content). Degree of grafting was calculated based on weight and ATR-FTIR data. Contact angle measurements were used to characterize the surface hydrophilicity of the membranes. Zeta potential measurements were performed to examine the surface charge of membranes. The performance of modified desalination membranes were characterized with water permeability and salt rejection, and the effects of membrane grafting chemistry on fouling resistance to feed protein solution chemistry were explored.

Chapter 2 Theory

2.1 Membrane desalination

With the development of human society, membrane desalination of brackish water and seawater has provided an effective technology of producing freshwater, to meet the increasing demand of drinking water [21]. Desalination is a general term for the process of removing salt from water to produce drinkable water. The main desalination processes categories are thermal processes and membrane processes. Nanofiltration (NF) and reverse osmosis (RO) are two main pressure driven membrane processes available for desalination. NF membranes are used most for softening brackish waters. The separation performances of nanofiltration are between ultrafiltration and reverse osmosis, and the membrane selectivity has often been attributed to the interchange of both molecular sieving mechanisms characteristic of ultrafiltration and solution diffusion mechanisms characteristic of RO [9]. NF membranes have relatively similar chemical structure with RO membrane, they are usually made of polyamide based thin film composites (TFC). The typical TFC membranes are composed of three layers of different polymeric materials (**Figure 2.1**). The top thin barrier layer is composed of polyamide and to provide the separation selectivity, it is prepared by interfacial polymerization and 100-200 nanometers thick. The second interlayer is an asymmetric porous polysulfone layer, the pores of this layer are in the ultrafiltration range, and the thickness is around 10-100 micrometers. The third support layer is a non-woven fabric layer providing mechanical strength (about 100-1000 micrometers thick) [22]. The performance of TFC membranes is determined by the density and thickness of the top layer as well as other physicochemical properties such as surface roughness, chemical structure, charge and hydrophobicity [23]. However, a fundamental distinguishing characteristic of NF membranes is their high rejection of multivalent ions but low rejection of monovalent ions, the RO membranes are typically characterized by high rejection of both monovalent ions and multivalent ions, but lower flux than that of NF membranes [9]. In general NF membranes have pore sizes between 0.5

and 2 nm and operating pressures between 5 and 40 bars; RO membranes do not have distinct pores and the operating pressures are between 10 and 150 bars [24-26].

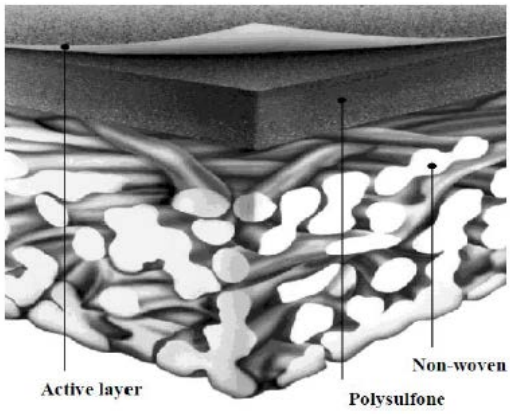

Figure 2.1. Structure of composite NF/RO membrane (www.dow.com).

Transport model

Two parameters are generally used for the description of membrane separation processes: solvent flux or permeability through the membrane, rejection of solutes.

In the pressure driven membrane process, such as NF, the solvent flux (J) is given by [27]:

$$J = \frac{\Delta P}{\eta R_{tot}} \quad (2.1)$$

Where ΔP is the effective transmembrane pressure, η is the permeate viscosity and R_{tot} the total resistance towards solvent flow.

The various resistances contribute with different extent to total resistance as depicted in Figure 2.2 [27]. In ideal case, only membrane resistance (R_m) exists. The membrane rejects the solutes to a certain extent, partial permeation will occur and non-permeated solute accumulates in the boundary layer. It results in a highly concentrated layer near the membrane and leads to the concentration polarization resistance (R_{cp}). The concentration of the accumulated solute molecules may become so high that a gel layer can be formed which leads to the gel layer

membrane resistance (R_g). With porous membranes, some solutes penetrate into the membrane and block the pores, leading to the pore blocking resistance (R_p). And solute adsorption on membrane surface, as well as the pores, will lead to the adsorption resistance (R_a) [27].

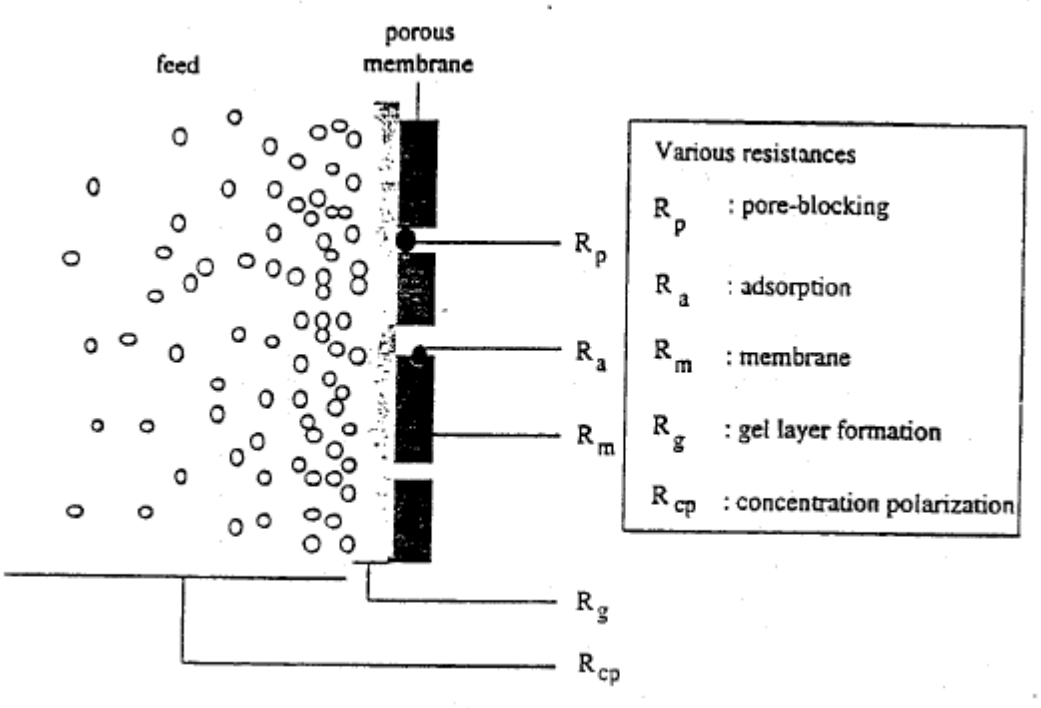

Figure 2.2. Overview of various resistances towards mass transport across a membrane in pressure driven processes [27].

The rejection of a component i (R_i) is defined as:

$$R_i = \frac{c_{f,i} - c_{p,i}}{c_{f,i}} \times 100\% \qquad (2.2)$$

Where $c_{p,i}$ and $c_{f,i}$ are the permeate concentration and the feed concentration of component i respectively.

In nanofiltration, the rejection of a neutral solute is mainly distributed to size exclusion. Due to its size a solute can pass the membrane only via a pore. It leads to a steric exclusion of the solute from the membrane. For charged solutes, one additional mechanism can be distributed to Donnan exclusion [28]. Donnan exclusion has a distinct effect on nanofiltration compared to other

pressure driven membrane processes. Solutes with the charge opposite to the membrane (counter-ions) are attracted, while solutes with a similar charge (co-ions) are repulsed. At the membrane surface exclusion between co-ions and counter-ions will occur, therefore this causes an additional separation [29].

2.2 Biofouling

2.2.1 Overview on membrane fouling

Fouling is defined as the process resulting in loss of membrane performance due to undesirable deposition of suspended or dissolved substances on its external surfaces, at its pore openings, or within its pores [30]. Diagnosis of the type/cause of fouling is an essential first step aiming at controlling fouling [31]. Autopsy gives conclusive information and further understanding about the types and extent of fouling in the membrane filtration plant and provides specific ways for reduction and control of fouling. A set of coherent tools has been developed for (a) determining the fouling potential of the feed water and (b) analyzing the fouling of NF and RO membranes. The tools presented can be used to (a) assess the cause of fouling, (b) further define criteria for feed water to predict and minimize the risk of fouling and (c) evaluate cleaning strategies [32].

The fouling categories of NF membrane based on fouling material can be generally divided into inorganic (mainly $CaCO_3$, $CaSO_4$, $BaSO_4$), organic (humic acids, carbohydrate and protein) and biological fouling [31-35]. While research traditionally focuses on one category or fouling mechanism at a time, it is well accepted that in most cases it is not one single category that can be identified. In most real life applications all three types of fouling go hand in hand. The types of foulants and where they usually occur in NF/RO systems are summarized in **Table 2.1** [36]. It can be seen, biofouling occurs throughout the filtration stages. Autopsy studies of NF and RO membranes fouled during the treatment of wastewaters and surface water have shown that more than 50% of the dry weights of the fouling layers are biological in origin [6, 37].

Table 2.1. Overview on where fouling occurs first [36].

Type of foulant	Most susceptible stage of NF/RO
Scaling/silica	Last membranes in last stage
Metal oxides, Colloids, Organic, Biofouling (rapid)	First membranes of first stage
Biofouling (slow)	Throughout the whole installation

2.2.2 Mechanism and characteristic of biofouling

Biofouling is a dynamic process of microorganisms adhesion, growth and biofilm formation. This phenomenon exists not only in membrane systems and also a major concern in heat exchangers, ship hulls, water treatment systems, and in bio-medical applications [1]. For membrane systems, biofouling has severe impacts not only on the performance in terms of flux and separation and also on the lifetime of membrane and modules.

Mechanism of biofilm formation

Although the function and appearance of biofilms in various environments may be different, all biofilms are formed according to the following basic sequence of events (**Figure 2.3**) [38, 39].

1. A conditioning film is formed by adsorbed macromolecular organic components (i.e. proteins and other organic molecules) on the substratum surface prior to microbial deposition; it can take place in seconds [10].
2. Microorganisms are transported towards the substratum surface through diffusion, convection, sedimentation, or by intrinsic bacterial motility.
3. Initial microbial adhesion.
4. Strong attachment or anchoring of microorganisms to the substratum surface through the production of extracellular polymeric substances (EPS) mostly composed of polysaccarides and proteins.

5. Surface growth of adhering microorganisms and continued secretion of EPS.
6. Localized detachment of isolated clumps of microorganisms caused by occasionally high fluid stress or other detachment forces operative in the environment of the biofilm, it occurs within hours [10].

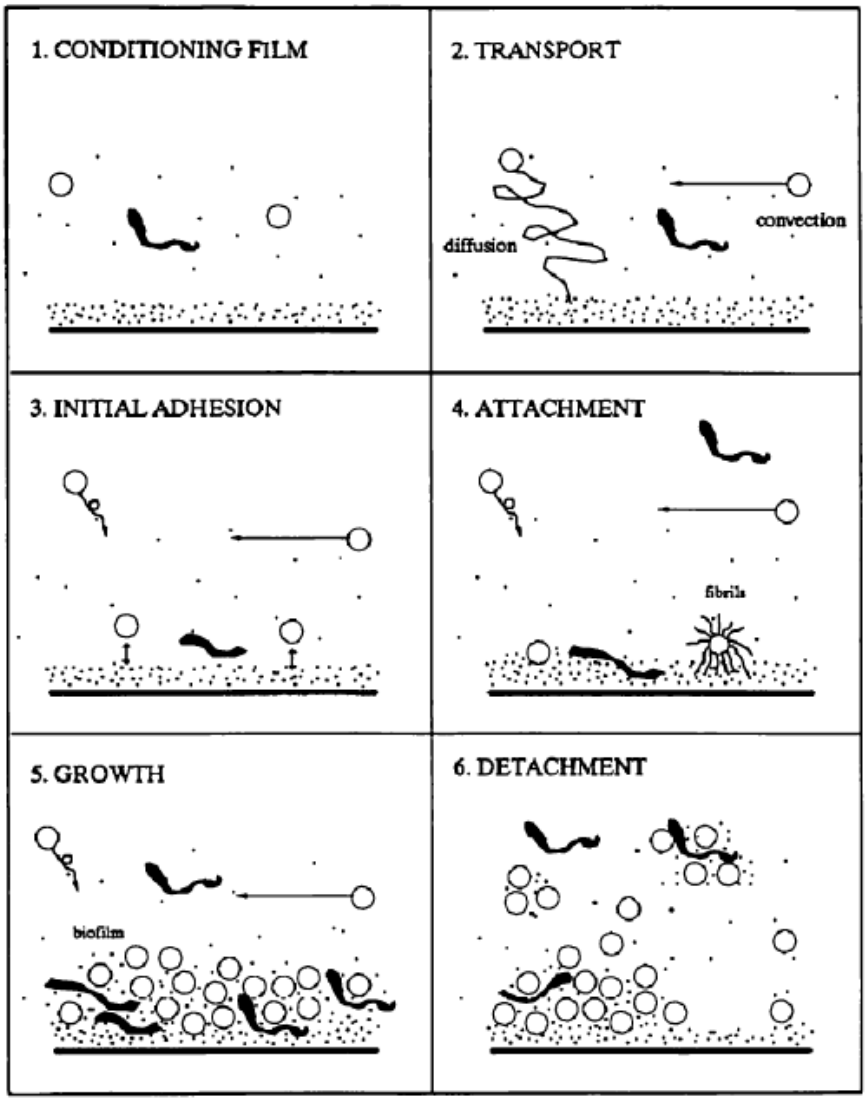

Figure 2.3. Schematic of biofilm formation step [39].

Bacteria adhesion to the surface

Bacterial adhesion to a surface can generally be recognized as consisting of two phases: a rapid reversible physical phase (stage 1 in Figure 2.3) and an irreversible phase (stages 4-5 in Figure

2.3). Much research has focused on the reversible initial deposition stage to control bacterial adhesion to surfaces. A widely adopted view is that release and adsorption of proteins to the surface is the first critical step in bacterial adhesion [40, 41]. When a protein approaches the surface it can (a) be adsorbed irreversibly to the surface through strong hydrophobic or electrostatic interactions or by chemical bond formation between the denatured protein and the substrate while going through conformational changes, (b) be adsorbed reversibly and removed, or (c) stay dissolved in the liquid medium and not be adsorbed to the surface [42]. Initial deposition of bacteria to a surface can be often described using the classic DLVO (Derjaguin-Landau-Verwey-Overbeek) theory as the basis [43, 44]. According to DLVO theory, the interactions between a particle and the surface can be predicted by a summation of the attractive van der Waals and the electrostatic double layer interactions that can be either attractive or repulsive. A schematic description of the DLVO interaction profiles and the summation of these two forces is presented in Figure 2.4 [9]. The resulting interaction energy in the case of repulsive double layer interaction may have two minima: a secondary minimum in which the cell reversibly attaches to the surface, and a much deeper primary minimum yielding a strong attachment, which may be viewed as irreversible [45]. Since bacteria and most synthetic and natural surfaces (including the surface of most NF and RO membranes) are negatively charged at ambient pH, the electrostatic interaction is usually repulsive [46]. In addition, composition of the aqueous environment including nutrient levels, ionic strength, pH, exposure to UV light, temperature and the characteristics of bacteria all affect the bacterial deposition [47].

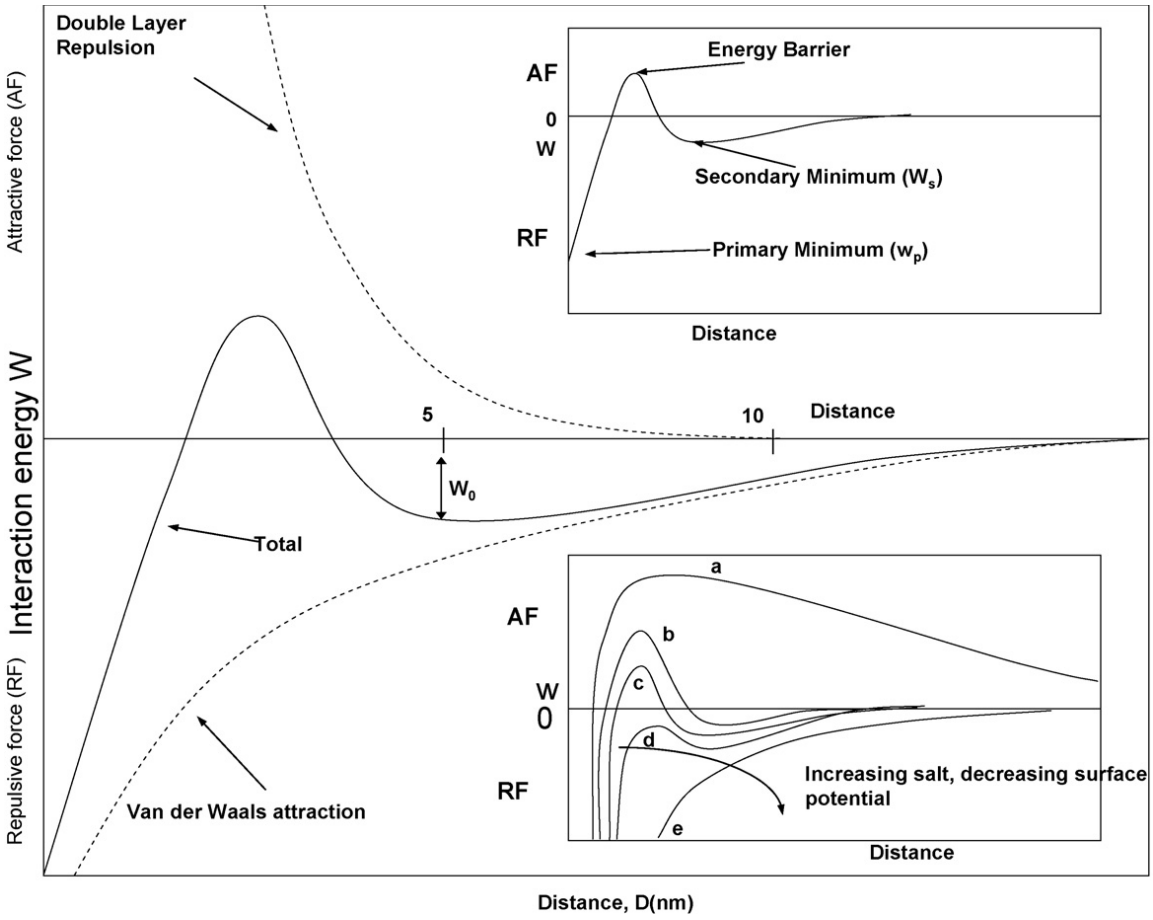

Figure 2.4. Schematic energy versus distance profiles of DLVO interaction profiles.

(a) Surfaces repel strongly; small colloidal particles remain 'stable'. (b) Surfaces come into stable equilibrium at secondary minimum if it is deep enough; colloids remain kinetically 'stable'. (c) Surfaces come into secondary minimum; colloids coagulate slowly. (d) The 'critical coagulation concentration'. Surfaces may remain in secondary minimum or adhere; colloids coagulate rapidly. (e) Surfaces and colloids coalesce rapidly.

2.2.3 Prevention and control of membrane biofouling

Membrane biofouling and its control remains a major operating problem due to the enormous diversity of microorganisms in feed water. Sudden outbreaks of biofilm growth in response to minor changes of conditions, e.g., temperature or water composition [4, 5], cause a severe loss of membrane performance (decreased flux and rejection), the need for more frequent cleaning and

ultimately shorter membrane lifetime. The prevention and control of membrane biofouling can be done using three strategies: early warning methods, physical pretreatment method and chemical methods.

Early biofouling warning enables to take preventive measures, either by pre-treatment optimizing or by preventive membrane cleaning. Cleaning at an early stage requires less chemicals and less down time and lowers the risk of irreversible fouling and membrane damage. Cleaning was more successful at early stage biofouled membrane systems [8].

Pretreatment systems using conventional microfiltration/ultrafiltration membrane processes are employed to produce feed water with a reduced fouling potential, by removing particulates, micro-pollutants and micro-organisms as well as preventing the formation of inorganic scales [49-51]. However, opposite to the other foulants, microorganisms can grow and multiply at the expense of feedwater nutrients, and even if they are removed by pretreatment to 99.99%, this can still be enough to form a biofilm [52].

Chemical methods for biofouling control include cleaning protocols, the use of biocides, and surface modification. Cleaning protocols can be optimized by varying types of chemical agents, the frequency of the cleaning, or the cleaning procedure [9]. However, cleaning is relatively expensive and not universally efficient. In spiral-wound and hollow fiber elements some sections of the flow channel may become blocked and inaccessible. In these conditions, cleaning solution may fail to reach certain fouled areas on the membrane leaves or fibers [53]. Biocides are disinfecting agents which are capable of inactivating micro-organisms. It can be achieved using tributyltin coating, chorine, oxidizing agents [6, 54]. However, leaching of tributyltin leads to massive pollution problems and detrimental effects on non-targeted organisms [55]. Chlorine and oxidizing agents may react irreversibly with RO or NF membranes, and they are problematic and have a negative affect their flux and salt rejection [53]. Moreover it was claimed that dead biomass and cell debris left after disinfection will be quickly biodegraded and used as nutrients by newly settled bacteria [56]. Depletion of the feed from nutrients is another operational mean of

inhibition [6]. However, biofilm formation may occur even under the most stringent starvation conditions, though not as rapidly or tenaciously as for unstarved cells [57].

The most promising approach is surface modification of membrane; it may require a minimal change in the existing desalination or water treatment technologies. In addition, the benefits in terms of the use of chemicals, frequency and ease of cleaning and increased membrane performance and lifetime may largely offset a marginal increase in the cost of membranes. And this approach is explored in the present study.

2.3 Membrane Surface Modification

2.3.1 Modification methods

In this section, a recent comprehensive feature article written by Ulbricht [58] is used as the main reference. Surface modification of membrane has been developed for changing surface characteristics to reach a variety of goals, such as minimize undesired (secondary) interactions (adsorption or adhesion) which reduce the performance (membrane fouling), or to introduce additional interactions (affinity, responsiveness or catalytic properties) for improving the selectivity or creating an entirely novel separation function [58]. Many different procedures have been explored for surface modification of desalination membranes to reduce fouling.

Physical methods

Attachment of functional layer onto a membrane surface could be done via the following ways [58]: (a) adsorption/adhesion the functional layer is only physically fixed on the base material. The binding strength can be increased via multiple interactions between functional groups in the macromolecular layer and on the solid surface, (b) interpenetration via mixing between the added functional polymer and the base polymer in an interphase, (c) mechanical interpenetration (macroscopic entanglement) of an added polymer layer and the pore structure of a membrane.

The stability of the functional layer or "coat" is dependent on the reversibility/irreversibility of the adsorption or more generally of the noncovalent attachment. And the thickness of the layer depends on the selected strategy; it can be significantly larger than for surface modifications controlled by interfacial reactions. Zhou et al. [59] describe an electrostatic self-assembly of polyethyleneimine on the membrane surface. Deposited polyethyleneimine surface layer tended to offer additional resistance to permeation, the improved fouling resistance and the increased surface hydrophilicity compensated for the reduction in membrane permeability.

Overall, in this way, the modification is simple and could improve the membrane performance with respect to the fouling resistance. However, loss of permeability after modification was also observed. More importantly, the stability of the coating/functional layer and incomplete surface coverage leading to the heterogeneity were other significant limitations.

Plasma treatment

Plasma is a complex gaseous state of matter, consisting of free radicals, electrons, photons, ions, etc. Plasma can be generated by continuous electrical discharge in either an inert or a reactive gas. Plasma treatment had been very intensively studied and typical applications are introduction of special function groups and hydrophilzation [58]. Pal et al. [60] used CO_2 plasma treatment to surface modify polyamide membrane. The results showed a reducing susceptibility to harsh chemicals or environmental agents, and increasing dye absorption. Kim et al. [61] modified commercial NF membrane using low pressure NH_3 plasma to increase the membrane hydrophilicity. Modification that resulted in more negatively charged surfaces could also better prevent Aldrich humic acid fouling on the membrane surface.

Chemical surface modification activated by plasma is flexible because of the variety of gases that can be used. Modification is surface selective and is restricted to the top several nanometers of the surface, so the bulk polymer properties are usually unaffected. Further, homogeneity of surface modification can be achieved due to under vacuum operation [58]. However, the ablation

tendency of the base polymer may be significant [62] and the complexity of the process including using vacuum equipment is the limitation. Then, the change in pore structure or pore etching leading to the retention loss, significant loss of membrane permeability were also observed. Modifications in small pores (diameter < 100 nm) are complicated because the dimension is smaller than the average free path length of the active species in the plasma [58].

Chemical reactions

The covalent bonding of polymer segments and chains to membrane surface can be achieved [58]: (i) heterogeneous reactions of the membrane polymer, (ii) "grafting-to" reaction, and (iii) "grafting-from" reaction.

Heterogeneous reactions of the membrane polymer. Chemical reactions on the surface of the membrane material could be classified into following two ways [58]:

(a) derivatization of or grafting onto the membrane polymer via reaction of intrinsic functional groups without material degradation (no polymer chain scission or change in bulk morphology).

(b) controlled degradation of the membrane material for the activation of derivatization or grafting reactions (at minimized polymer chain scission or change of bulk morphology).

Reactions according to (a) may be based on end groups of the membrane polymer (e.g. amino or carboxylic groups in polyamides or hydroxyl groups in polysulfone). For example, surface coupling of poly(ethylene glycol) to desalination membranes showed an improved fouling resistance to charged surfactants and emulsion but decreased water flux [63]. However, most of the other established membrane polymers are chemically rather stable, and, therefore, controlled heterogenous functionalizations are complicated or even impossible.

"Grafting-to" reaction. "Grafting-to" reaction is performed by coupling polymer molecules to surface. Introducing macromolecular functional layers to the surface of membranes could be done via the following strategies [58]: (a) direct coupling on reactive side groups or end groups of the membrane, (b) primary functionalization of the membrane□ introduction of amino, aldehyde,

epoxide, carboxyl or other reactive groups on the surface and subsequent coupling, (c) adsorption on the membrane surface and subsequent physically activated coupling.

Wei et al. [64] and Kang et al. [13] describe reactions with acyl chloride and/or carboxylic groups in the polyamide film for attachment of monomers that lead to membranes that are either resistant to chlorine attack and show antimicrobial properties or are fouling resistant, respectively.

"Grafting-from" reaction. During "grafting-from" reaction, monomers are polymerized using an initiation at the surface. Synthesis of macromolecular layers via "grafting from" a polymer membrane surface had used almost exclusively radical polymerization until now [58]. "grafting-from" reaction can be initiated via: (a) degradation of the membrane polymer (main chain scission or cleavage of side groups), via physical excitation with radiation or plasma, (b) decomposition of an initiator in solution and radical transfer (here hydrogen abstraction); radicals in solution may initiate a homopolymerization as a side reaction or leading to grafting via radical recombination, (c) adsorption of a photoiniator (e.g. benzophenone derivative) on the surface and selective UV excitation (the reactivity of the benzpinakol radical is too low to start a polymerization in solution) (**Figure 2.5)**.

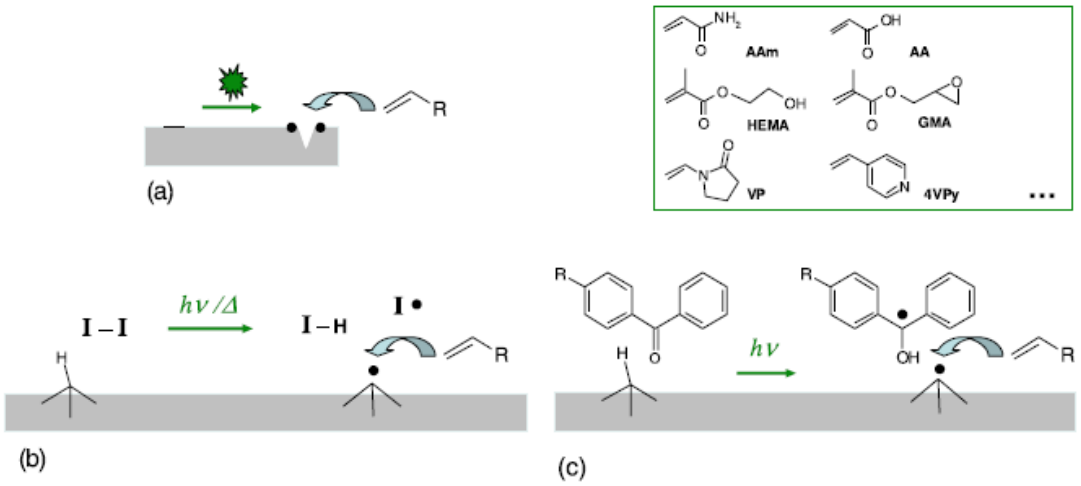

Figure 2.5. Heterogenous radical graft copolymerizations (grafting-from) of functional monomers on membrane polymers can be initiated (formation of starter radicals) [58].

Chemical activation for the generation of radicals on the membrane surface has been explored. Through decomposition of peroxides in a solution in contact with the membrane, a radical transfer to the membrane material can also yield starter radicals (**Figure 2.5b**). Several studies used such a method to grow a number of different hydrophilic polymers from the surface of polyamide membranes in order to reduce membrane fouling [65-68]. Such 'grafting-from' functionalizations without additional activation by external means could also be applied for the modification of membranes in modules. However, branching or crosslinking of the grafted chains by reactions in solution cannot be avoided.

Several studies also used surface initiated atom transfer radical polymerization (ATRP) to minimize polymerization in solution and provide polymer growth with low polydispersities. The typical procedure is immobilizing ATRP initiator on substrate by the immersion of a hydroxyl functionalized membrane in an organic solvent containing an ATRP initiator and the subsequent surface initiated growth of polymer [69-71]. However many membranes do not have a high density of function groups on the surface, and may also incompatible with organic solvents used

for initiator immobilization [72]. Since most of membrane surfaces are negatively charged, the cationic macroinitiators have been developed for initiator immobilization as presented in **Figure 2.6** [72]. The cationic macroinitiator readily adsorbs onto oppositely charged surfaces through strong electrostatic interactions, as reported previously in adsorption on silicon [73], silica beads, [74, 75] modified colloidal particles [76], and polymeric substrates [77]. And ATRP can be successfully carried out from the immobilized macroinitiator. But one drawback to ATRP is that control of polymerization is often achieved at the expense of the polymerization rate.

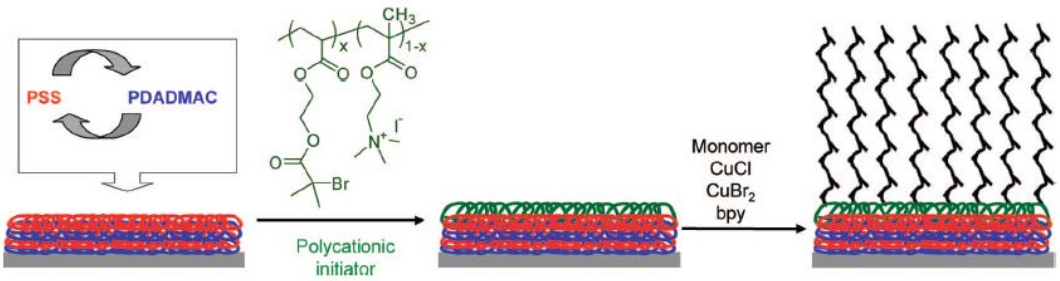

Figure 2.6. Growth of polymer brushs from macroinitiator adsorbed on polymeric substrates [72].

Physical activation (electron beam, plasma treatment or direct UV excitation) had been explored to create free radicals from early on because this excitation can be applied to many membrane polymers. As consequences, unwanted changes in membrane morphology and/or an even modification in the interior of porous membrane are the side effects of this approach. The extent of these side effects depends on the sensitivity of the membrane material and the excitation used. "Photo grafting-from" has been increasingly used and developed. It has relatively low cost, and works under mild reaction conditions, potentially reducing or even avoiding negative effects on the bulk polymer. To minimize homopolymerization in solution, a general method is immobilizing initiators on membranes and the subsequent surface-initiated growth of gel layers. One route has been developed for initiator immobilization via direct initiator adsorption.

For direct initiator adsorption, the typical ‘‘Type II’’ photoinitiator benzophenone (BP) or its derivatives can be immobilized on polymer substrates via: (a) weak physical interaction between the polymer surfaces and the photoinitiator [78, 79], (b) ionic interaction between respective functional groups on the surfaces and the photoinitiator [80], (c) entrapping in surface layer by preswelling base membrane polymer and subsequent solvent exchange [81]. And then it generates starter radicals by hydrogen abstraction from the surrounding chemical species including substrate polymer surface. However, this approach has an obvious disadvantage. Usually the hydrogen atoms in many commercial membrane polymers are not very reactive to the excited BP. In that case, the selection of solvent should be considered very carefully, in particular only solvents without labile hydrogen (e.g., water or acetonitrile) should be used to minimize homopolymerization and enhance the surface-selectivity [82].

This work builds on these previous studies to design a novel cationic photoreactive macroinitiator (**Figure 2.7**) for functionalization of membranes. Quaternizated poly(2-dimethylamino-ethyl methacrylate) segments can anchor via strong ion exchange groups to membranes with excess negative charge (carboxylic acid or sulfonic acid groups). “Type I” photoinitator benzoin ethyl ether which is coupled in poly(2-hydroxyethyl methacrylate) segments can generate start radicals directly by bond cleavage. Therefore, the immobilization of photoinitiator will be more stable and control over side and over graft copolymerization will increase.

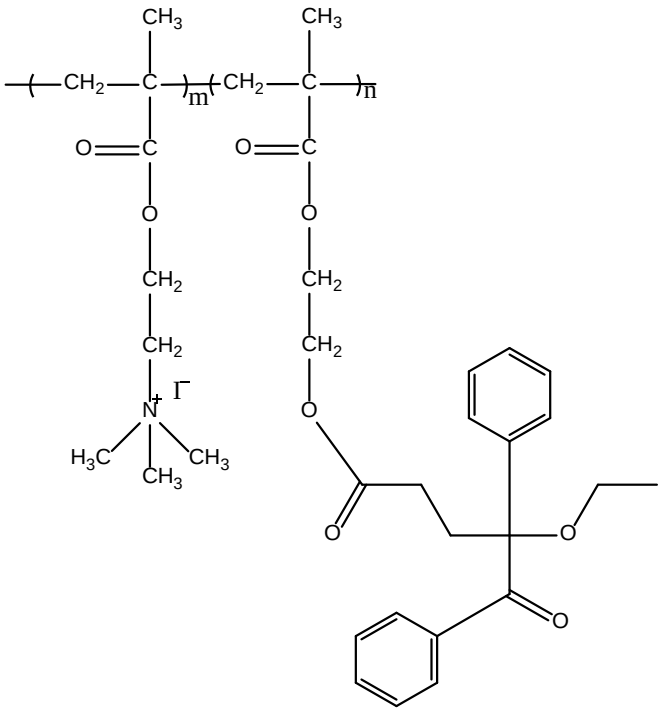

Figure 2.7. Chemical structure of the cationic photoreactive macroinitiator.

2.3.2 Polymer for grafting

Due to the general importance of proteins and their presumed primary role in bioadhesion (cf. section 2.2.2), much research has focused on developing “protein-resistant” surfaces. A large number of studies focus on optimizing the chemical composition of solid surfaces and identifying chemical motifs responsible for low protein adsorption. This led to formulation of the “four rules” that confer “protein resistance”, namely, surface moieties must be hydrophilic, be hydrogen-bond acceptors but not hydrogen-bond donors and bear zero net charge [10-12].

Hydrophilicity. The main driving force for protein adsorption are hydrophobic interactions [83]. Adsorption to hydrophobic surfaces appears rapid, and binding may be stronger than to hydrophilic surfaces. Many researches claim that protein adhesion to hydrophilic surfaces (high wettability) is much lower than to hydrophobic surfaces. As presented in **Figure 2.8**, an AFM tip modified with different functional groups was used to measure the energy of adhesion to a $HS(CH_2)_{11}COOH$ SAM (self-assembled monolayer) surface covered with immobilized proteins

on Au coated glass substrates in aqueous solution. The results showed that for all proteins, hydrophobic groups (-CH3, -OPh, -CF_3, -CN and -OCH_3) had definitively higher adhesion force than hydrophilic groups (-OH, -EG_3OH and -$CONH_2$) [84].

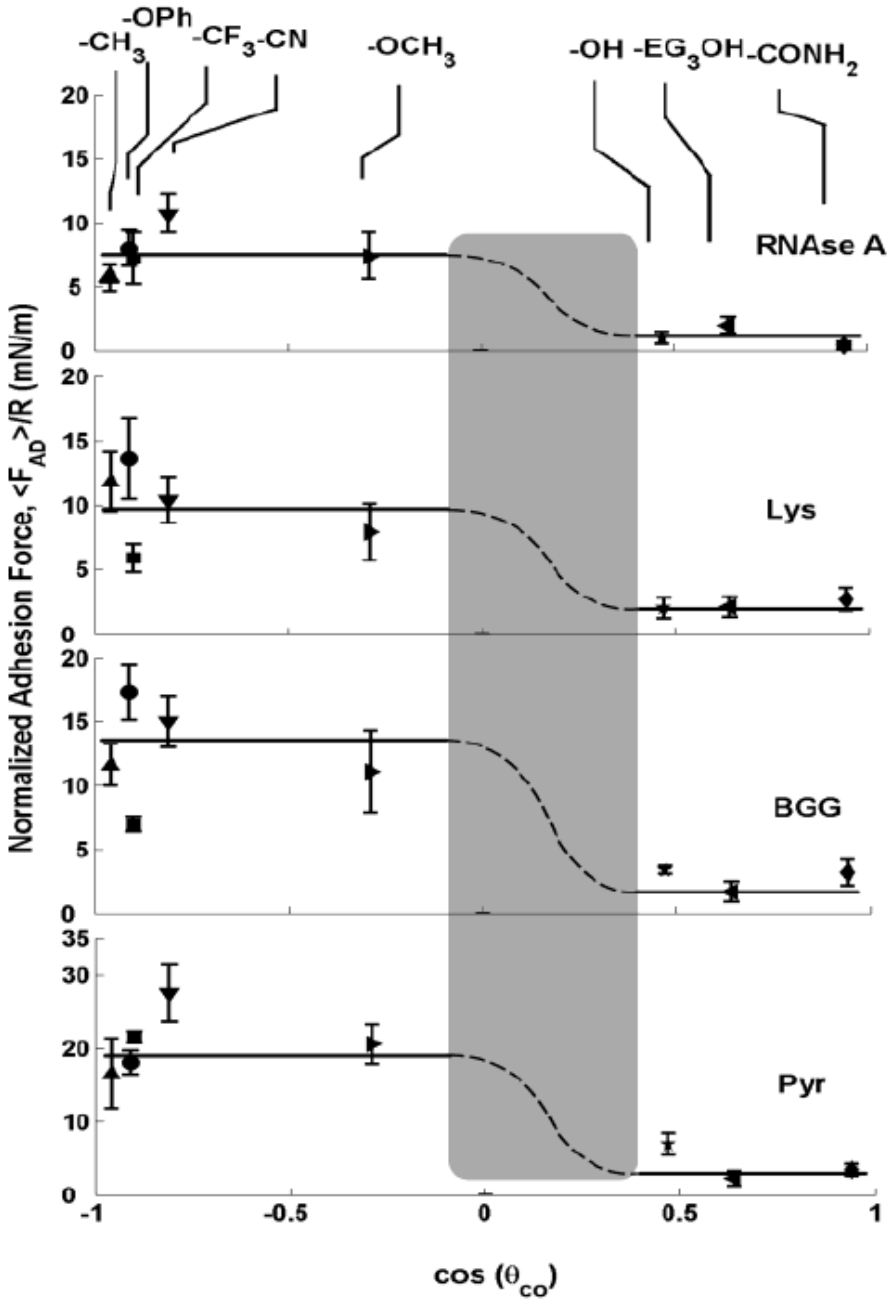

Figure 2.8. Effect of protein adhesion force of AFM tip on contact angle [84].

Surface charge. The cell envelope of bacteria is composed mostly of phospholipids, lipo-polysaccharides, polysaccharides and proteins, most of which are charged at ambient pH and may interact with charged regions on the surface. In most cases, bacteria adhere more readily to positively charged surfaces than to negatively charged surfaces, because the net charge of most bacteria is negative [39]. Nevertheless, even surfaces with overall negative charge have been shown to have different heterogeneities with positive areas [85] and some bacterial strains are positively charged, therefore negatively charged surfaces may not be universally efficient and neutral surfaces may be commonly more efficient in reducing adhesion of a wide variety of bacteria onto the surface [86, 87].

Surface roughness. Surface roughness also plays a role on bacterial adhesion. In general, rough surfaces enhance bacterial adhesion, since they create regions of lower shear stresses and stronger bacteria-surface interactions and offer a larger surface area for bacteria to settle than smooth surfaces [86, 88, 89] (**Figure 2.9**).

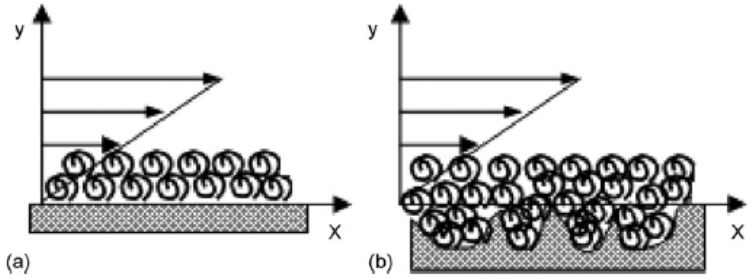

Figure 2.9. Schematic of the effect of surface roughness on membrane fouling [89].

Polymers for anti-biofouling

Poly(ethylene glycol) and its derivatives. Immobilizing poly(ethylene glycol) (PEG) is one most common approach used for preventing protein adsorption [90, 91] and bacterial adhesion [92, 93]. Also, PEG has the advantages of very low toxicity and low cost. The mechanisms for high protein resistance of PEG are not yet fully understood. One is the relatively high solubility in water (hydrophilicity), leading to low van der Waals interactions with the protein, and neutral polymer

[94, 95]. Also, PEG is very hydrophilic, neutral and the poly ethylene oxide chain of the PEG has many proton-accepting groups and thus fully meets the four rules of protein resistance [12]. In addition, PEG brushes employ an extra steric exclusion, which utilizes a secondary minimum in the energy-distance dependence, to reduce protein and cell adsorption [96-98].

Zwitterionic polymers. Zwitterionic substances have also been extensively studied as an antifouling material. They have negatively and positively charged groups but a zero net charge. Grafting of the phospholipid zwitterionic polymer on surface showed an effective protein or platelet adhesion resistance [99-101]. Susanto et. al [14] reported that polyethersulfone ultrafiltration membrane surfaces coated with poly(sulfobetaine methacrylate) were efficient in reducing protein fouling.

Biomimetic materials:

(a) *Carbohydrates*. The external region of a cell membrane is dominated by glycosylated molecules and is known as glycocalyx, which is known to prevent undesirable non-specific interactions. Indeed, a synthetic glycocalyx mimicking surface showed reduced cell adhesion [102].

(b) *Peptides*. Surfaces coated with certain polypeptides, may exhibit high protein resistance. They were found to be specifically fouling-resistant when combining positively and negatively charged amino acids in the same ratio [103], i.e., yielding amphoteric or even zwitterionic surface (cf. above).

2.3.3 Hydrogel

Hydrogels are three-dimensional networks of hydrophilic polymer chains with properties between liquids and solids. They are chemically or physically crosslinked polymers that can imbibe large amounts of water without dissolving and without loosing their shapes [104]. They are emerging today as promising novel materials in biology and medicine [105]. Studies performed over the last two decades demonstrated the efficiency of grafted hydrogels as bio-inert coating biomedical

devices (e.g. urinary tract catheters) and biosensors [106, 107]. The experiments with blood cells carried out by Ikeda's group showed a clear correlation between degree of swelling of the hydrogels and reduction of cell adhesion [16], in agreement with the recent conclusions by Rubner et al. [17]. Interestingly, these results pointed to the existence of an optimal water content of about 85-90%, similar for different gels and explained by a tradeoff between the reduced adhesion to the gel surface and the increased penetration of cells and mediator molecules into the gel and onto the underlying substrate.

In this work, the physical principle (high swelling) is explored for creating biofouling-resistant membranes through designing and grafting a thin highly swollen gel onto the membrane surface. Importantly, these favorable physical characteristics also combined with known chemical criteria for bio-inert surface, particularly, the use of intrinsically "low-fouling" moieties as building blocks for the grafted gel. A few recent studies reported the use swollen hydrogels as coatings for reduced biofouling by marine organisms of materials working in sea environment [18, 108]. The observed efficiency was however limited, apparently because the used polymers failed to meet the known chemical criteria for bio-inert surfaces, such as avoiding charged polymers or hydrogen bond donors. Therefore, poly(ethylene glycol) methylether methacrylates (**Figure 2.10**) had been selected to prepare highly swollen gels coating and to meet criteria for protein and bacteria resistance, in particular the absence of hydrogen donor groups [11].

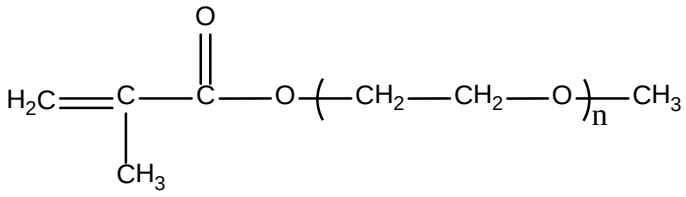

Figure 2.10. Chemical structure of poly(ethylene glycol) methylether methacrylate.

Free radical polymerization is common method to synthesize hydrogel. The basic mechanism of free radical polymerization can be generally divided into three steps: initiation, chain propagation,

termination [109]. The reaction is initiated by formation of initial free radicals from dissociation of initiator. Then the initial radical is transferred to monomer forming a primary radical (initiation). The primary radical attacks another monomer molecule and the process continues in growing a long chain (chain propagation). Finally, the reaction are terminated by three alternative mechanisms: (a) coupling two radical chains join at the reactive ends to form a non-reactive chain of a length equal to the sum of the two chain lengths, (b) disproportion, where a radical is transferred from a radical chain to another radical chain resulting in two unreactive chains, (c) chain transfer in which a radical abstracts a hydrogen or other atom or species from some compound present in the system (termination) [109].

The initial radical can be created by dissociation of redox initiator or photo initiator. In redox initiation, ammonium persulfate (APS) and N,N,N‘,N‘-tetramethylethylene diamine (TEMED) redox initiator pair are typically used to produce initial radical by an electron transfer from a reductant TEMED to an oxidant APS. In photo initiation, UV light is commonly used to produce excited photo initiator in a short time. In this work, bulk hydrogel was synthesized via redox free radical polymerization due to low activation energy and formation of homogeneous hydrogel. However redox reaction takes a long time, then the photo polymerization was used to graft hydrogel from membrane surface to complete modification in minutes.

The swelling behaviors of hydrogels are mainly dependent on the chemical nature of the polymers composing the gel as well as the structure and crosslinked network which includes physical entanglement and chemical crosslinking [104, 110]. The structure of an idealized hydrogel is presented in **Figure 2.11**. The most important parameter that determines the structure and properties of swollen hydrogels is network mesh size ξ. The network mesh size is defined as the average distance between consecutive crosslinking points and serves as an indicator of the screening effect of the network on solute diffusion. The term ξ also indicates the maximum size of solutes that can pass through gel network [111]. The mesh size can be determined theoretically or using a number of experimental techniques. Two direct techniques for measuring this

parameter are quasi-elastic laser-light scattering [112], and scanning electron microscopy [113-115]. Some indirect experimental techniques for determination of the hydrogel mesh size include NMR relaxation times measurement [116], mercury porosimetry experiments [117], protein exclusion experiments [118], equilibrium swelling experiments [20, 119-121] and rheological measurements [122, 123]. This study used swelling and rheological data to estimate the mesh size.

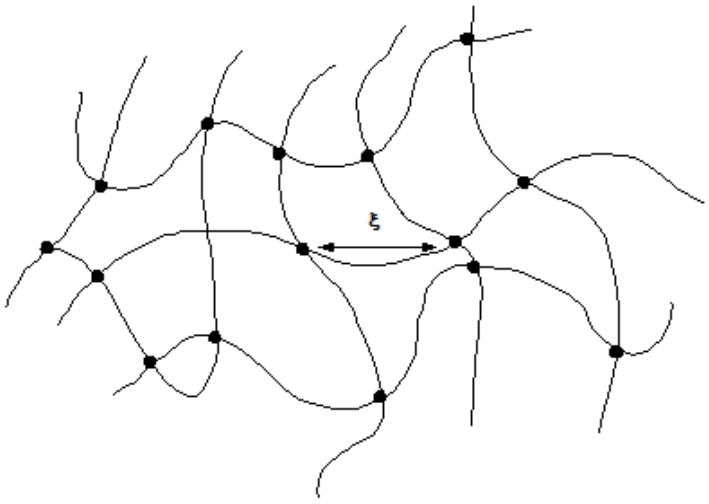

Figure 2.11. Schematic representation of the cross-linked structure of a hydrogels. ξ is the network mesh size.

Mesh size estimated from swelling data. Based on gel swelling in water, the network mesh size is related to the elongation of the polymer chains in any direction which can be calculated from polymer volume fraction of swollen gel and the end-to-end distance of polymer chains in the unperturbed state between crosslinking points [104]. For an isotropically swollen gel the mesh size of the swollen polymeric network can be estimated by the following equation according to Peppas et al. [124]:

$$\xi=(C_n/n)^{1/2} l \upsilon_{2,s}^{-1/3} \qquad (2.3)$$

where C_n is the polymer Flory characteristic ratio (14.6 for polymethacrylic acid in an aqueous NaCl solution [125] had been used in this work because data for polyPEGMEMA could not be

found), l is the carbon-carbon bond length (154 pm), n is the crosslinking density which is theoretically equal to the molar ratio of crosslinker monomer and functional monomer assuming full conversion (quantitative network yield), and $\upsilon_{2,s}$ is the equilibrium polymer volume fraction of a fully swollen hydrogel, determined by the following equation.

$$\upsilon_{2,s} = \frac{\frac{W_d}{\rho}}{\frac{W_d}{\rho}+\frac{W_s-W_d}{\rho_w}} = \frac{\frac{1}{\rho}}{\frac{1}{\rho}+\frac{SR-1}{1}} = \frac{1}{1+\rho SR-\rho} \qquad (2.4)$$

Where SR is the swelling ratio of gel, ρ is the density of polymer, ρ_w is the density of water.

Mesh size estimated from rheological data. Based on rheological data and rubber elasticity theory [126], a chemically crosslinked hydrogel is a network of tetrafunctional connectivity in which four strands radiate from each cross-link, the strands are of equal length, and the crosslinks are fixed in a way that when external sample dimensions change with deformation the crosslinks move in a affine manner. The mesh size can then be estimated from the equilibrium storage modulus at infinitesimal deformations using the following equation [123]:

$$\xi=(RT/G'N_A)^{1/3} \qquad (2.5)$$

Where R is ideal gas constant, T is the measuring temperature, N_A is Avogadro's constant, G' is linear storage modulus measured with frequency sweep experiments.

Chapter 3 Experiments

3.1 Materials

Poly(ethylene glycol) methylether methacrylate (PEGMEMA), with PEGs of average molecular weight 200, 400 and 1000 $g \cdot mol^{-1}$, and 2-dimethylamino-ethyl methacrylate(DMAEMA) were purchased from Polysciences. Ethylene glycol dimethacrylate (EGDMA), ammonium persulfate (APS), N,N,N‘,N‘-tetramethylethylene diamine (TEMED), ethanol, methanol, Hexane, and tetrahydrofuran (THF) were purchased from Acros Organics. Diethylene glycol dimethacrylate, triethylene glycol dimethacrylate, N,N’-methylenebisacrylamide (MBAA), 3-methacryloxypropyl-trimethoxysilane (MPS), Fluorescein isothiocyanate labeled bovine serum albumin (FITC-BSA), deuterium oxide (D_2O), 2-Hydroxyethyl methacrylate (HEMA), benzophenone (BP), benzoin ethyl ether (BEE), ethyl acrylate and bromine and phosphorous (red) were purchased from Sigma Aldrich. 2, 2’-Azobis (2-methylpropionitrile) (AIBN), Iodomethane, potassium hydroxide (KOH) and lysozyme (Lys) from hen egg white were purchased from Fluka. Bovine serum albumin (BSA) and Fibrinogen (Fib) from bovine plasma was purchased from MP Biomedicals. Hydrochloric acid, Magnesium chloride ($MgCl_2$), Sodium chloride (NaCl) and Sodium hydroxide (NaOH) were purchased from VWR chemicals. N-Methyl-2-pyrrolidone (NMP) was purchased from Merck. All solutions were prepared using water produced by a Milli-Q water purification system. All chemicals were used as received without further purification.

NF membranes

Flat sheet samples of NF270 membranes (Dow-Filmtec) were kindly supplied by the manufacturers and NTR7450 membranes (Hydranautics/Nitto Denko) were kindly supplied by Prof. Viatcheslav Freger’ group. The top layer of NF270 is composed of polyamide and that of NTR7450 composed of sulfonated polyether-sulfone. Prior to use, the membranes are washed in 1 : 1 (v : v) mixture of ethanol and water for 1 hour and then stored with pure water [127] .

3.2 Bulk hydrogel preparation and characterization

3.2.1 Polymerization procedures

PolyPEGMEMA hydrogels were prepared by free radical solution polymerization of PEGMEMA. A predetermined amount of PEGMEMA was dissolved in water, and then EGDMA as the crosslinking reagent was added. This prepolymerization mixture was purged with nitrogen for 5 min to remove dissolved oxygen. Then, the redox initiator pair, APS and TEMED, was added and the mixture was allowed to react under nitrogen at room temperature for 24 h. In further experiments, a 1 : 1 (v : v) mixture of ethanol and water was used as solvent in order to improve the solubility of EGDMA. The synthesis procedure of PolyPEGMEMA hydrogels is presented in **Figure 3.1.**

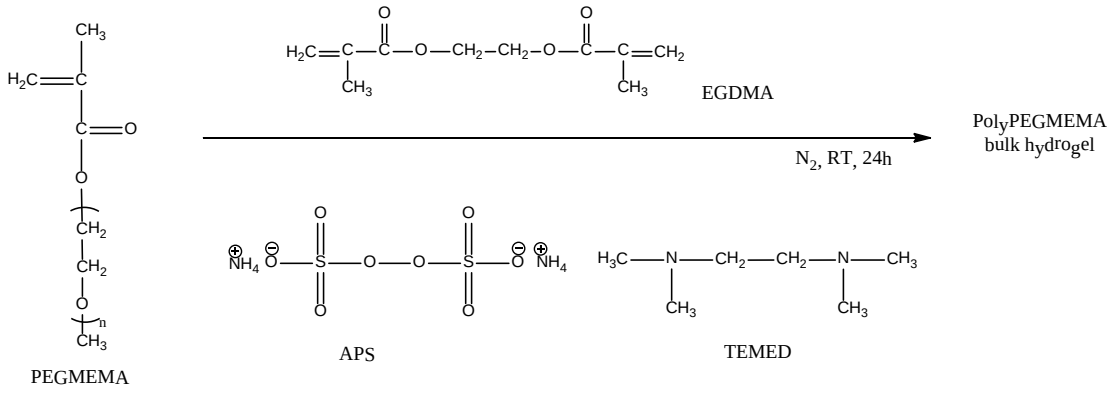

Figure 3.1. Preparation of polyPEGMEMA bulk hydrogel.

3.2.2 Chemical structure characterization

ATR-IR

IR spectra of dry hydrogel samples were recorded using an ATR unit in a Varian Resolution Pro 4.0 on Varian 3100 FTIR spectrometer.

NMR

PolyPEGMEMA hydrogels were prepared in D_2O according to the preparation protocol above. Either EGDMA or MBAA was used as crosslinker, respectively. The resulting gels were washed in D_2O for two days to remove unreacted monomer and the sol fraction. NMR spectra were recorded on an Avance 400 spectrometer (Bruker AG, Karlsruhe, Germany) at 400.13 MHz for protons and 100.63 MHz for ^{13}C nuclei.

3.2.3 Hydrogel yield

The resulting gel was soaked in pure water for five days to remove unreacted monomer and the sol fraction. The supernatant solution was analyzed using a Shimadzu TOC-V analyzer, each sample was measured at least 3 times and average values were used for further calculations. The yield of polymeric hydrogel was calculated as:

$$\text{Yield}=\frac{m_{feed}-m_{unreacted}}{m_{feed}}\times 100\% \qquad (3.1)$$

where m_{feed} is the mass of monomer in the reaction mixture and $m_{unreacted}$ is the mass what had not been incorporated in the hydrogel network.

Gel permeation chromatography (GPC) was used to analyze the fractions of soluble polymer in supernatant solution. All analyses used a MZ HEMA Bio linear column coupled with a Shodex RI-101 detector at 23 °C. Water containing 0.01 $mol \cdot L^{-1}$ NaN_3 was used as the eluent at a flow rate of 1 $mL \cdot min^{-1}$. PEG standards were used for calibration.

3.2.4 Swelling tests

A hydrogel sample was first immersed in and equilibrated with pure water for 5 days. The hydrated sample was then wiped gently with filter paper to remove excess water and weighed. Subsequently it was dried by freeze dryer (Christ Alpha 1-4, Osterode am Harz, Germany) for 3

days, and then the weight was determined again. The swelling ratio (SR) was calculated as follows:

$SR=w_s/w_d$ (3.2)

where w_s and w_d are the weights of a swollen gel at equilibrium and of a dry gel, respectively. Average values and standard deviations are based on measurements on at least 3 parallel samples.

3.2.5 Rheological measurements

The gelation during syntheses of bulk hydrogels was monitored by rheological measurements in an Anton Paar Physica MCR 301 rheometer (Graz, Austria). The samples were continuously measured in an oscillation mode at constant angular frequency of 2 $rad \cdot s^{-1}$ and a fixed strain of 1 %. In order to establish the extent of the linear viscoelastic regime for further investigations of the mechanical properties of the fully swollen hydrogels, the gel samples were cut into 15 mm diameter disks using a hollow punch, and frequency sweep experiments were performed in the range of 0.1 - 100 $rad \cdot s^{-1}$ at a normal force of 0.2 N and a fixed strain of 1 % using a 15 mm diameter TruGap plate. All runs were repeated at least three times, and average data are presented or used for further calculations.

3.2.6 Mesh size calculation

The correlation length or the network mesh size is indicative of the distance between consecutive junctions, cross-links, or tie points. All these network parameters can be measured though a range of experimental techniques or calculated by application of network deformation theories. Here, the mesh size was estimated from swelling and rheological data using equation 2.3 and 2.5 respectively.

3.2.7 Protein sorption test

Studies of biomolecule uptake were performed with three proteins of different sizes, i.e., lysozyme (Lys), bovine serum albumin (BSA), and fibrinogen (Fib). The bulk gels were cut into 14 mm diameter disks and soaked in 0.01 mol·L^{-1} PBS solution (pH 7.4) overnight to reach equilibrium. These films were then transferred to a 6-well plate, and each well was filled with 5 mL (V_o) of 1 g·L^{-1} (c_o) protein solution in PBS (pH 7.4). The protein was allowed to equilibrate for 24 h at ambient temperature while the plate was stirred on a shaker at 90 rpm to ensure good contact of the protein with the gel surface. Next, the gel film was rinsed 3 times with Milli-Q water, and then placed into 10 ml (V) 0.1 mol·L^{-1} NaOH solution for 48 h to thoroughly desorb the protein from the gel samples. The protein concentration (c) in the NaOH solution was analyzed using a Thermo Scientific Pierce Micro BCA protein assay kit. Protein partition coefficient K was calculated as according to the following equations:

$$K=\frac{C_{gel}}{C_{sol}}=\frac{\frac{C\times V}{V_{gel}}}{\frac{C_o\times V_o - C\times V}{V_o}} \qquad (3.3)$$

$$V_{gel}=\frac{w_d}{\rho_{polymer}}+\frac{w_s-w_d}{\rho_{water}} \qquad (3.4)$$

where w_s and w_d are the weights of a swollen gel at equilibrium and of a dry gel, respectively; w_s was measured after the protein desorption experiment, then w_d was determined after freeze drying.

Confocal laser scanning microscopy of protein sorption

The protein sorption on bulk gel surface and penetration into the network were measured using a confocal laser scanning microscopy (CLSM). Excitation/Emission maxima for FITC were 485 nm and 515 nm, respectively. 1 g·L^{-1} BSA composed of FITC BSA and normal BSA (1:50, g:g) was used. Rinsed gel samples were mounted on 76 mm x 26 mm microscopic slides without cover. Microscopy was performed using a Zeiss inverted Axiovison 10 microscope at x10

magnification (Oberkochen, Germany). Three dimensional images were produced using Axio Vison V.6.

3.3 Surface anchored gels

3.3.1 Preparation of glass anchored gels

Glass microscopy slides were immersed in a Piranha solution composed of sulfuric acid and hydrogen peroxide (7:3, v : v) for 1 h, subsequently dried in a nitrogen stream and then immediately used for silanization. The clean glass slides were immersed in a 1 : 1 (v : v) mixture of ethanol and Milli-Q water containing 0.4 % MPS and 0.05 % glacial acetic acid. After 30 min, the slides were removed from the bath and dried in a nitrogen stream. The silane layer was then cured by placing the slides in an oven at 115 °C for 30 min. Finally, the slides were ultrasonicated in ethanol for 1 min, further rinsed with ethanol and then dried. Silanized glass slides were sandwiched between two flat glass plates separated using a 0.1 mm Teflon tape as spacer. A gel was then prepared in the space between the plates similar to preparation of bulk gels. The synthesis procedure of glass anchored gels is presented in **Figure 3.2**.

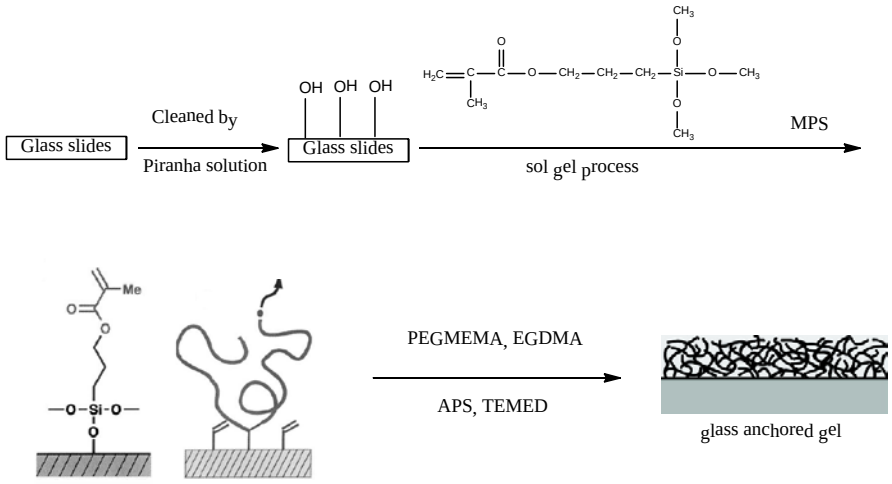

Figure 3.2. Preparation of glass anchored gel.

3.3.2 Contact angle measurements

The hydrophilicity of the glass anchored gels was determined with the contact angle system OCA 15 plus (Dataphysics, Filderstadt, Germany). An air bubble or a heptane droplet was placed under the surface of glass anchored gels, both of which were submerged in Milli-Q water, and captive bubble contact angles were measured. The average value of each contact angle was obtained for at least five different bubbles at different locations on the substrate surface. The time dependence of contact angle was also measured.

3.3.3 Bacterial deposition on the surface

The rate of bacteria deposition was measured using commercially available parallel plate flow cells (Biosurface Technologies). A glass anchored gel was mounted in a cell and thus formed the bottom of a parallel plate channel with a transparent upper plate. The cell was mounted on the stage of a microscope equipped with a digital camera. *P. Fluorescence* bacteria were used to examine bacterial deposition. The bacteria were pre-cultured for 12 hours and then cultivated for another 12 hours in Lysogeny broth (LB) medium. Bacteria were then diluted in 0.1 mol·L^{-1} NaCl solution to yield a bulk concentration, $C_b = 1.67 \times 10^7$ bacteria·cm^{-3}. This suspension was pumped through the flow cell at a rate of 2 mL·min^{-1}. Bacterial deposition was monitored using a Zeiss Axioscope fluorescence microscope at x10 magnification. Deposition coefficient (DC) was calculated according to the following equation:

$$DC = \frac{\frac{dN}{dt}}{A \times C_b} \qquad (3.5)$$

where dN/dt is the average slope of the curve bacteria number versus time, and A is the area of viewed image.

To estimate the effect of gravity on bacterial deposition to the surface, the bacteria suspension was pumped for 30 minutes while the flow cell was upside down and the images of deposited

bacteria were taken from five parallel surface areas every 10 minutes using a Zeiss Axioscope fluorescence microscope at x10 magnification.

3.3.4 Biofilm growth

For biofilm growth, the bacteria suspension was allowed to flow through the cells for 1 hour to allow deposition on the substrate surface in the same way as in deposition experiments (Section 3.3.3). The images of deposited bacteria were taken from five parallel surface areas using a Zeiss Axioscope fluorescence microscope at x10 magnification. Thereafter, LB medium diluted x2 was pumped through the cell for 48 hours and biofilm growth was then observed using Zeiss LSM 510 META microscope at x20 magnification.

Biofilm images were quantitatively analyzed using COMSTAT, a script for MATLAB 6.5 (The MathWorks Inc., Natick, Massachusetts) written by Arne Heydorn of the Technical University of Denmark in Lyngby (www.comstat.dk). This yielded three dimensional biofilm structure using Z-stacks of CSLM images. The software also yielded the average thickness, substratum coverage and roughness [128, 129].

3.4 Membrane modification and characterization

3.4.1 Synthesis and analysis of macroinitiator

The preparation procedures for the cationic macroinitiator are presented in **Figure 3.3.** First, a benzoin ethyl ether derivative with bromide group was synthesized from benzoin ethyl ether as described in previous literature [130]. Then a random copolymer of DMAEMA and HEMA was synthesized via free radical polymerization, and subsequently the DMAEMA residues were fully quaternized by use of excess iodomethane, and finally the hydroxyl groups of the HEMA residues were completely esterified with benzoin ethyl ether (BEE) derivative.

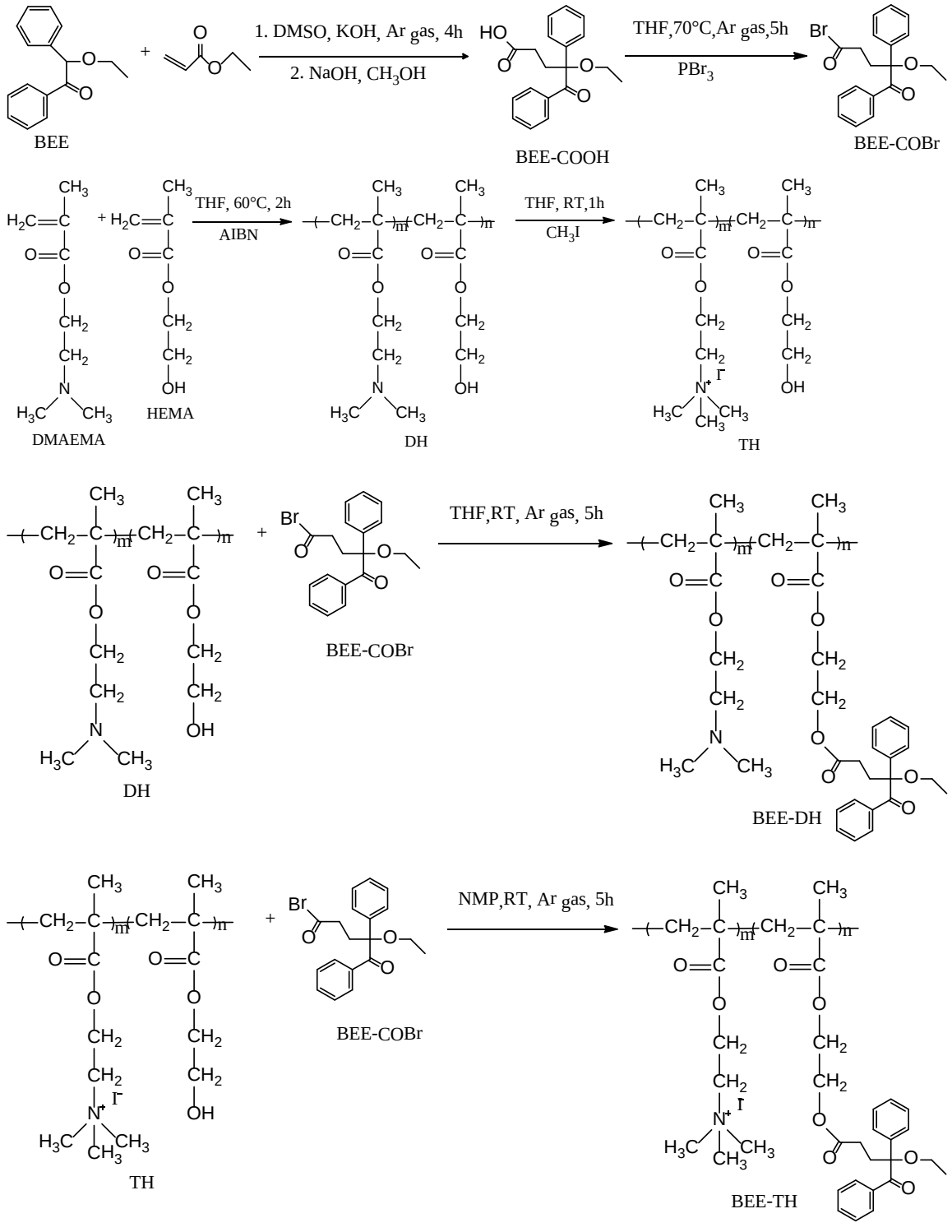

Figure 3.3. Reaction steps for synthesis of cationic macroinitiator.

Synthesis of 4-ethoxy-5-oxo-4,5-diphenylpentanoyl bromide (BEE-COBr) [130]. Benzoin ethyl ether (20 g) was dissolved in 32 mL DMSO. Ethyl acrylate (8 mL) and potassium hydroxide (2 mL; 4 $mol \cdot L^{-1}$) were added into the solution. The reaction took 4 h under argon gas at room temperature. Hydrochloric acid (6.4 mL; 1 $mol \cdot L^{-1}$) was added to adjust the pH values of the solution to neutral. The resulting solution was evaporated under vacuum at 80 °C to remove DMSO. The residue was dissolved in 200 mL water and dried by freeze-drying for 24 h. The dry powder was dissolved in NaOH solution (160 mL; 1 $mol \cdot L^{-1}$) containing 6% methanol (9.6 ml) and hydrolyzed for 24 h at room temperature. The solution was dried by freeze-drying for 48 h and the remaining product was dissolved in dichloromethane to remove the hydroxide. After removing dichloromethane under vacuum, the residue was dissolved in 200 mL water and dried by freeze-drying for 24 h to obtain 16.4 g of 4-ethoxy-5-oxo-4,5-diphenylpentanoic acid (BEE-COOH), yield 89%. BEE-COOH (8 g) and phosphorous (red) (20 mg) were dissolved in 160 mL dry THF. Bromine (4.1 g) was dissolved in 40 mL dry THF and added dropwise. The reaction took 5 h at 80 °C under argon gas. The resulting suspension was filtered and the clear solution was evaporated under vacuum to remove the solvent THF. The residue was dried under vacuum at 40 °C for 24 h and obtained 4.5 g of BEE-COBr, yield 30%.

Synthesis of poly(DMAEMA-co-HEMA) (DH). DMAEMA (5.9 g), HEMA (1.4 g), and AIBN (83.8 mg) were added to 10 mL dry THF. The mixture was degassed by nitrogen purge, and then polymerization was carried out under nitrogen at 60°C with stirring for 2 h. The highly viscous polymer solution was diluted with 10 ml of THF, and the polymer was precipitated into water at pH 11. After filtration, the polymer was dried under vacuum, redissolved in 15 mL of THF, and precipitated into hexane (500 mL). Filtration and drying under vacuum at room temperature for 24 h gave 3.0 g of the copolymer, yield 41%.

Synthesis of poly(TMAEMA-co-HEMA) (TH). Poly(DMAEMA-co-HEMA) (2.0 g) was dissolved in 30 mL of THF; iodomethane (1.25 ml) was dissolved in 10 mL THF and added to the stirred

solution at room temperature. Within 2 min, the reaction mixture became turbid and had a butterlike color. After 1 h of stirring, the solution was added dropwise to vigorously stirred hexane (500 mL) to precipitate the polymer as a fine powder. Washing with hexane and drying under vacuum at room temperature for 24 h gave 2.7 g of the copolymer, yield 81%.

Synthesis of BEE-DH. BEE-COBr (1 g) was dissolved in 20 mL dry THF. Poly(DMAEMA-co-HEMA) (1.5 g) was dissolved in 20 mL dry THF and added dropwise. The reaction took 5 h at room temperature under argon gas. The resulting solution was added dropwise to vigorously stirred hexane to precipitate the polymer. The polymer was dried under vacuum at 40°C for 48 h and obtained 1.6 g of BEE-DH, yield 72%.

Synthesis of BEE-TH. BEE-COBr (0.6 g) was dissolved in 20 mL dry N-methyl-2-pyrrolidone (NMP). Poly(TMAEMA-co-HEMA) (1.5 g) was dissolved in 20 mL dry NMP and added dropwise. The reaction took 5 h at room temperature under argon gas. The resulting solution was added dropwise to vigorously stirred THF to precipitate the polymer. The polymer was dried under vacuum at 40°C for 24 h, then redissolved in pure water, and dried by freeze-drying for 48 h and obtained 2.8g of BEE-TH, yield 77%.

NMR

^{1}H NMR spectra of macroinitiator and it precursors were recorded on a Bruker DMX-300 instrument at 300 MHz.

GPC analysis

Macroinitiators were analyzed using a PSS Gram linear column coupled with a differential refractometer-viscometer detector at 23°C. Dimethylformamide containing 0.01mol·L^{-1} LiBr was used as the eluent at a flow rate of 1mL·min^{-1}. Polymethyl methacrlylate standards were used for calibration.

3.4.2 Macroinitiator immobilization

The pre-weighed pristine membrane sample was with the active layer upwards placed in a backward sealed cell, a solution of copolymer (DH, TH, BEE-DH, BEE-TH) in a mixture of 1 : 1 (v : v) ethanol and water was added for 1 h and then taken out again. The membrane was shortly washed five times for 10 s in pure water. For membrane used in determination of membrane functionalization, it was dried at 45°C overnight and weighted. The degree of modification was determined gravimetrically:

$$preDG\_W = (m_1-m_0)/A \qquad (3.6)$$

where m_0 is the pristine membrane sample weight, m_1 is the premodified membrane sample weight, and A is the outer surface area of the membrane. All membranes used for preDG determination were not used for flux and fouling experiments.

3.4.3 Photo grafting of membrane

After washing (mentioned above), the premodified membrane was quickly wiped with filter paper to remove the adhering solvent, then placed between two filter paper, put in a Petri dish with monomer (PEGMEMA 200, 400, 1000) solution in 1 : 1 mixture of water and ethanol containing the crosslinker (CL) EGDMA, with 1.2 $mmol \cdot L^{-1}$ photoinitiator BP for DH and TH premodified membrane or without BP for BEE-DH and BEE-TH premodified membrane, and covered with a smaller Petri dish. After 10 min equilibration, UV irradiation followed (effective UV intensity was about 11 $mW \cdot cm^{-2}$). Thereafter the membrane was washed with pure water at room temperature for 1 day, dried by freeze drying for 2 days and weighed to determine the degree of grafting (DG_W) as following:

$$DG\_W = (m_2-m_1)/A \qquad (3.7)$$

where m_2 is the gel modified membrane sample weight. Average values and standard deviations are based on measurements on at least 3 parallel samples. All membranes used for DG

determination were not used for flux and fouling experiments. Membranes used in performance test are not dried during the whole modification process

3.4.4 Membrane characterization

ATR-IR

IR spectra (average of 32 scans at 4 cm^{-1} resolution) of dry membrane samples were recorded using an ATR unit with a single reflection diamond/ZnSe crystal plate in a Spectra Manager V1.54 on Jasco FTIR 430 spectrometer. FTIR data were also used to determine the degree of grafting (DG_IR) of modified membranes as follows:

$$preDG\_IR = I_{pol}/I_{mem} \qquad (3.8)$$

$$DG\_IR = (I_{gel}-I_{pol})/I_{mem} \qquad (3.9)$$

Where I_{pol} is the intensity of a characteristic carbonyl peak of the copolymer at 1720 cm^{-1}, I_{gel} is the intensity of a characteristic carbonyl peak of the gel layer at 1720 cm^{-1} and I_{mem} is the intensity of a characteristic polysulfone (part of the pristine membrane) peak at 1584 cm^{-1}. These bands usually change insignificantly upon modification, unless the thickness of the grafted layer is commensurable or exceeds the penetration depth of evanescent IR wave (~1 μm with the used crystal) [131]. Average values and standard deviations are from measurements at least 5 spots on each sample for at least 3 parallel samples.

Contact angle

Contact angle was measured using an optical contact angle measurement system (OCA 15 Plus; Dataphysics GmbH, Filderstadt, Germany). Before the measurements all the samples were dried by freeze drying overnight. Static sessile drop method was used. A water drop (5 μL) was injected from a syringe with a stainless steel needle onto the sample surface. At least five measurements at different locations were averaged to obtain contact angle for one membrane sample.

Zeta potential

The membrane surface charge was investigated via an outer surface streaming potential measurement. Experiments were carried out in a SurPASS electrokinetic analyzer (Anton Paar GmbH, Graz, Austria). The slit-type channel was 2 cm in length and 1 cm in width and had a variable cell height that was set to approximately 100 μm for all experiments. Flow in the measurement cell was induced by linearly ramping the differential pressure from 0 to 400 mbar in both directions. A 0.001 $mol \cdot L^{-1}$ KCl solution was used as the electrolyte, 0.1 $mol \cdot L^{-1}$ HCl and 0.1 $mol \cdot L^{-1}$ NaOH were used to adjust the pH in the range of pH 2-10 at room temperature. Before measurement, the membrane was equilibrated by soaking in a 0.001 $mol \cdot L^{-1}$ KCl solution overnight. The Zeta Potential of membranes was calculated using the Helmholtz-Smoluchowski equation.

3.4.5 Membrane performance test

All experiments were conducted with a dead-end stirred-cell filtration system. The system was pressurized by argon. To avoid the effects of membrane compaction on the interpretation of modification and fouling data, each sample was first compacted by the filtration of pure water at a pressure of 14 bars for at least 0.5 h.

To know the effect of modification on membrane water permeability, the water flux was measured before and after modification at a constant pressure of 14 bar. All pure water fluxes were measured (by the gravimetric method) until the consecutively recorded values (for periods of 10 min) were considered to be constant (i.e., they differed by less than 4%). The water permeability of membrane was calculated as:

$$P = \Delta V/(\Delta t \times \Delta p \times A) \qquad (3.10)$$

Where ΔV is the permeate volume during a time Δt, Δp is the pressure difference across the film.

Salt rejection experiments were conducted using a NaCl and $MgCl_2$ solution (100 mL, 5 $g \cdot L^{-1}$) respectively, as the feed. A 15 mL of permeate was collected. The permeate and feed solutions were analyzed by conductivity meter (Touch Control Metrohm, Swiss) at 25°C. Salt rejection was calculated as:

$$R = (1-C_p/C_f)\times 100\ \% \qquad (3.11)$$

Where C_p is the permeate concentration and C_f is the feed concentration.

3.4.6 Membrane fouling test

Static protein adsorption experiments

Protein solution was filtered through a 0.45 μm microfilter (Sartorius, Germany) to remove undissolved material prior to use. The water permeability and NaCl (5 $g \cdot L^{-1}$) rejection were initially measured. Subsequently a protein solution (20 mL; 10 $g \cdot L^{-1}$) containing BSA (pH 4.8 in 0.01 $mol \cdot L^{-1}$ PBS) or Lys (pH 7.4 in 0.01 $mol \cdot L^{-1}$ PBS) respectively, was added to the cell. Thereafter, the outer membrane surface was irradiatedirradiated for 1 h without any flux. Then the protein solution was removed, and the membrane surface was washed five times with pure water. Water fluxes and NaCl rejection after exposures were measured again in order to evaluate the irreversible fouling.

Protein filtration experiment

The water permeability and NaCl (5 $g \cdot L^{-1}$) rejection were initially measured, and then a protein solution (100 mL 1 $g \cdot L^{-1}$) containing BSA (pH4.8 in 0.01 $mol \cdot L^{-1}$ PBS) or Lys (pH 7.4 in 0.01 $mol \cdot L^{-1}$PBS), respectively, was added to the cell. Thereafter, 50 ml solution was filtered. Then the residual solution was removed, and the membrane surface was washed five times with pure water. Water fluxes and NaCl rejection after filtration were measured again in order to evaluate the irreversible fouling.

The relative reduction of membrane performance was calculated as:

$$\text{Reduction} = (P_0 - P_a)/ P_0 \times 100\% \qquad (3.12)$$

P_0 and P_a are water permeability (NaCl rejection) before and after protein adsorption (filtration), respectively.

Chapter 4 Results and discussion

4.1 PolyPEGMEMA bulk gel

4.1.1 Chemical structure characterization

PolyPEGMEMA in dry state had been analysed by FTIR spectroscopy (**Figure 4.1**). The absorption bands at 1100 cm^{-1} and 1728 cm^{-1} were attributed to C-O-C and C=O peaks respectively. The signal at 1386 cm^{-1} was attributed to C=C stretching, most probably from the crosslinker monomer EGDMA. However, that band was only observed for samples prepared at low initiator concentration and it could not be detected for samples prepared at initiator content of 0.5 mol% or higher. This indicated that the dangling double bonds had also been converted into carbon-carbon single bonds in polymer chains of the hydrogel network.

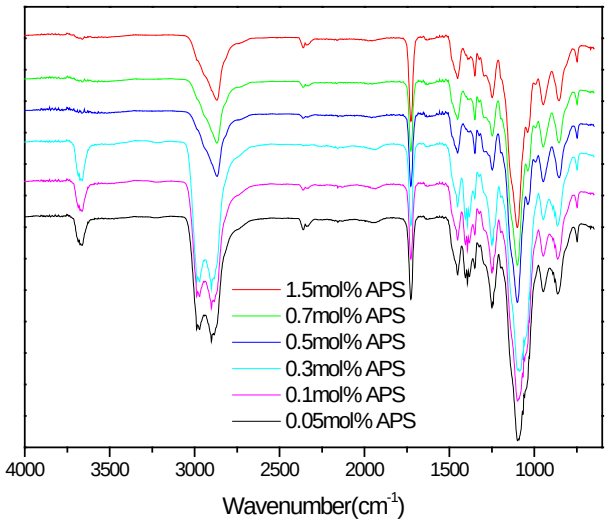

Figure 4.1. FTIR spectra of polyPEGMEMA400 hydrogels as a function of APS content at 0.5 $mol \cdot L^{-1}$ PEGMEMA and EGDMA : PEGMEMA = 12.6 mol%.

Since the sensitivity of IR analyses was limited, another insight could be gained through a solid state NMR analysis. With NMR it is possible to directly distinguish between structures involving unreacted and reacted double bonds of the crosslinker. Hydrogels with a crosslinker content higher than used later on had been prepared in order to enable an easier quantification; an alternative cross-linker, MBAA, was also used for comparison. The assignment of all peaks in the ^{1}H and ^{13}C NMR spectra had been done for the monomers and the hydrogels, using also ^{1}H COSY and ^{13}C DEPT NMR analyses. All spectra could be fully interpreted in association with Heteronuclear Single Quantum Coherence (HSQC) and Heteronuclear Multiple Bond Correlation (HMBC) relationships differentiating proton-carbon coupling [132, 133] .

The chemical structures of monomer PEGMEMA and the crosslinkers EGDMA and MBAA are shown in **Figure 4.2**. The ^{1}H NMR spectrum of PEGMEMA 200 (**Figure 4.3**) shows signals for a single proton at 6.20 ppm (H-1a), for another one at 5.77 ppm (H-1b), for three methyl protons at 3.41 ppm (H-7) and for three other methyl protons at 1.97 ppm (H-3). A cumulated signal for 18 protons between 4.37 ppm and 3.647 ppm can be assigned to the PEO chain (H-5 and H-6). The ^{13}C NMR spectrum of PEGMEMA 200 shows 15 carbon signals. The DEPT 90° spectrum did not show any signal, indicating the absence of a methine group. The DEPT 135° spectrum shows two positive peaks (at 60.63 ppm and 20.01 ppm) which consequently derive from methyl groups, eleven negative peaks (at 125.59 ppm and between 73.95 and 66.73 ppm) which consequently derive from methylene groups, and two suppressed peaks at 171.96 ppm (C-4) and 138.29 ppm (C-2) which derive from quaternary carbons. The connection of these functional groups was determined on the basis of HSQC correlations. Two distinguishable cross-peaks corresponding to the CH_2 signal at 125.59 ppm (C-1) correlate to the proton signal at 6.20 ppm (H-1a) and 5.77 ppm (H-1b). The other CH_2 carbon signals at 73.59 - 66.73 ppm (C-5, C-6) show cross-peak multiplets that correlate with the protons signals at 3.65 - 4.37 ppm (H-5, H-6). Moreover, the CH_3 carbons at 20.01 ppm (C-3) and 60.63 ppm (C-7) show cross-peaks that correlate with the protons signal at 1.97 ppm (H-3) and 3.41 ppm (H-7), respectively. Similarly, all protons and

their corresponding carbons in the monomers PEGMEMA 400 and 1000 as well as in the crosslinkers EGDMA and MBAA were successfully assigned by ^{1}H, ^{13}C NMR and DEPT spectra in association with the HSQC connectivities shown in **Table 4.1** and **4.2**.

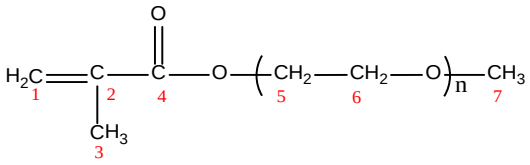

PEGMEMA

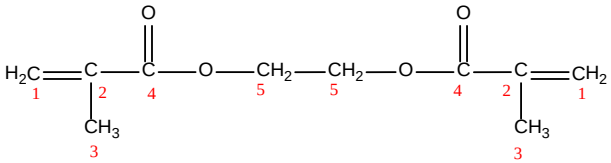

EGDMA

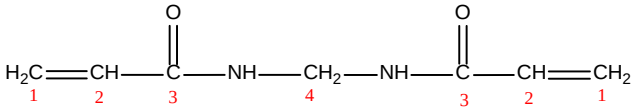

MBAA

Figure 4.2. Chemical structures of the monomer PEGMEMA and of the crosslinker monomers EGDMA and MBAA.

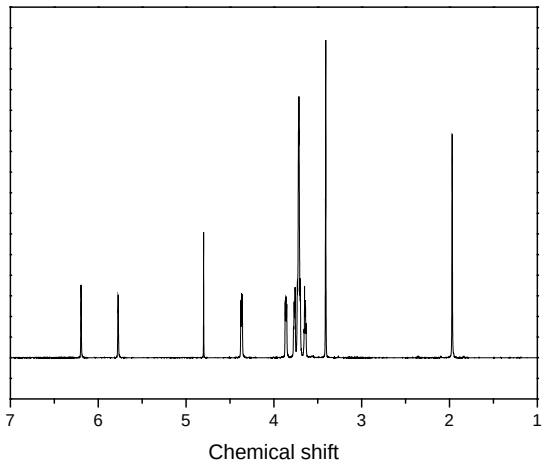

Figure 4.3. The ^{1}H NMR spectrum of PEGMEMA 200 monomer.

Table 4.1. Comparative 1H 13C NMR, DEPT and HSQC assignments for the monomers PEGMEMA 200, 400 and 1000.

Position	PEGMEMA 200			PEGMEMA 400			PEGMEMA 1000		
	^{1}H δ(ppm)	^{13}C δ(ppm)	DEPT HSQC	^{1}H δ(ppm)	^{13}C δ(ppm)	DEPT HSQC	^{1}H δ(ppm)	^{13}C δ(ppm)	DEPT HSQC
1	5.77, 6.20	129.59	CH_2	5.69, 6.12	129.55	CH_2	5.69, 6.11	129.53	CH_2
2	--	138.29	C	--	138.23	C	--	138.24	C
3	1.97	20.01	CH_3	1.89	19.95	CH_3	1.89	19.94	CH_3
4	--	171.96	C	--	171.94	C	--	172.01	C
5,6	3.65 ~ 4.37	66.73~ 73.59	CH_2	3.57 ~ 4.30	66.68~ 73.51	CH_2	3.56~ 4.29	66.66 ~ 73.50	CH_2
7	3.42	2.98	CH_3	3.33	60.57	CH_3	3.33	60.56	CH_3

Table 4.2. Comparative ^{1}H ^{13}C NMR, DEPT and HSQC assignments for the crosslinkers EGDMA and MBAA.

Position	EGDMA			MBAA		
	^{1}H δ (ppm)	^{13}C δ (ppm)	DEPT HSQC	^{1}H δ (ppm)	^{13}C δ (ppm)	DEPT HSQC
1	5.54, 6.07	125.90	CH_2	5.79 ~ 5.84, 6.22 ~ 6.29	130.76	CH_2
2	--	135.91	C	6.22 ~ 6.29	132.06	CH
3	1.89	18.17	CH_3	--	171.22	C
4	--	167.01	C	4.74	46.96	CH_2
5	4.35	62.27	CH_2			

In comparison, the ^{1}H NMR spectrum of PEGMEMA 200 gel (a-1) shows methylene protons related unreacted double bonds (unsaturated ethylene bonds) observed at 5.76 ppm and 6.18 ppm.

In addition, the methyl proton signals have shifted slightly downfield from 3.41 ppm to 3.43 ppm (H-7). In ^{13}C NMR DEPT 135° spectrum, three positive peaks observed at 19.22 ppm, 20.99 ppm and 60.63 ppm which derive from methyl groups, negative peaks observed between 67.38 ppm and 73.76 ppm which dreive from methylene groups and three suppressed peaks observed at 47.31 ppm, 47.61 ppm and 181.50 ppm which derive from quaternary carbons. The connection of these functional groups was determined on the basis of H-H COSY, HSQC and HMBC correlations. The cross-peak multiplets observed at 0.95 ppm, 1.11 ppm and 1.20 ppm (H-3') in the H-H COSY spectrum correspond to the methylene proton related to the reacted double bond (saturated bond) at 3.66 ppm (H-5), similarly the cross-peak multiplets observed at 1.96 ppm (H-3) correspond to methylene proton related to the unreacted double bond at 5.76 ppm (H-1). In the HSQC spectrum, the cross-peak multiplets observed at 0.95 ppm and 1.20 ppm (H-3') correspond to the CH_3 carbon related to the reacted double bond at 19.22 ppm (C-3'), the proton signal at 1.11 ppm (H-3') corresponds to the carbon signal at 20.99 ppm (C-3'). Similarly the cross-peak multiplets observed at 1.96 ppm (H-3) correspond to CH_3 carbon related unreacted double bond at 20.00 ppm (C-3), at 3.43 ppm (H-7) correspond to CH_3 carbon at 60.78 ppm (C-7), and at 2.61 ppm (H-1') correspond to CH2 carbon in reacted double bond at 46.09 ppm (C-1'). The cross-peak multiplets in the HMBC spectra correspond to the CH_3 signal at 1.961 ppm (H-3) and correlate to the carbon signals at 44.54 ppm and 53.44 ppm. Similarly, the methylene carbon at 2.61 ppm (H-1') shows two cross-peaks that correlate with carbon signals at 46.20 ppm and 56.05 ppm (C-2'). All protons and their corresponding carbons in PEGMEMA 200, 400 and 1000 gel were successfully assigned by ^{1}H, ^{13}C NMR and DEPT in association with HSQC, HMBC relationships, as shown in **Table 4.3** and **4.4**. Based on above data, the content of residual double bonds per total methacrylate content was determined. The results are presented in **Table 4.5**.

Table 4.3. Comparative ^{1}H ^{13}C NMR, DEPT and HSQC assignments for PEGMEMA 200, 400 and 1000 gels with higher EGDMA content.

Position	a-1			b-1			c-1		
	^{1}H δ (ppm)	^{13}C δ (ppm)	DEPT HSQC	^{1}H δ (ppm)	^{13}C δ (ppm)	DEPT HSQC	^{1}H δ(ppm)	^{13}C δ (ppm)	DEPT HSQC
1	5.76, 6.18	--	CH_2	5.76, 6.18	44.63	CH_2	5.76, 6.19	44.63	CH_2
1’	2.61	46.09	CH_2	2.61	46.21	CH_2	2.61	46.08	CH_2
2	--	--	--	--	--	--	--	129.51	C
2’	--	46.20, 56.05	C	--	46.20, 56.05	C	--	46.20, 56.05	C
3	1.96	20.00	CH_3	1.96	20.00	CH_3	1.96	19.93	CH_3
3’	0.95, 1.11, 1.20	19.22, 20.99	CH_3	0.95,1.19	19.31	CH_3	1.20	19.53	CH_3
4	--	181.50	C	--	--	--	--	--	--
5,6	3.50 ~4.50	67.00 ~74.00	CH_2	3.50 ~4.50	67.00 ~74.00	CH_2	3.50 ~4.50	66.00 ~74.00	CH_2
7	3.43	60.78	CH_3	3.41	60.65	CH_3	3.40	60.62	CH_3

Table 4.4. Comparative ^{1}H ^{13}C NMR, DEPT and HSQC assignments for PEGMEMA 400 gel with higher MBAA and lower EGDMA content respectively.

Position	b-3			b-4		
	1 H δ (ppm)	13C δ (ppm)	DEPT HSQC	1 H δ (ppm)	13C δ (ppm)	DEPT HSQC
1	5.86, 6.29	--	CH_2	5.76, 6.19	44.63	CH_2
1’	2.59	46.21	CH_2	2.57	46.33	CH_2
2	--	--	--	--	--	--
2’	--	46.20, 56.17	C	--	46.20, 56.28	C
3	--	--	--	1.96	20.12	CH_3
3’	0.93	19.71	CH_3	0.97, 1.10	19.27, 21.19	CH_3
4	--	181.00	C	--	181.07	--
5,6	3.50 ~ 4.50	66.00 ~ 74.00	CH_2	3.50 ~ 4.50	70.00 ~ 74.00	CH_2
7	3.41	60.64	CH_3	3.66	60.65	CH_3

Table 4.5. Content of residual double bonds per total methacrylate content in polyPEGMEMA gels.

Code	Monomer	Crosslinker	[M] ($mol \cdot L^{-1}$)	Crosslinker/ PEGMEMA (mol%)	APS/ PEGMEMA (mol%)	Content of double bonds (mol%)
a-1	PEGMEMA200	EGDMA	0.3	30	0.5	0.6
b-1	PEGMEMA400	EGDMA	0.3	30	0.5	2.7
c-1	PEGMEMA1000	EGDMA	0.3	30	0.5	3.5
b-4	PEGMEMA400	EGDMA	0.5	12.6	0.5	1.6
b-3	PEGMEMA400	MBAA	0.3	30	0.5	6.1

Overall, the content of residual double bonds in the hydrogels was rather low. For the same preparation conditions, the values increased systematically with the PEG chain length; generally, a bulkier side group led to less complete crosslinking. For medium PEG size (400 $g \cdot mol^{-1}$), a lower crosslinker content (at higher total monomer concentration) led to a reduction of the fraction of unreacted double bonds by a factor of ~2. This can be related to the higher flexibility of the forming network which presumably leads to a more efficient diffusion of the crosslinker to the reactive sites and hence to a more complete reaction. This result also indicates that PEG size could still affect the conversion for the compositions investigated subsequently, where the crosslinker content had been varied between 1 and 12.5 mol%. However, the very small absolute values of the fraction of dangling double bonds also suggests that under the reaction conditions used in this study, they had only a minor effect on hydrogel structure.

The cross-linker MBAA which is much better water-soluble than EGDMA led to a significantly higher fraction of unreacted double bonds. This can be explained by the lower reactivity of acrylamides compared to methacrylates [134].

4.1.2 Correlations between varied synthesis conditions and compositions, network polymer yield and hydrogel swelling

Preparation of hydrogels in water

A series of polyPEGMEMA hydrogels was prepared with various PEG chain lengths and varying synthesis conditions. Variations in monomer concentration as well as initiator and crosslinker content in the prepolymerization mixture were expected to affect network structure and material properties. The yield of network polymer calculated from TOC analyses and the swelling ratios of the resulting polyPEGMEMA gels are presented in **Figures 4.4** and **4.5**.

For increasing PEGMEMA concentration, the polymer yield increased and the swelling ratio significantly decreased. This implied a denser network structure because of the higher polymer volume fraction. As APS content increased, the conversion for PEGMEMA200 and 400

decreased and the swelling ratio increased while the opposite was observed for PEGMEMA1000. It could be expected that higher initiator content would reduce the average molecular weight of linear polyPEGMEMA, thus shortening the macromolecular chains. In the course of a crosslinking polymerization, this would lead to reduced connectivity of the network, i.e., a reduced crosslinker density, which could explain the results for PEGMEMA200 and 400. An alternative consequence, leading to a similar result, would be an increasing fraction of soluble polymer; an increase in the swelling ratio would then be due to lower volume fraction of network polymer. Significant but very small fractions of soluble polymer could be detected by GPC analyses only for PEGMEMA400 (**Figure 4.6**) while no soluble homopolymer could be found for PEGMEMA200 and 1000. Therefore, this is probable not the reason. For PEGMEMA1000 with the largest side group, chain propagation rate is lowest, i.e., more starter radicals could compensate this leading to a higher conversion. For increasing EGDMA content, the conversion increased and the swelling ratio decreased. However, beyond 8% the decrease in swelling with further increase in crosslinker content was minor. Because no effect onto conversion of double bonds was expected (cf. above), the reason could be that network chains became less flexible. For PEGMEMA1000, increasing EGDMA content only resulted in a slight change in swelling ratio. Hence, for this monomer even at low EGDMA fraction the entanglement of the long side chains could reduce the swelling in addition to the constraints of the covalent network structure.

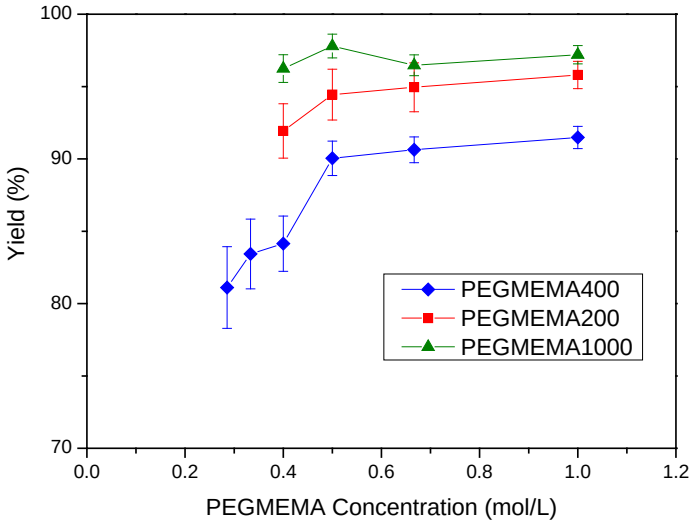
100
90
80
70
Yield (%)
0.0
0.2
0.4
0.6
0.8
1.0
1.2
PEGMEMA Concentration (mol/L)
PEGMEMA400
PEGMEMA200
PEGMEMA1000

(a)

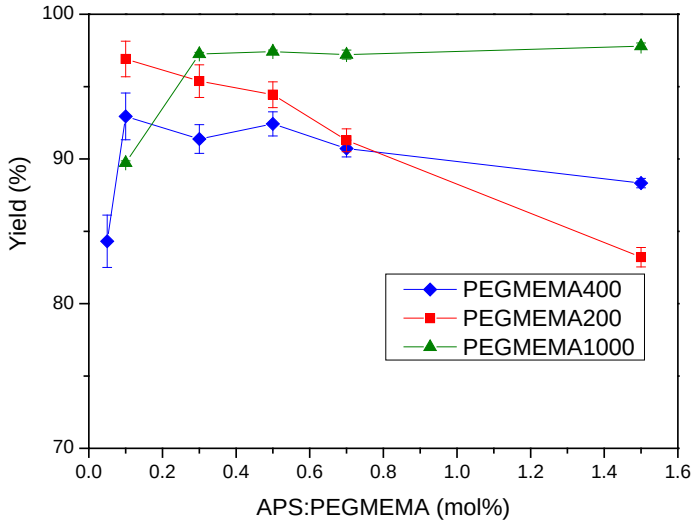
100
90
80
70
Yield (%)
0.0
0.2
0.4
0.6
0.8
1.0
1.2
1.4
1.6
APS:PEGMEMA (mol%)
PEGMEMA400
PEGMEMA200
PEGMEMA1000

(b)

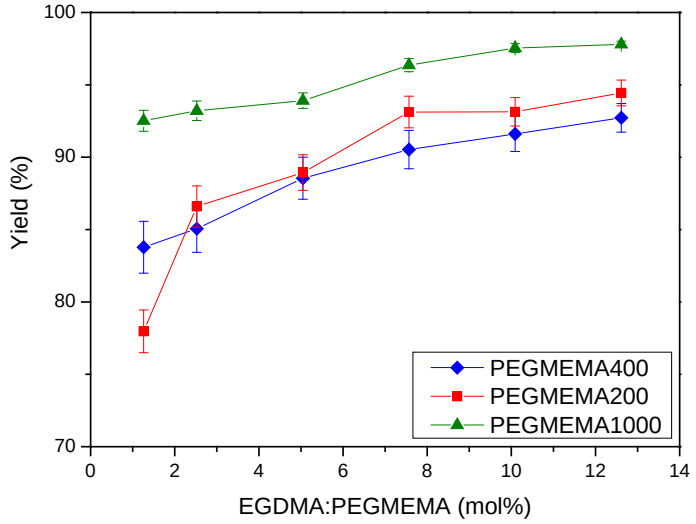

(c)

Figure 4.4. Polymerization efficiency as a function of (a) PEGMEMA concentration at the following conditions: EGDMA : PEGMEMA = 12.6 mol%, APS : PEGMEMA200 = 0.5 mol%, APS: PEGMEMA400/PEGMEMA1000 = 1.5 mol%; (b) APS content at 0.5 mol·L^{-1} PEGMEMA, EGDMA : PEGMEMA = 12.6 mol%; and (c) EGDMA content at 0.5 mol·L^{-1} PEGMEMA, and APS : PEGMEMA200 = 0.5 mol%, APS : PEGMEMA400 = 0.3 mol%, or APS : PEGMEMA1000 = 1.5 mol %.

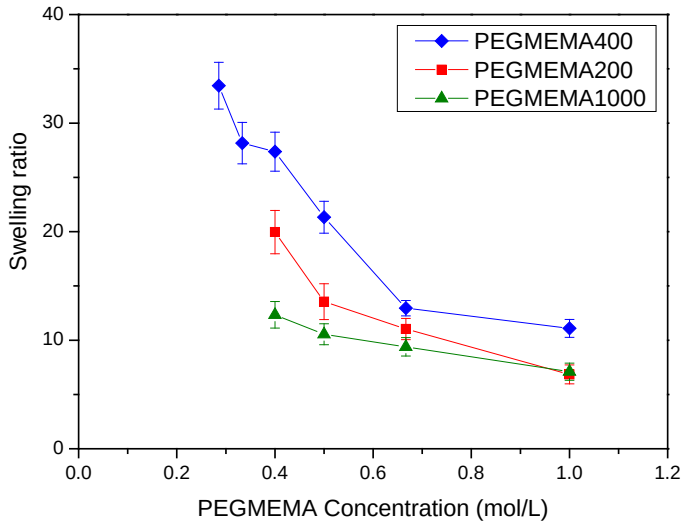

(a)

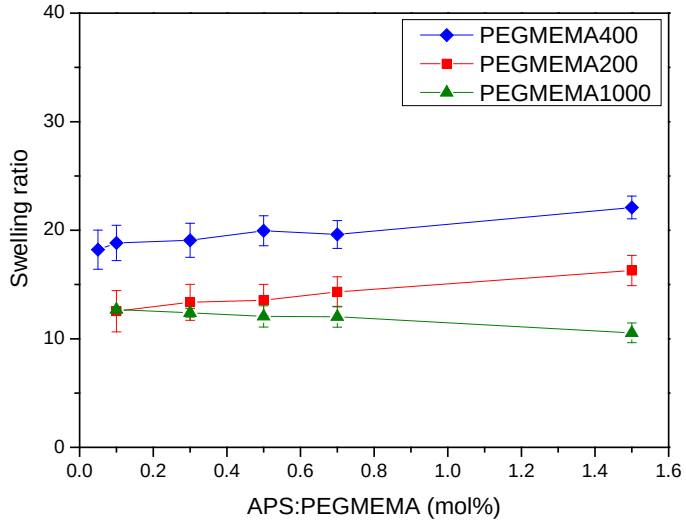

(b)

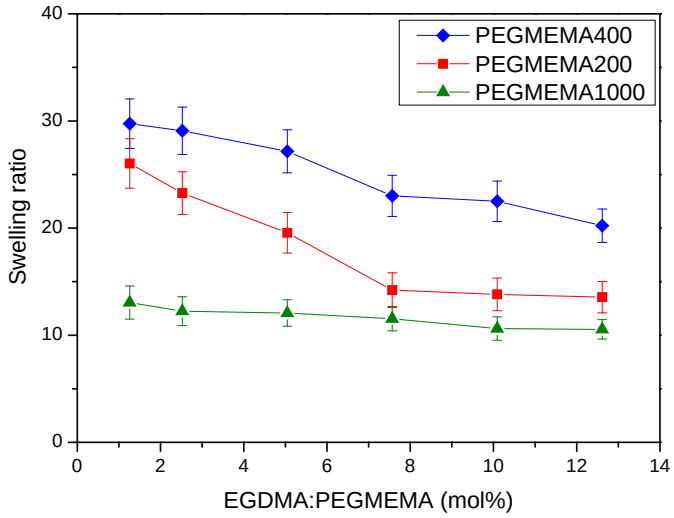

(c)

Figure 4.5. Swelling ratio as a function of (a) PEGMEMA concentration at EGDMA : PEGMEMA = 12.6 mol%, APS : PEGMEMA200 = 0.5 mol%, and APS : PEGMEMA400/PEGMEMA1000 = 1.5 mol%; (b) APS content at 0.5 mol·L^{-1} PEGMEMA, and EGDMA : PEGMEMA = 12.6 mol%; and (c) EGDMA content at 0.5 mol·L^{-1} PEGMEMA, and APS : PEGMEMA200 = 0.5 mol%, APS : PEGMEMA400 = 0.3 mol%, or APS : PEGMEMA1000 = 1.5 mol%.

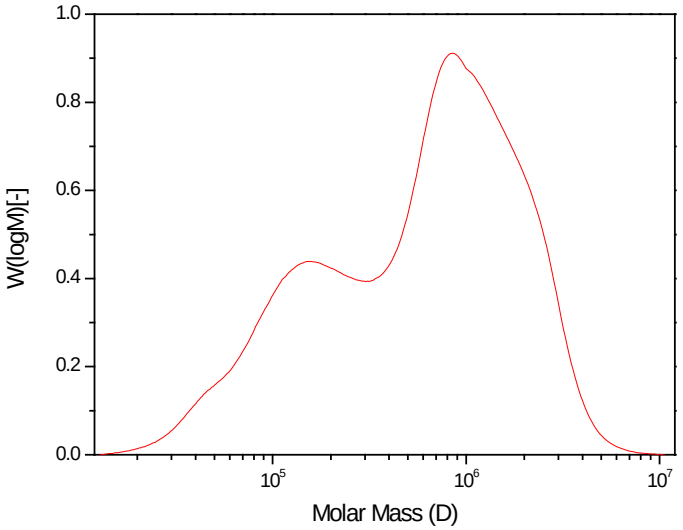

Figure 4.6. GPC curve of the washing solution of polyPEGMEMA400 gel prepared at 0.5 mol·L^{-1} PEGMEMA, EGDMA : PEGMEMA = 1.3 mol%, and APS : PEGMEMA = 0.3 mol%.

Further, yield of network polymer also influenced the swelling degree for gels prepared using the same solution composition (**Figure 4.7**). Obviously, higher conversion led to a lower swelling degree due to higher density of chemical and physical crosslinks in the network. However, for polyPEGMEMA1000 gels, swelling ratio showed only slight changes with conversion, presumably, because the network was more significantly influenced by physical chain entanglement due to long PEG side groups that chemical cross-links (cf. above).

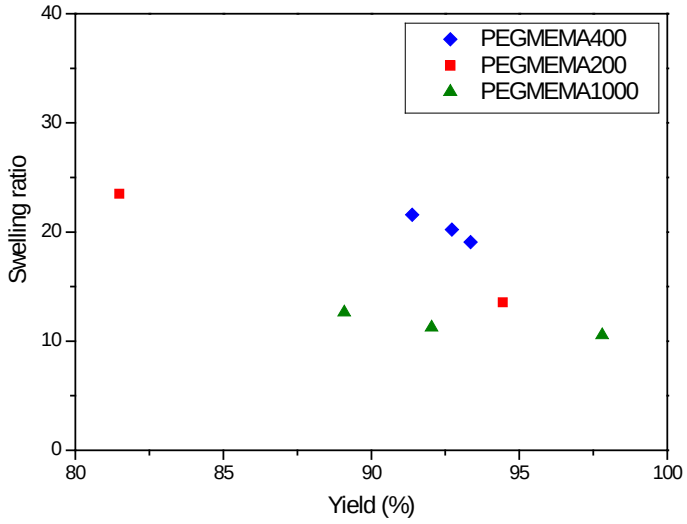

Figure 4.7. Effect of polymerization efficiency on swelling degree in polyPEGMEMA gels prepared at 0.5 mol·L^{-1} PEGMEMA, EGDMA : PEGMEMA = 12.6 mol%, and APS : PEGMEMA200 = 0.5 mol%, APS : PEGMEMA400 = 0.3 mol%, or APS : PEGMEMA1000 = 1.5 mol%. Data are included in this correlation where the conversion had been lower than for typical preparations because the room temperature had been higher than normal (22°C).

Effect of crosslinker structure

The length of crosslinker can also influence swelling behavior. This was examined using a series of monomers where the two methacrylate groups are linked by 1, 2 or 3 ethyleneglycol units. **Figure 4.8** presents the yield of network polymer and the swelling ratio obtained when varying the crosslinker molecular structure at otherwise identical conditions. With increasing the length of crosslinker, the polymer yield decreased and the swelling ratio increased indicating a looser network in the hydrogels. However, the effects of spacer length and network connectivity cannot clearly be distinguished.

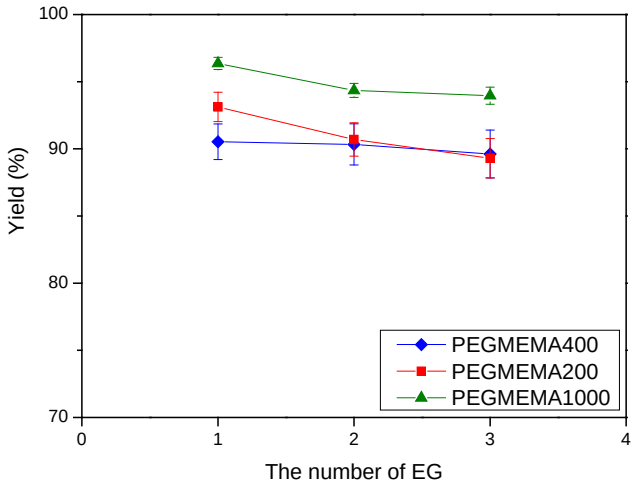

(a)

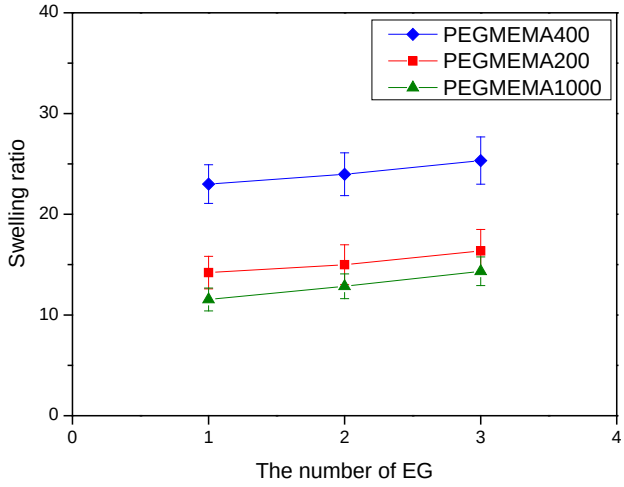

(b)

Figure 4.8. (a) Polymerization efficiency and (b) swelling ratio, depending on crosslinker length, i.e., number of ethylenglycol units in the dimethacrylate, in polyPEGMEMA gels prepared at 0.5 mol·L^{-1} PEGMEMA, dimethacrylate : PEGMEMA = 7 mol%, and APS : PEGMEMA200 = 0.5 mol%, APS : PEGMEMA400 = 0.3 mol%, or APS : PEGMEMA1000 = 1.5 mol%.

Hydrogel preparations in water/ethanol

Since EGDMA is poorly soluble in water, a mixture of water and ethanol was used as a solvent instead of pure water. The extent of ethanol evaporation from the solution during washing was

difficult to determine; the resulting error of the data obtained with TOC analyses was very high. Therefore, the yield of network polymer for this solvent is not reported here. The influence of solvent on swelling ratio of hydrogels is presented in **Figure 4.9**. Generally, the solvent did not much affect the swelling ratio of resulting gel prepared with high crosslinker content. However, at EGDMA content below 7.5 mol% for the polyPEGMEMA400 and 200 gels, the swelling ratio after preparation in a mixture of water and ethanol was significantly higher than that prepared in water.

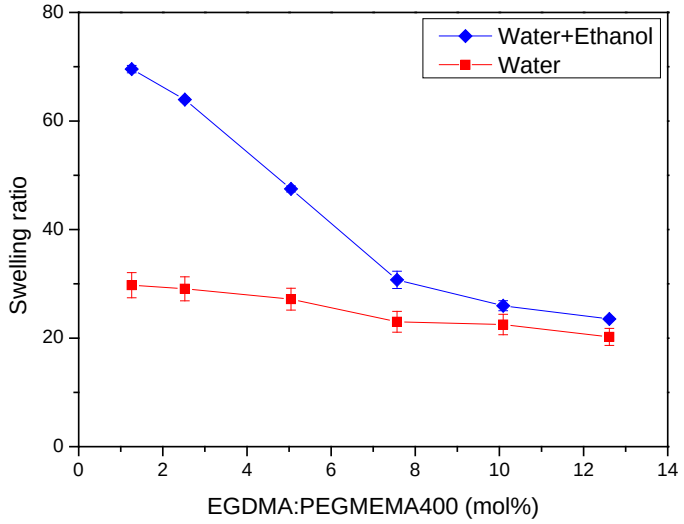

(a)

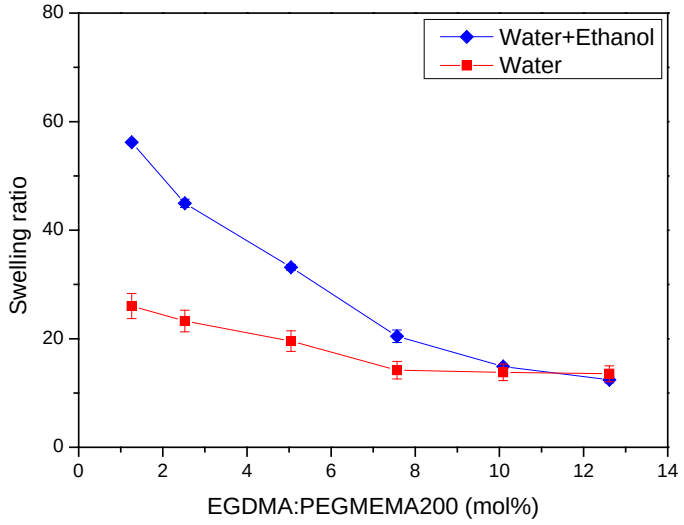

(b)

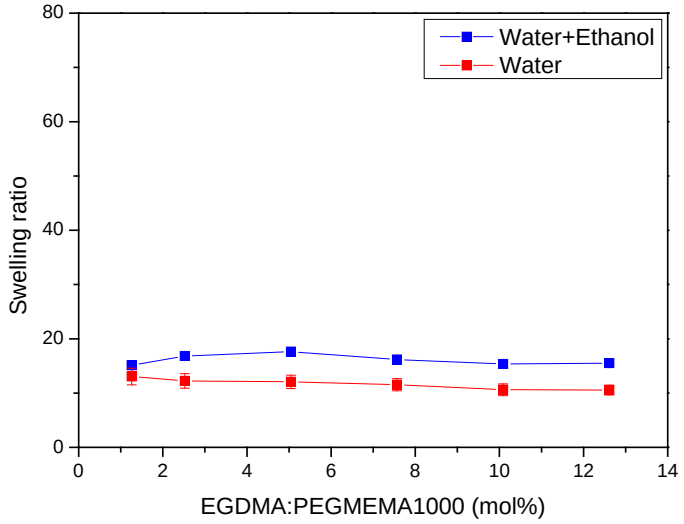

(c)

Figure 4.9. Effect of EGDMA content on swelling degree for two different solvents: (a) polyPEGMEMA400; (b) polyPEGMEMA200; and (c) polyPEGMEMA1000 gels; all prepared at 0.5 mol·L^{-1} PEGMEMA, and APS : PEGMEMA200 = 0.5 mol%, APS : PEGMEMA400 = 0.3 mol%, or APS : PEGMEMA1000 = 1.5 mol%.

All gels prepared in the mixed solvent showed a smoother surface and were more transparent than those prepared in pure water (**Figure 4.10**). This indicated that the gels prepared in the mixed solvent were more homogeneous. The insolubility of EGDMA in water obviously led to more heterogeneous gels, caused by a larger extent of phase separation. The lower swelling of gels prepared in water, especially at a low level of chemical crosslinking, could then be related to the presence of phase-separated domains acting as additional crosslinkers. All subsequent preparations of PEGMEMA/EGDMA-based gels were conducted using a mixture of water and ethanol as a solvent.

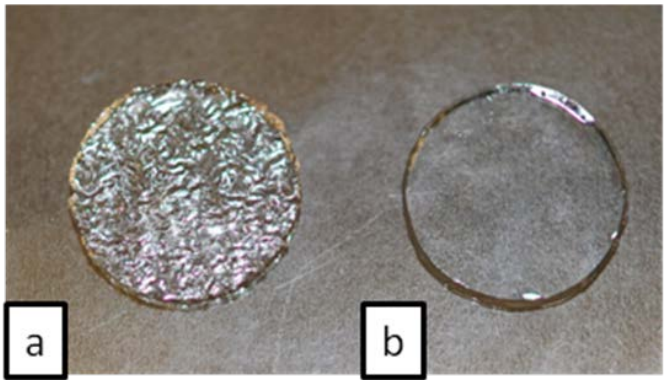

Figure 4.10. Typical images of gels prepared in (a) water; (b) 1 : 1 (v : v) mixture of water and ethanol.

Overall, the presented swelling results lead to one interesting and unexpected finding. The hydrogels prepared under similar conditions using PEGMEMA400 have higher equilibrium swelling than PEGMEMA200 and PEGMEMA1000. It is known that for a given chemical structure and hydrophilicity, swelling of hydrogels mainly depends on the total degree of cross-linking. The latter includes both physical entanglement and chemical cross-links which could depend on the PEGMEMA monomer in a non-monotonic manner. In order to elucidate this point rheological experiments were performed.

4.1.3 Rheology

In situ preparation and the mechanical properties of bulk gels were both characterized using oscillation rheometry. *In situ* preparation of hydrogel process can be monitored *via* corresponding changes in the storage modulus G' and loss modulus G" as a function of preparation time (**Figure 4.11**). Generally the polymerization process can be divided into three regions. First, G'< G", the system exhibits a viscous liquid behavior. With increasing time, G" increases while G' rises sharply until they are equal, this time is called gelation time [135]. After this time, G'>G", the

system exhibits an elastic response. The gelation times of selected polyPEGMEMA gels are presented in **Figure 4.12a**. Two important trends could be noted. First, a higher EGDMA content in the gel leads to faster gelation; this is expected due to more efficient branching during chain growth. Second, the gelation times for 12.6 mol% EGDMA increased in the order of PEG molar mass 200 → 1000 → 400, which correlated well with swelling (**Figure 4.12b**).

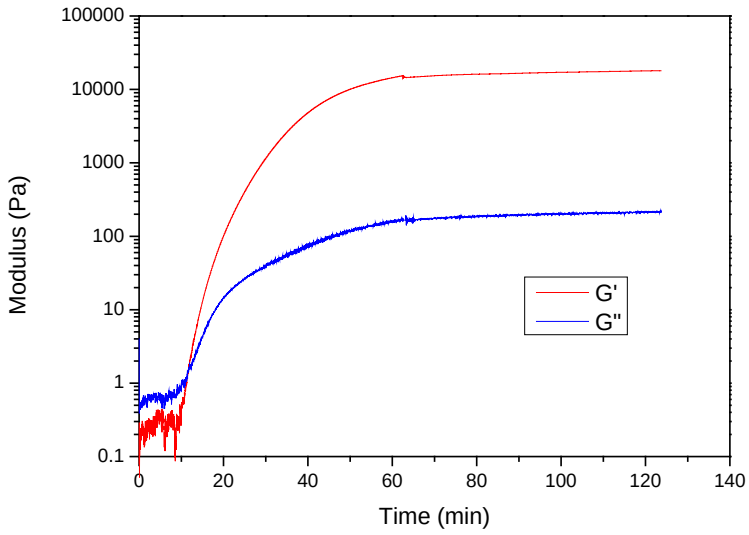

Figure 4.11. Changes in storage modulus and loss modulus as function of preparation time in PEGMEMA400 gels prepared at 0.5 mol·L^{-1} PEGMEMA, EGDMA : PEGMEMA = 12.6mol%, and APS : PEGMEMA = 0.3 mol%.

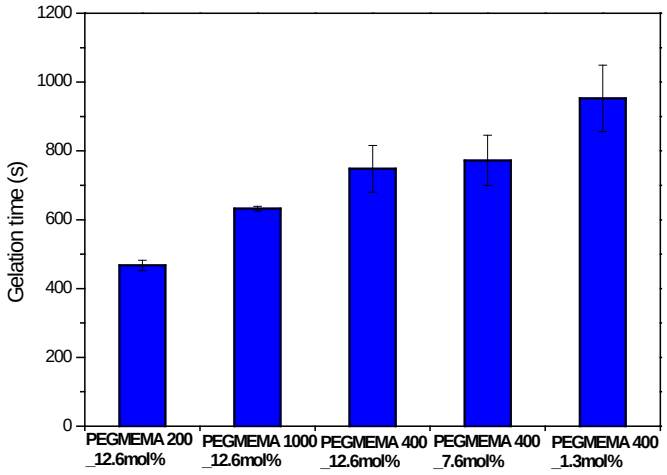

(a)

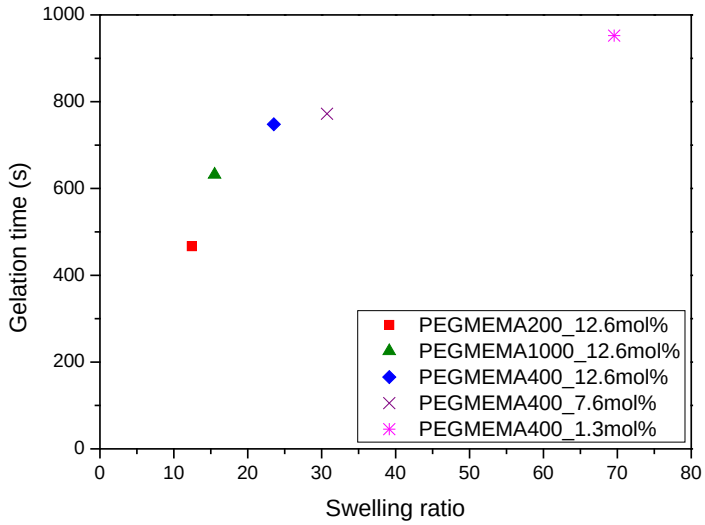

(b)

Figure 4.12. (a) Changes in gelation time with for various preparations; (b) correlation of swelling ratio and gelation time.

The mechanical properties of fully swollen gels were characterized by its storage modulus measured in frequency sweep experiments (**Figure 4.13**). G' was constant in the angular frequency range of 0.1 - 2.5 rad·s^{-1}. This value was further used to estimate the mesh size of the gel. The plateau values of storage modulus G' of hydrogels with varying EGDMA content and PEG side chain length are presented in **Figure 4.14**. For polyPEGMEMA200 and 400 gels, the plateau value of G' increased monotonically with increasing EGDMA content; the gel became mechanically stronger due to decreased swelling. Data for the polyPEGMEMA1000 gels were not much influenced by the EGDMA content, but G' values for low degree of crosslinking were much higher than for the other two gel types. In addition, the rough surface of PEGMEMA1000 gel yielded a higher standard deviation of storage modulus. Overall, the absolute values were very low what correlates well with the high degrees of swelling.

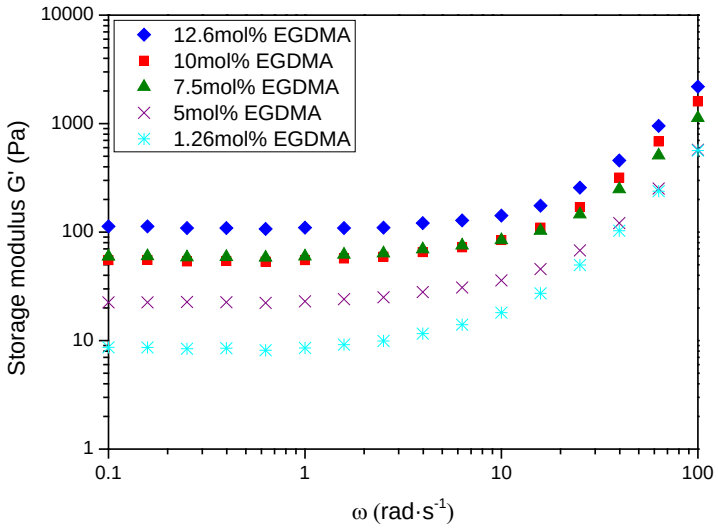

(a)

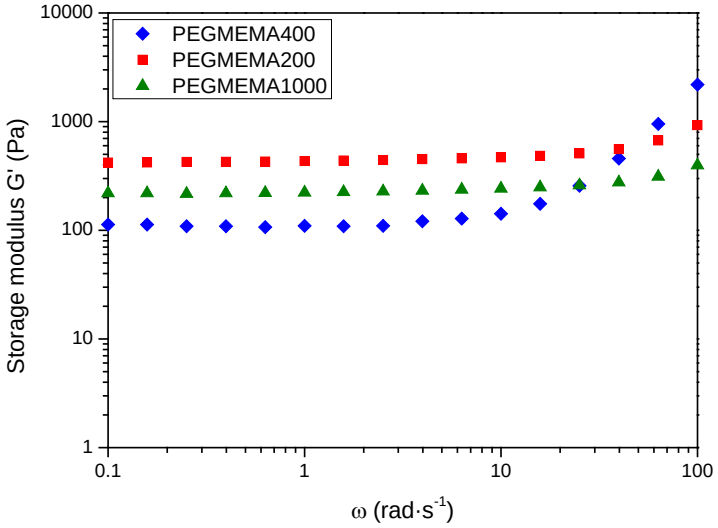

(b)

Figure 4.13. Storage modulus as a function of angular frequency: (a) with variation of EGDMA content in PEGMEMA 400 gel, (b) in polyPEGMEMA 200, 400 and 1000 gels at EGDMA : PEGMEMA = 12.6mol%.

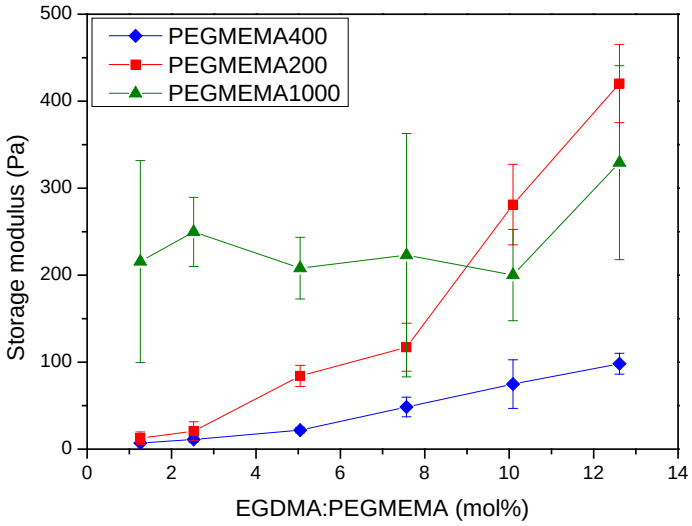

Figure 4.14. The plateau values of storage modulus as function of EGDMA content in polyPEGMEMA gels (all gels were prepared in a 1 : 1 (v : v) mixture of water and ethanol at 0.5 mol·L^{-1} PEGMEMA, and APS : PEGMEMA200 = 0.5 mol%, APS : PEGMEMA400 = 0.3 mol%, or APS : PEGMEMA1000 = 1.5 mol %).

4.1.4 Network structure

The network correlation length which corresponds to the mesh size of the hydrogel was estimated from swelling and rheological data using equations 3.3 and 3.4, respectively. This information, which helps describe the physical nature of gels, is an important parameter in applications such as protein release from hydrogels [20]; in the present context it is also relevant to the discussion of the uptake of proteins in antifouling coatings.

Figure 4.15a presents the effect of EGDMA content and PEG side chain length on mesh size of PEGMEMA gels estimated from swelling data. All calculations were done under the assumption of full conversion of monomer and of double bonds in the cross-linker monomer into a statistical chemical network (cf. above). Obviously, varying PEG side chain length and EGDMA content in polyPEGMEMA200, 400 and 1000 strongly influenced the apparent gel mesh size. It increased with decreasing EGDMA content; it also increased in the following order of PEG molecular weight: 1000 → 200 → 400.

The mesh sizes of polyPEGMEMA gels estimated from rheological data (**Figure 4.15b**) are in a range of 12 to 70 nm. The same trend as for swelling-based data was observed, except for the less pronounced crosslinker effect for polyPEGMA1000. However, the absolute values were about 4 times higher than those estimated from swelling data (cf. Figure 4.15a). This discrepancy is most probably due to the very low G' values; those are more typical for the viscous than for the visco-elastic state. However, the used model had been derived from rubber elasticity theory. **Figure 4.16** shows that there was a clear correlation between G' values and swelling ratio for all hydrogels, irrespective the monomer used. In contrast, the relationship of G' to mesh size calculated from swelling was different for each PEG molecular weight.

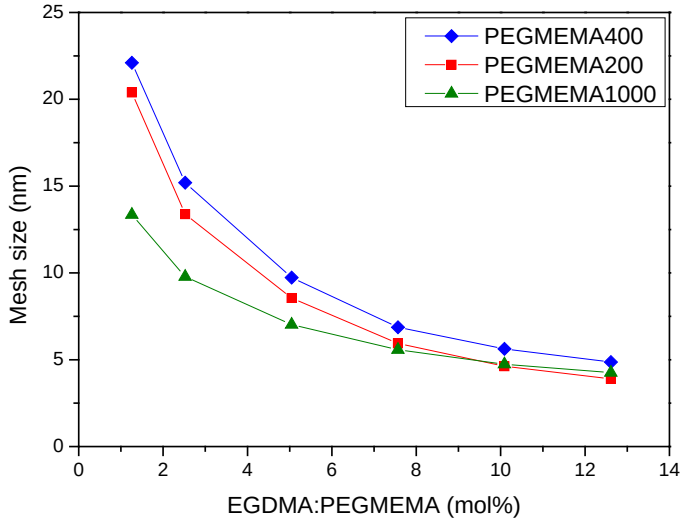

(a)

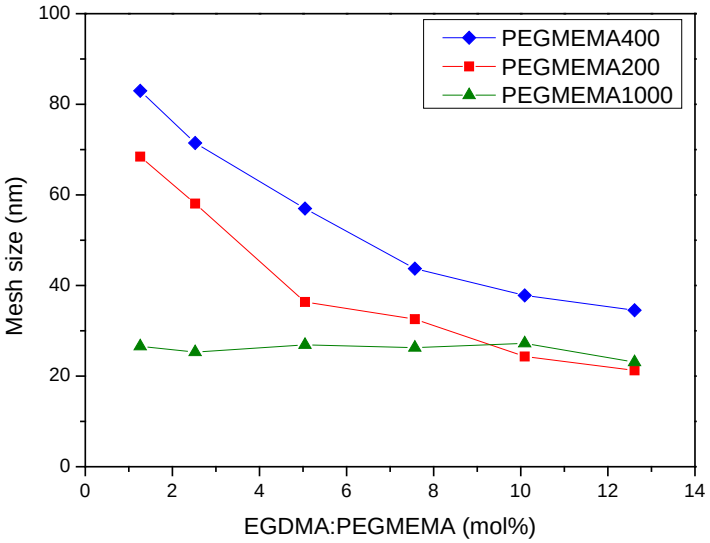

(b)

Figure 4.15. Mesh size of polyPEGMEMA gels with various EGDMA contents estimated from (a) swelling; (b) rheological data (all gels were prepared in a 1 : 1 (v : v) mixture of water and ethanol at 0.5 mol·L^{-1} PEGMEMA, APS : PEGMEMA200 = 0.5 mol%, and APS : PEGMEMA400 = 0.3 mol%, APS : PEGMEMA1000 = 1.5 mol%).

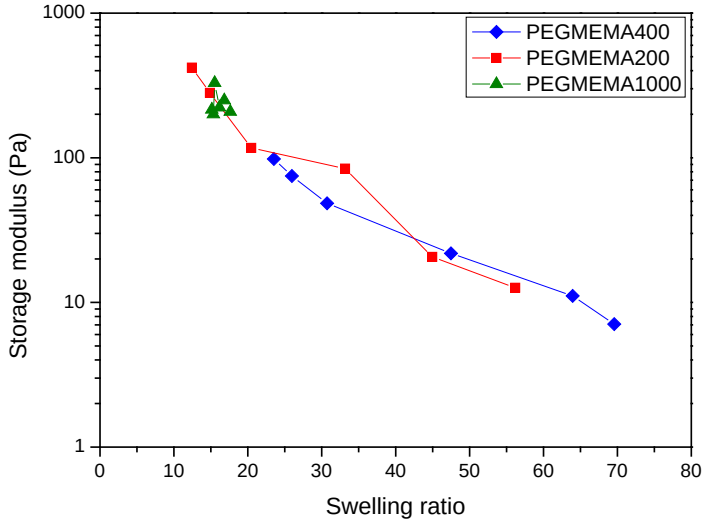

Figure 4.16. Correlation of storage modulus with degree of swelling for polyPEGMEMA gels with various EGDMA contents (all gels were prepared in a 1 : 1 (v : v) mixture of water and ethanol at 0.5 mol·L^{-1} PEGMEMA, APS : PEGMEMA200 = 0.5 mol%, and APS : PEGMEMA400 = 0.3 mol%, APS : PEGMEMA1000 = 1.5 mol%).

There are only very few related studies on polymeric hydrogels where both swelling ratio and modulus from rheology had been measured [136]. However, as a typical example, for a series of PEG vinyl sulfone-based hydrogels, mesh size was then exclusively calculated from swelling ratio while the modulus was only discussed with respect to other materials properties [137]. It should be noted that the G' values had been much higher than in the present study. On the other hand, the influence of model assumptions onto mesh sizes for polyPEGMA-based hydrogels calculated from swelling ratios has been discussed critically [138]. Overall, the mesh sizes based on swelling can be compared with many more reported values in the literature [20] than the ones based on G' data. The values achieved for higher contents of EGDMA with all three PEGMEMA monomers suggest that the resulting materials, if they can be prepared defect-free, should prevent the uptake of biomacromolecules with diameters beyond about 5 nm. On the other hand, the rate

of bacteria deposition can be expected to be minimal for the gels with largest mesh size, i.e., lowest crosslinker contents (cf. [120]).

The unexpected influence of PEG chain length at lower EGDMA content, which had been found in swelling and rheology data, is presumably related to the superposition of two different effects. The higher hydration efficiency of PEG400 relative to PEG200, i.e., higher content of hydrophilic EG units per monomer, may lead to the largest mesh sizes for polyPEGMA400. However, for the even larger PEG1000, increased entanglement between the long side chains seems to invert this trend and reduce the mesh sizes as well as increase mechanical strength.

4.1.5 Protein sorption

Protein sorption measurements were used to characterize the potential fouling resistance of various polyPEGMEMA gels. This should also improve biofouling resistance of the gel surface.

Effect of protein concentration and soaking time

In order to elucidate the influence of feed BSA concentration, the BSA sorption in polyPEGMEMA400 gels was investigated (**Figure 4.17**). The diffusion rate into the gel is lower at lower external concentration. Therefore, the data for low concentration may differ more from the equilibrium ones that those for high concentration. Protein sorption also can be affected by soaking time (**Figure 4.18)**. A plateau of BSA sorption was reached after 1 day. Therefore, the following experiments were conducted using a BSA concentration of $1 g \cdot L^{-1}$ and 1 day for soaking.

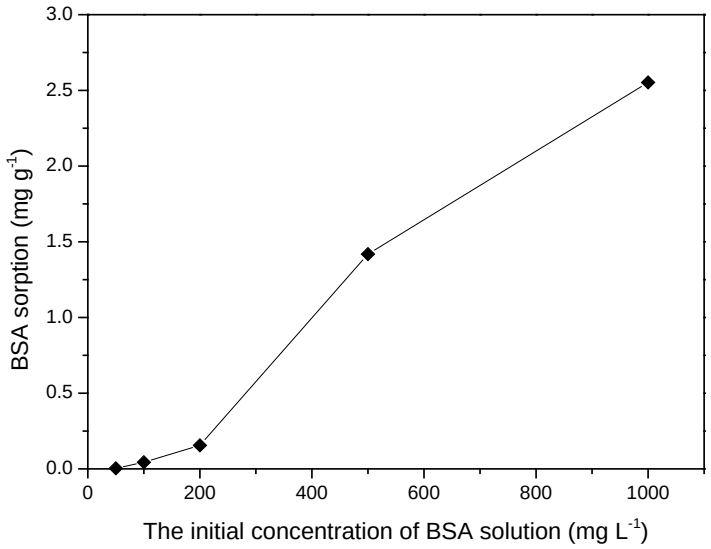

Figure 4.17. BSA sorption per dry gel mass as function of the initial BSA solution concentration in polyPEGMEMA400 gels prepared at 0.5 mol·L^{-1} PEGMEMA 400, EGDMA : PEGMEMA 400 = 7.5 mol%, APS : PEGMEMA400 = 0.3 mol%, and soaked for 1h.

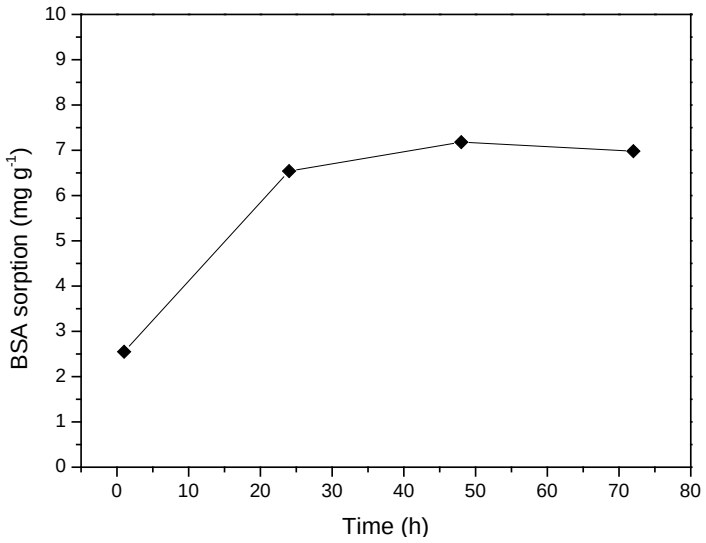

Figure 4.18. The amount of BSA sorption as function of time in polyPEGMEMA400 gels prepared at 0.5 mol·L^{-1} PEGMEMA 400, EGDMA: PEGMEMA 400 = 7.5 mol%, APS: PEGMEMA400 = 0.3 mol%, and soaked in 1 g·L^{-1} initial BSA.

Washing time Determination

After soaking in protein solution, the gels were washed in order to elute protein. Washed gels with time were monitored using CLSM measurement (**Figure 4.19**). In blank gel without BSA sorption, there is no any signal detected (**Figure 4.19a**), which is means, the gel do not have an influence on the FITC-protein detected by CLSM. After 1 day BSA sorption, protein penetrated into the gel around 200 μm (**Figure 4.19b**). Then the gel was taken out to washing, it could be seen, there is still protein remained in the gel after 1 day (**Figure 4.19c**). After 2 days the protein was nearly completely washed out expect for some protein which was stll entrapped in the gel network (**Figure 4.19d**). It also proved in **Figure 4.20**, protein concentration in washing solution reached the equilibrium after 2 days washing. In addition, it is an interesting finding that protein could penetrate only up to 200 μm into the gel. This is consistent that the BSA has a diameter of 7.7 nm [139], so it could diffuse into the hydrogel, which has a mesh size of about 22 nm (estimated from swelling data). Simultaneously permeated BSA molecules could be accumulated in the network of gel, and then stop from deeper penetration. On the other hand, the protein partition coefficients of these gels are surprisingly low (<0.04, cf. below), this also fits to the fact that protein will not use the entire gel volume.

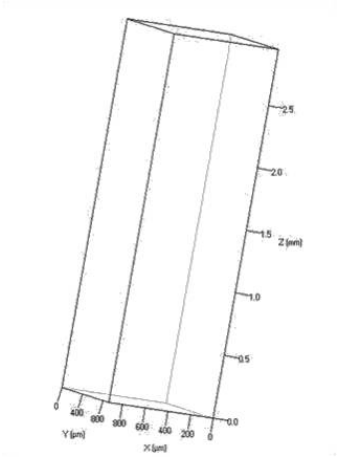

(a)

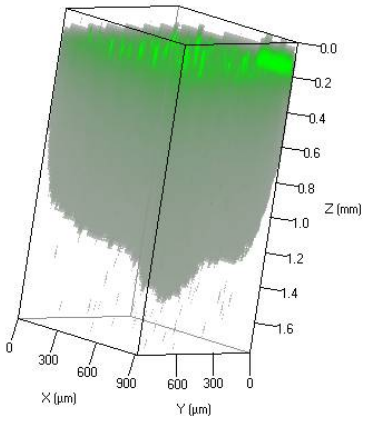

(b)

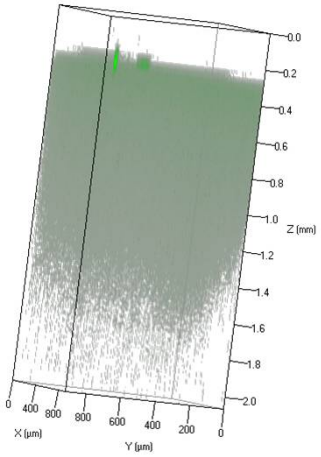

(c)

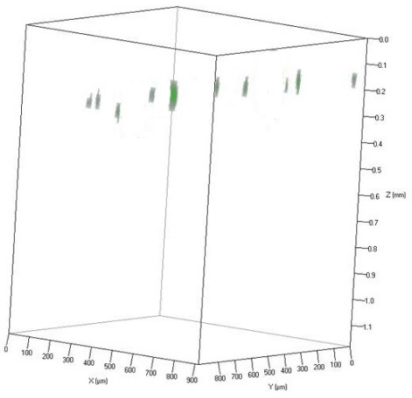

(d)

Figure 4.19. CSLM 3D images of polyPEGMEMA400 gels prepared in 0.5 mol·L^{-1} PEGMEMA400, EGDMA: PEGMEMA=12.6 mol%, APS: PEGMEMA= 0.3 mol% (a) Blank gel (b) after 1 day BSA sorption (c) after 1 day NaOH washing (d) after 2 days NaOH washing.

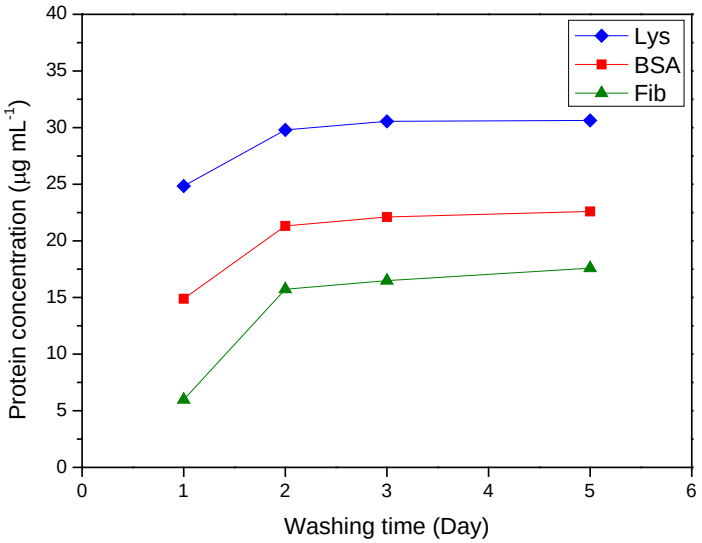

Figure 4.20. Protein concentration in washing solution with increasing washing time using polyPEGMEMA400 gel prepared at 0.5 mol·L^{-1} PEGMEMA 400, EGDMA: PEGMEMA 400=12.6 mol%, APS: PEGMEMA 400 = 0.3 mol%.

Partition coefficient

The partition coefficient for protein between polyPEGMEMA gel and protein solution as function of EGDMA content in polyPEGMEMA gels is presented in **Figure 4.21**. For polyPEGMEMA200 and 400 gels, protein uptake correlated well with the cross-linker content; a higher degree of crosslinking was linked to a smaller partition coefficient. For the polyPEGMEMA1000 gels no significant effect of crosslinker could be seen (analogous to the effect onto swelling; cf. **Figure 4.8c**). On the other hand, the amount of Lys (diameter 1.8 nm) [140] sorbed into the hydrogels was larger than that of BSA (diameter 7.7 nm) [139], and much larger than that of Fib (9 x 45 nm) [141]. This is due to the protein size effect (graphs showing the protein size effects for each type of gel as function of crosslinker content are presented in **Figure 4.22**). All results indicated that size exclusion of protein from the hydrogel played a major role. Overall, the very low absolute K values indicated also a weak affinity between protein and the

polyPEGMEMA segments, but may also be influenced by a limited penetration depth into the samples (cf. Figure. 4.19).

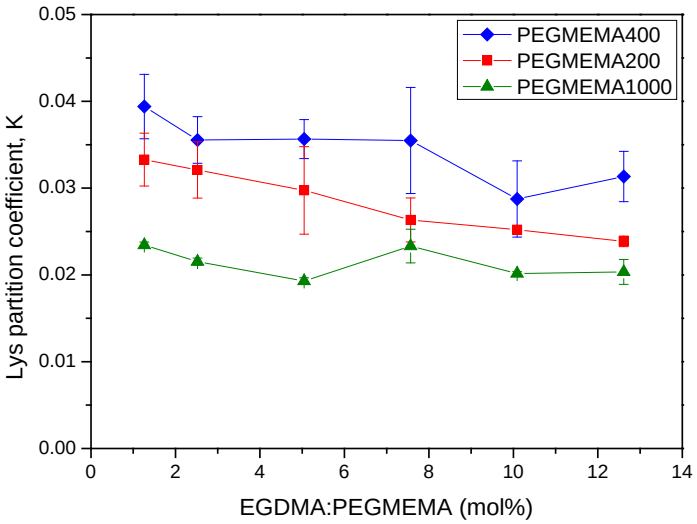

(a)

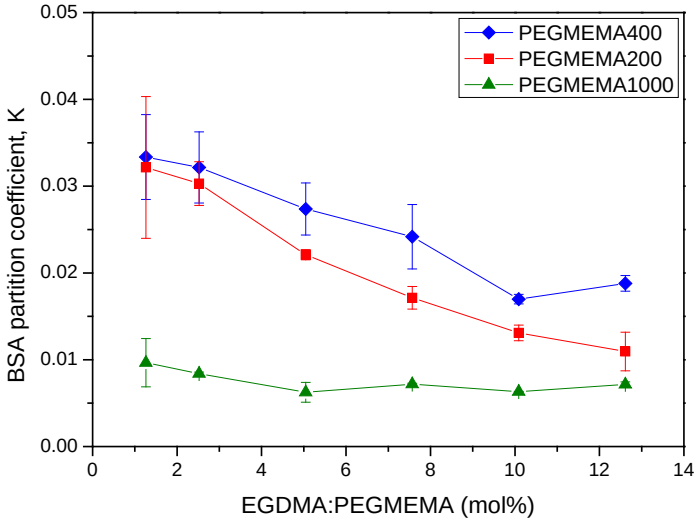

(b)

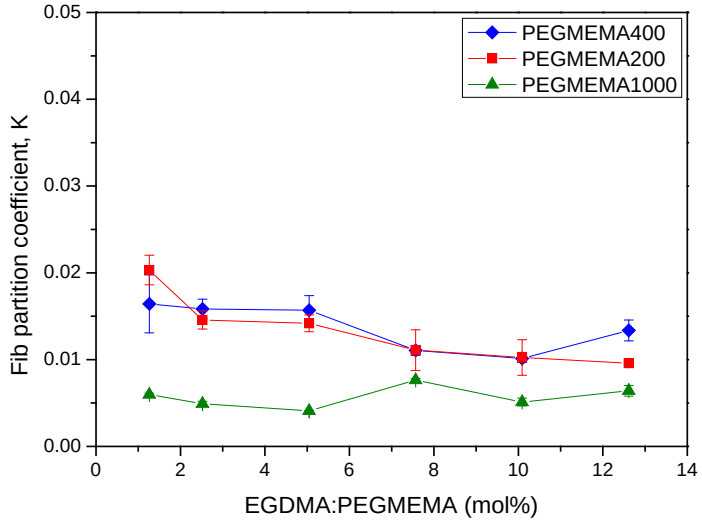

(c)

Figure 4.21. Partition coefficient for (a) Lys, (b) BSA, and (c) Fib; as function of EGDMA content in polyPEGMEMA gels prepared at 0.5 mol·L-1 PEGMEMA, APS: PEGMEME 200 = 0.5 mol%, APS : PEGMEMA 400 = 0.3 mol%, APS : PEGMEMA1000 = 1.5 mol%.

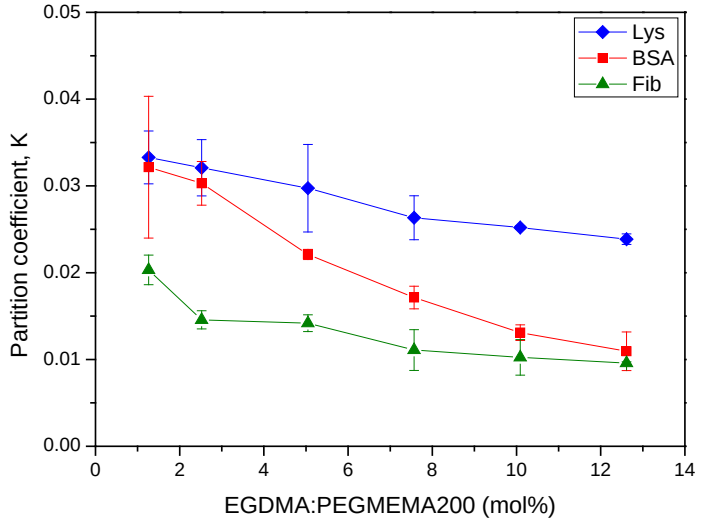

(a)

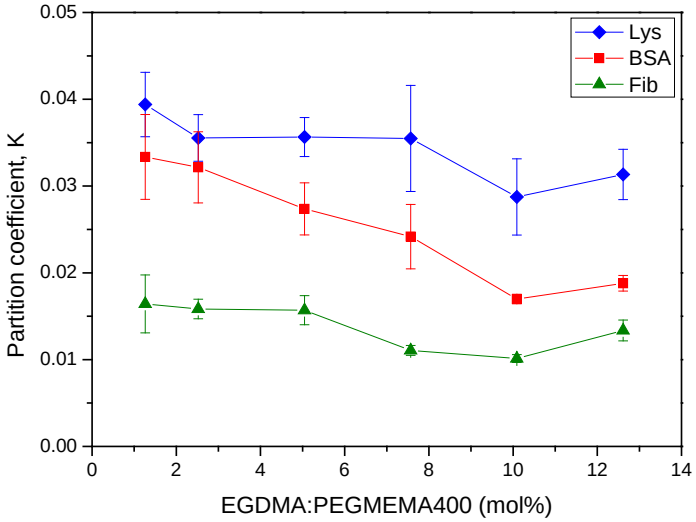

(b)

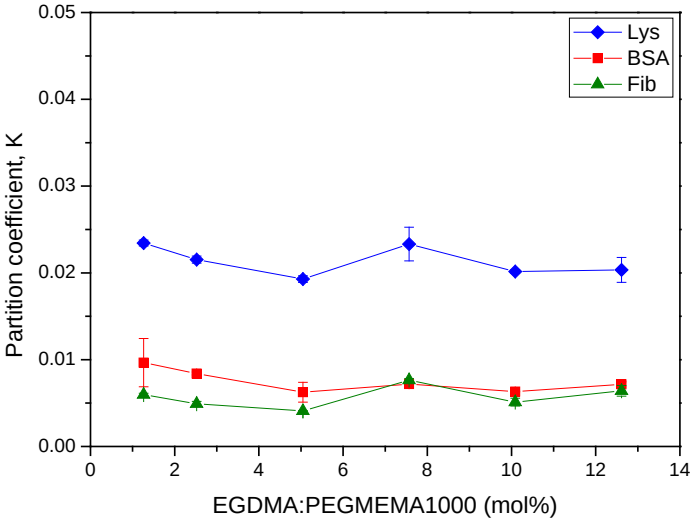

(c)

Figure 4.22. Protein size effects on partition coefficient for (a) PEGMEMA200 (b) PEGMEMA400 and (c) PEGMEMA1000; as function of EGDMA content in polyPEGMEMA gels prepared at 0.5 mol·L^{-1} PEGMEMA, APS: PEGMEME200 = 0.5 mol%, APS : PEGMEMA400 = 0.3 mol%, APS : PEGMEMA1000 = 1.5 mol%.

In an attempt to link protein sorption into the gels with the other results related to hydrogel structure, the partitioning coefficient for protein was correlated with mesh size from swelling ratio (**Figure 4.23**) and with storage modulus (**Figure 4.24**). It can be clearly seen that a correlation with mesh size calculated from swelling is only observed for the two gels polyPEGMEMA200 and 400, while for PEGMEMA1000 K it is small and independent of swelling-based mesh size. In contrast, a "universal" correlation for all gels can be seen when protein sorption is correlated with G'. Protein uptake is systematically decreasing with increasing mechanical strength of the hydrogels. The mesh size calculation based on the swelling data is only considering chemical crosslinking; obviously, size exclusion for polyPEGMEMA1000 is more efficient than assumed based on chemical crosslinking. The protein sorption is clearly related to polymer network structure [119, 142, 143]. Furthermore, the protein sorption tendency can be explained as steric repulsion free energy at the interface between the protein and the hydrogel. The steric repulsion free energy can be attributed to osmotic and elastic effect. The gel with higher elastic modulus has a denser network structure, which means a lower osmotic pressure and a higher elastic force; this corresponds to a lower interfacial free energy and results in a lower protein sorption [95, 144]. On the other hand, the storage modulus accounts for both chemical and physical crosslinking of the network. Therefore, the protein partitioning results provide additional, independent evidence that in the polyPEGMEMA1000 hydrogels additional physical crosslinking (most probably entanglement between the relatively long PEG chains) contributed to the network structure [145] (cf. section 4.1.4).

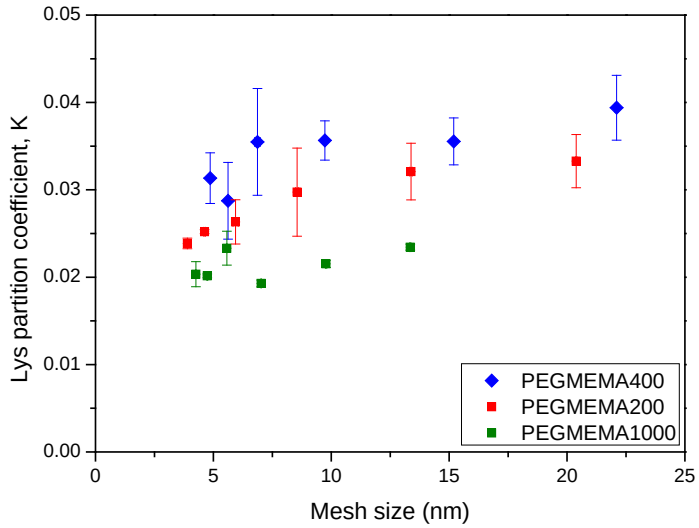
Lys partition coefficient, K
Mesh size (nm)
PEGMEMA400
PEGMEMA200
PEGMEMA1000

(a)

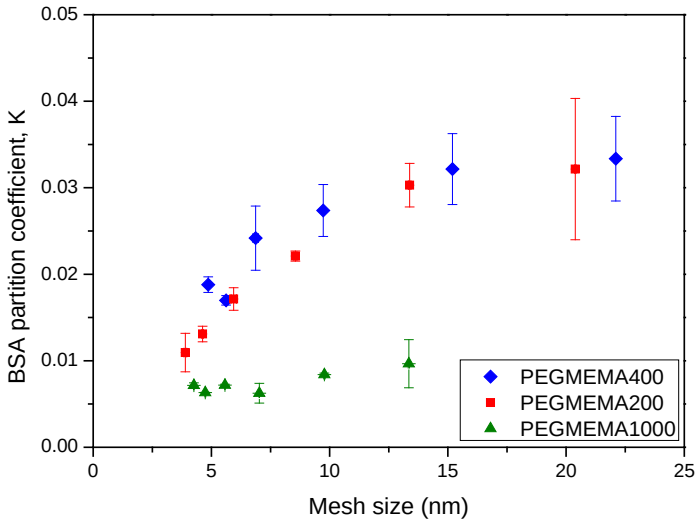
BSA partition coefficient, K
Mesh size (nm)
PEGMEMA400
PEGMEMA200
PEGMEMA1000

(b)

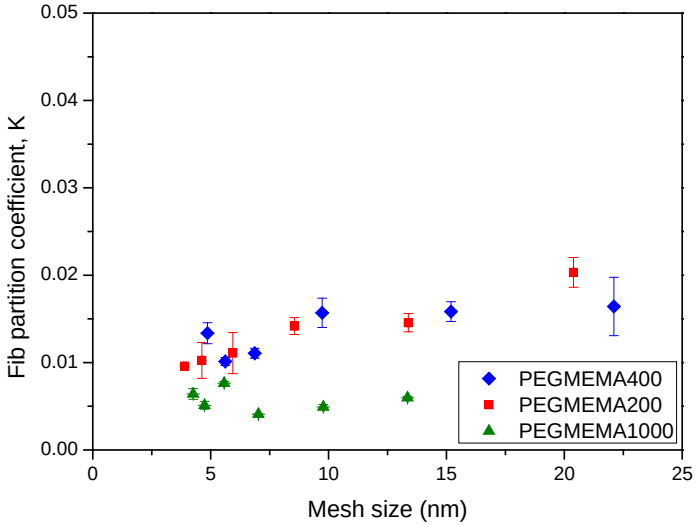

(c)

Figure 4.23. Correlation of protein partitioning coefficients for (a) Lys, (b) BSA, and (c) Fib in hydrogels with different degree of chemical crosslinking with mesh size calculated from swelling degree.

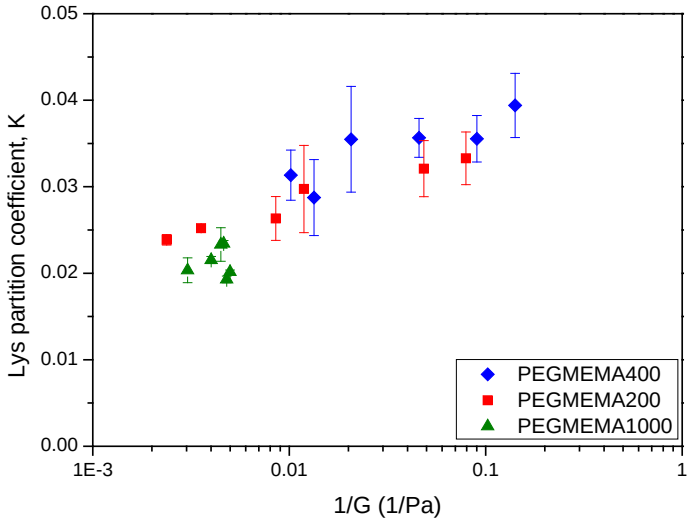

(a)

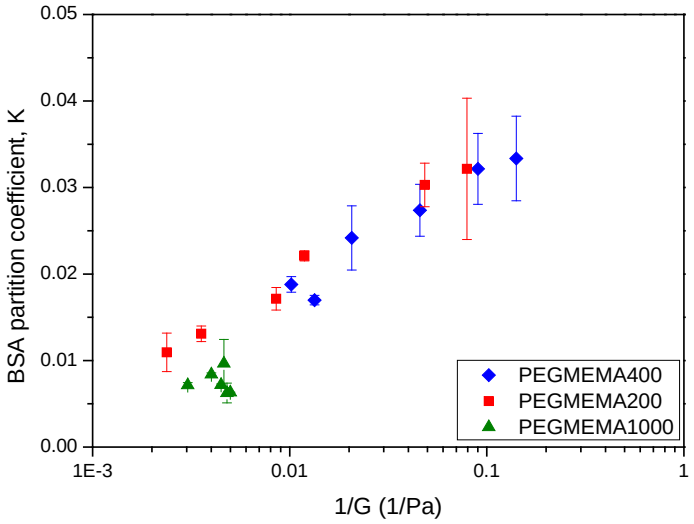

(b)

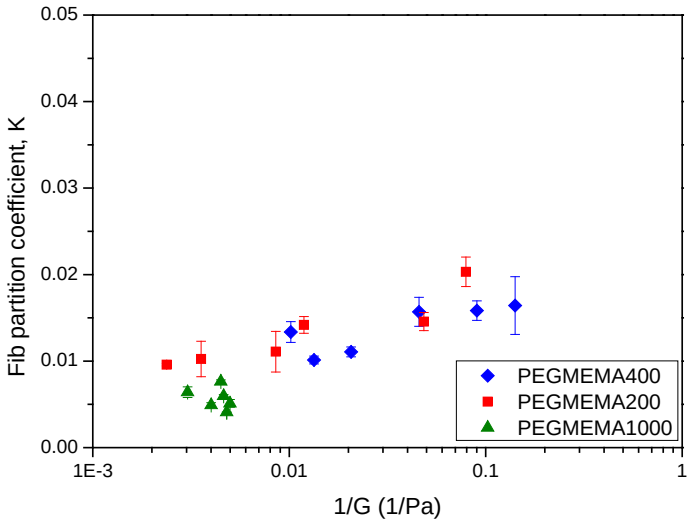

(c)

Figure 4.24. Correlation of protein partitioning coefficients for (a) Lys, (b)BSA, and (c)Fib in hydrogels with different degree of chemical crosslinking with storage modulus from rheology.

4.2 Surface anchored gel

4.2.1 Surface hydrophilicity

Contact angle measurements were used to characterize the surface hydrophilicity of various polyPEGMEMA gels. All other factors being equal, a more hydrophilic surface is often more resistant to the adsorption of proteins or adhesion of cells, cf. section 2.3.2. **Figure 4.25** presents contact angles between the surface of PEGMEMA gels and an air or a heptane bubble. In most cases, for gels prepared with the same PEG chain length, contact angle increased with decreasing EGDMA content. Hence, with higher degree of swelling, the contribution of less polar chain segments of the polymer network to surface energy was reduced.

Dynamic captive bubble contact angle measurements were also carried out. One interesting finding was that the contact angle of gels containing low crosslinker content increased with time while it was constant for higher degree of crosslinking (**Figure 4.26**). Hence, the high mobility of the weakly crosslinked hydrogel will allow a rearrangement of less hydrophilic macromolecular segments in the vicinity of the air/water interface.

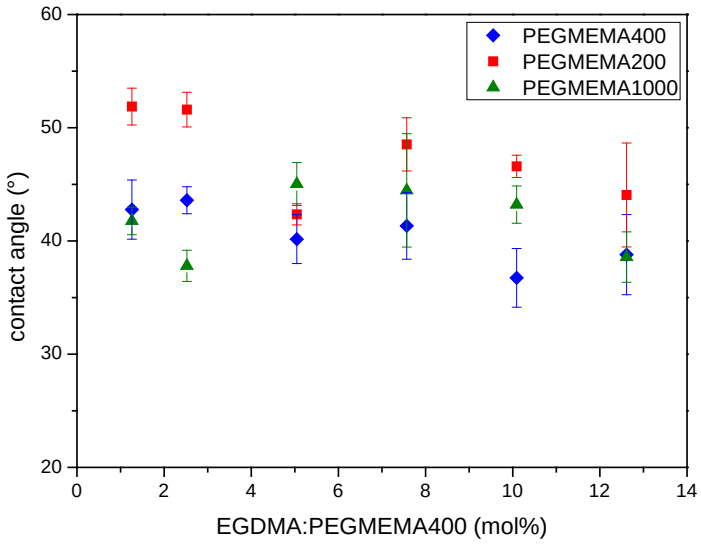

(a)

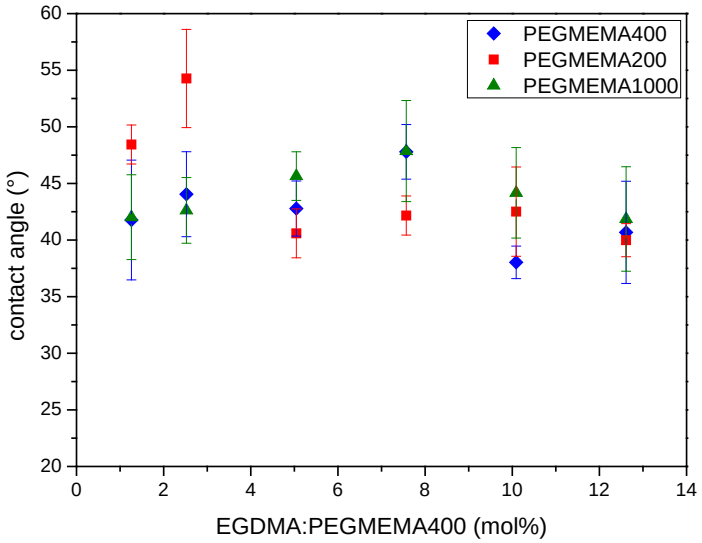

(b)

Figure 4.25. Contact angle in water between the surface of glass anchored gel and (a) air bubble, (b) heptane droplet; stable values obtained at the latest after 8 min.

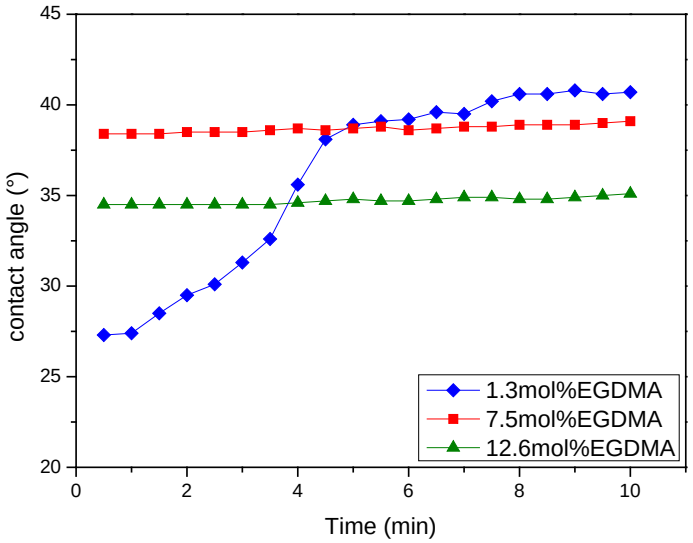

Figure 4.26. Captive air bubble contact angle as a function of time for polyPEGMEMA400 gels with different content of crosslinker prepared with 0.5 mol·L^{-1} PEGMEMA and at APS : PEGMEMA400 = 0.3 mol%.

4.2.2 Bacteria deposition

Single bacteria strains are commonly used in deposition experiments as favorable indicators for bacteria / surface interactions [146-153]. With focus on effects of physicochemical properties with relevance to biofouling, they do not completely exhibit the entire complexity of actual biofoulants (cf. [153]). *Pseudomonas fluorescens* are GFP-tagged and negatively charged bacteria, at pH 7 with zetapotential -40 ± 5 mV. Moreover, it is hydrophilic at a partitioning coefficient of 17 ± 4% between n-dodecane and water. These surface characteristics are fairly representative of many bacteria [44, 154], including many biofilm-forming ones [155], and make *P. fluorescens* a convenient model organism in the field of bacterial deposition, biofilm and biofouling studies [156-158].

Deposition coefficient

Deposition coefficients for polyPEGMEMA gels are presented in **Figure 4.27**. The values were much lower than for glass used as reference (8×10^{-5} cm·min^{-1}) and substrate for the grafted hydrogels. PolyPEGMEMA200 showed higher deposition than more swollen PEGMEMA400 gel. However, polyPEGMEMA1000 gels had the lowest deposition even though they also had the lowest swelling degree. A possible additional effect of PEG chain length could render the outer surface more repelling than observed for shorter PEG chains. Such sterical mechanism had been evoked [92, 96]. It had also been criticized when applied to adsorption of proteins (small bioparticles), but it could have relevance for cells (large bioparticles).

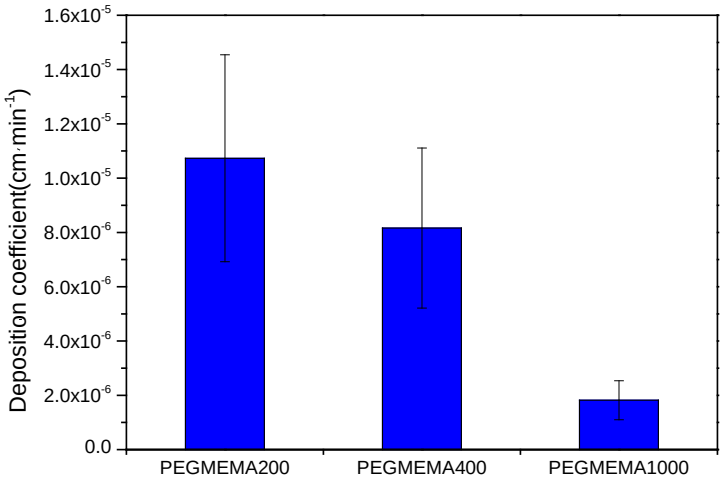

Figure 4.27. Bacteria deposition coefficient for three polyPEGMEMA gels (crosslinker content 12.6 mol%; for other preparation conditions see Figure 4.8); data for glass: 8 x 10^{-5} cm·min^{-1}.

Effect of gravity

Gravity also plays a substantial role on bacterial deposition. To clarify the role of gravity, bacterial deposition experiments were performed, in which the effect of gravity was reversed by turning the cells upside down. The results showed that a few bacteria adhered after 30 minutes to all surfaces including the reference bare glass surface **(Figure 4.28)**. This result was consistent with recent conclusion by Chen et al. [159] that gravitational force has a considerable effect in bacterial deposition in a parallel plate flow chamber, especially under low flow velocities. They used a higher flow velocity (average 23.6 m/h) compared to the velocity used in this work (5.9 m/h), it means that a large effect of gravity should be expected in this work. This indeed confirms that gravity has a strong effect on the deposition results shown in **Figure 4.25**. Nevertheless, this effect was identical for all tests and different gels were compared on a consistent basis.

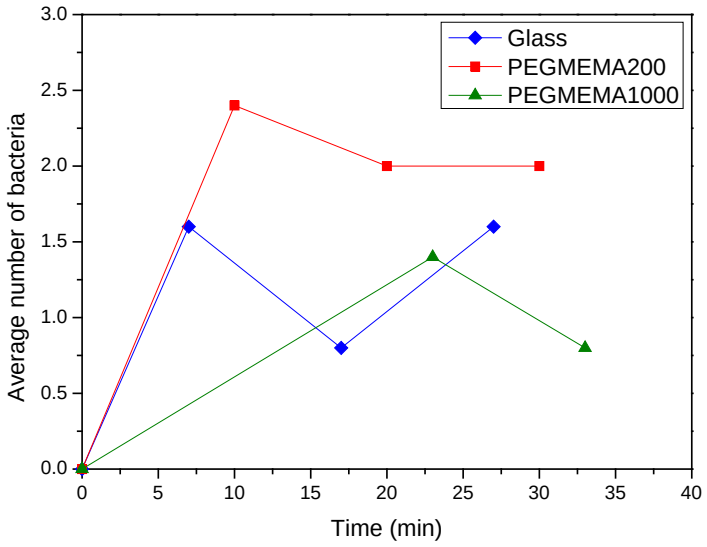

Figure 4.28. Average number of bacteria deposited on polyPEGMEMA gel (crosslinker content 12.6 mol%; for other preparation conditions see Figure 4.8) and glass using an upside down flow cell.

4.2.3 Biofilm growth

Even though it is known that initial bacteria deposition is the first stage of the biofilm formation, it may not be related to ultimate biofilm formation in a straightforward way. In order to test biofouling resistance more directly and compare it with initial deposition results, we carried out successive initial bacteria deposition and accelerated biofouling experiments with two hydrogels, PEGMEMA200 and PEGMEMA1000, and a bare glass as a control. As a first step, bacteria were pumped for 1 hour to provide seeding of the surface with bacteria for subsequent biofouling tests. The results are presented in **Figure 4.29**.

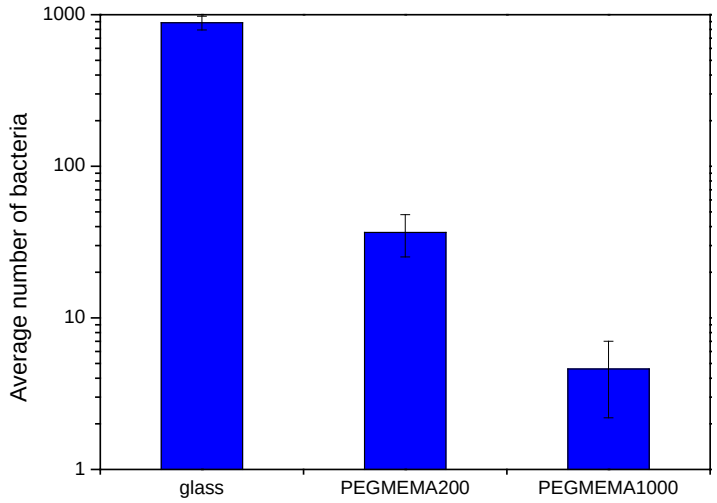

Figure 4.29. Average number of bacteria deposited on polyPEGMEMA gel (crosslinker content 12.6 mol%; for other preparation conditions see Figure 4.8) and glass in PEGMEMA gel and glass after 1 hour.

It can be seen that glass showed a much higher bacteria deposition compared with the PEG hydrogels. PEGMEMA 200 showed higher bacteria deposition than PEGMEMA 1000 hydrogels, as was observed also in deposition experiments (cf. section 4.2.1). Following initial seeding, biofilm formation was incubated by pumping a diluted LB medium through the flow cell for 48 hours. At the end of the run the flow cells were disassembled and the biofilm that had developed was observed using CLSM; the resulting images are presented in **Figure 4.30**.

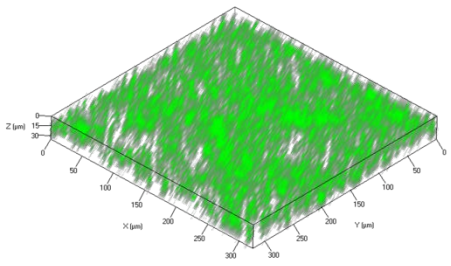

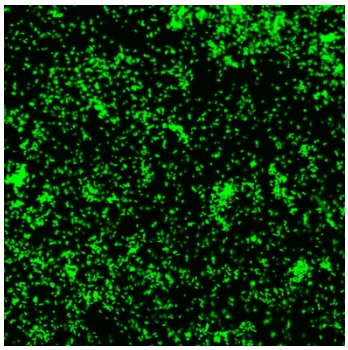

(a)

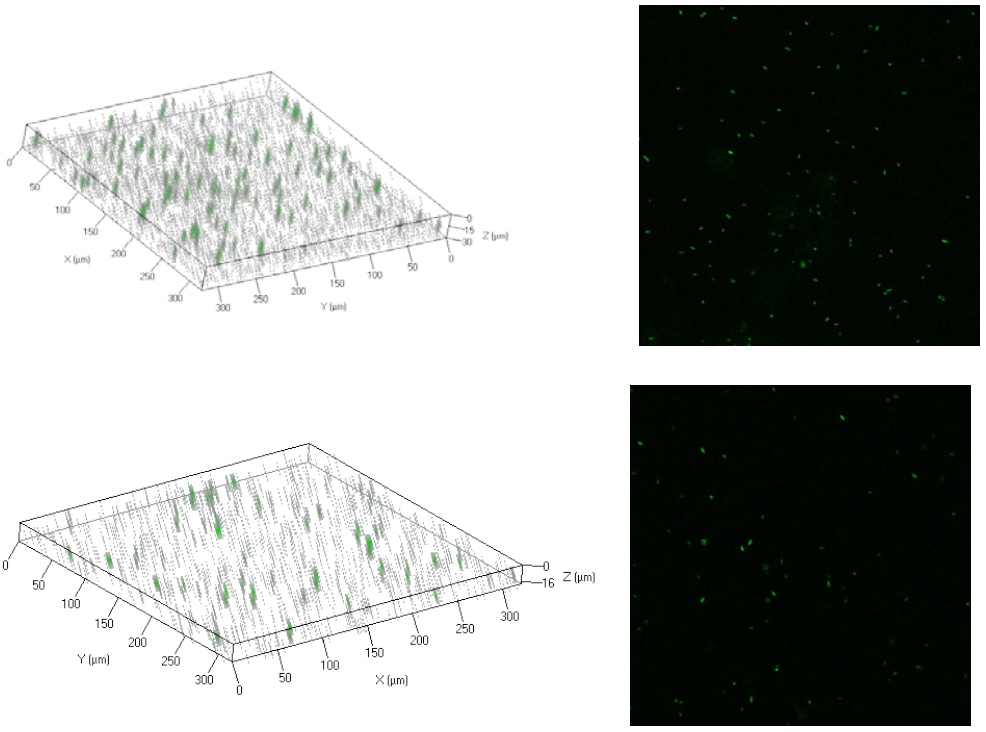

Figure 4.30. Confocal fluorescence microscopy 3D and surface images of (a) glass, (b) polyPEGMEMA200, and polyPEGMEMA1000 gels (crosslinker content 12.6 mol%; for other preparation conditions see Figure 4.8) after biofilm growth for 48 hours.

The CLSM images of the biofilm were analyzed using the COMSTAT software. **Figure 4.31** presents the COMSTAT results for biovolume per unit area and quantifies the striking difference observed in the CLSM images of **Figure 4.30**. Actually, significant biofilm growth occurred only on glass used as a reference material, which was consistent with much higher deposition after 1 hour. On the other hand, very few bacteria were observed on the gel samples. It is likely that COMSTAT might not accurately quantify single bacteria sparsely distributed on the surface, and therefore a comparison between the two hydrogels using COMSTAT analysis may not be a reliable tool for the understanding of the tendency of different gels to support or prevent the growth of biofilm. Nevertheless it is obvious that the biomass present on both hydrogels was

greatly reduced compared to glass, by two orders of magnitude. This result can be explained by the weak adhesion of bacteria to the surface, which reduces initial deposition and enables easy detachment by shear force.

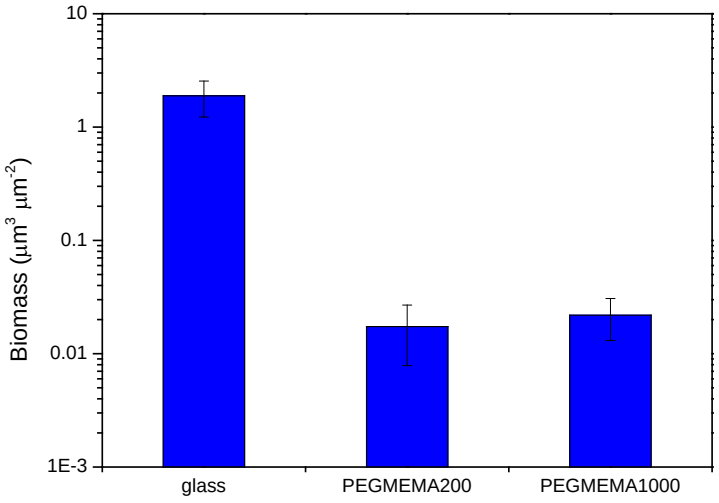

Figure 4.31. COMSTAT analysis for biofilm growth on polyPEGMEMA gel (crosslinker content 12.6 mol%; for other preparation conditions see Figure 4.8) and glass after 48 hours.

4.3 Macroinitiator synthesis and characterization

One objective of the present study was to examine the feasibility of a simple, generic route for the irreversible surface grafting of a (cross-linked) hydrogel layer onto a commercially available membrane. Bruening and coworkers [77] recently reported the physical adsorption of an atom transfer radical polymerization (ATRP) macroinitiator onto polymeric substrates surfaces for the grafting of polymer brushes via surface-initiated ATRP (cf. section 2.3.1). This work takes advantage of the well-known tendency of polyelectrolytes to adsorb onto oppositely charged surfaces in relatively flat conformations in the presence of low (or zero) levels of electrolyte. Given that most desalination membrane surfaces are negatively charged, a cationic photoreactive macroinitiator was synthesized.

DMAEMA was first statistically copolymerized with HEMA via free radical polymerization and the yield was 41 %. This copolymer is insoluble in water but easily dissolves in THF and DMF. The molar ratio between DMAEMA and HEMA in the copolymer determined from the ^{1}H NMR integration ratios (**Figure 4.32**) was 3.54. This was very close to the initial feed molar ratio 3.45 of monomers in the polymerization solution, the target copolymer composition. GPC analysis of this copolymer precursor indicated a M_n of 147,000 g/mol and a polydispersity of 2.25 (**Figure 4.33**). The subsequently quaternized copolymer is stable and water-soluble but insoluble in common organic solvents. The NMR spectrum of TH shows downfield shift of the methyl groups attached to nitrogen (e of TH in **Figure 4.32**), indicating successful quaternization. Finally, the cationic and photoreactive macroinitiator was obtained by esterification of the hydroxyl group of HEMA units in the copolymer. The NMR spectrum of esterified copolymer BEE-DH and BEE-TH showed benzene ring group peaks at chemical shift of 7-8 ppm, the integration ratios between benzene ring groups and methyl groups indicated a degree of esterification of approximately 100%.

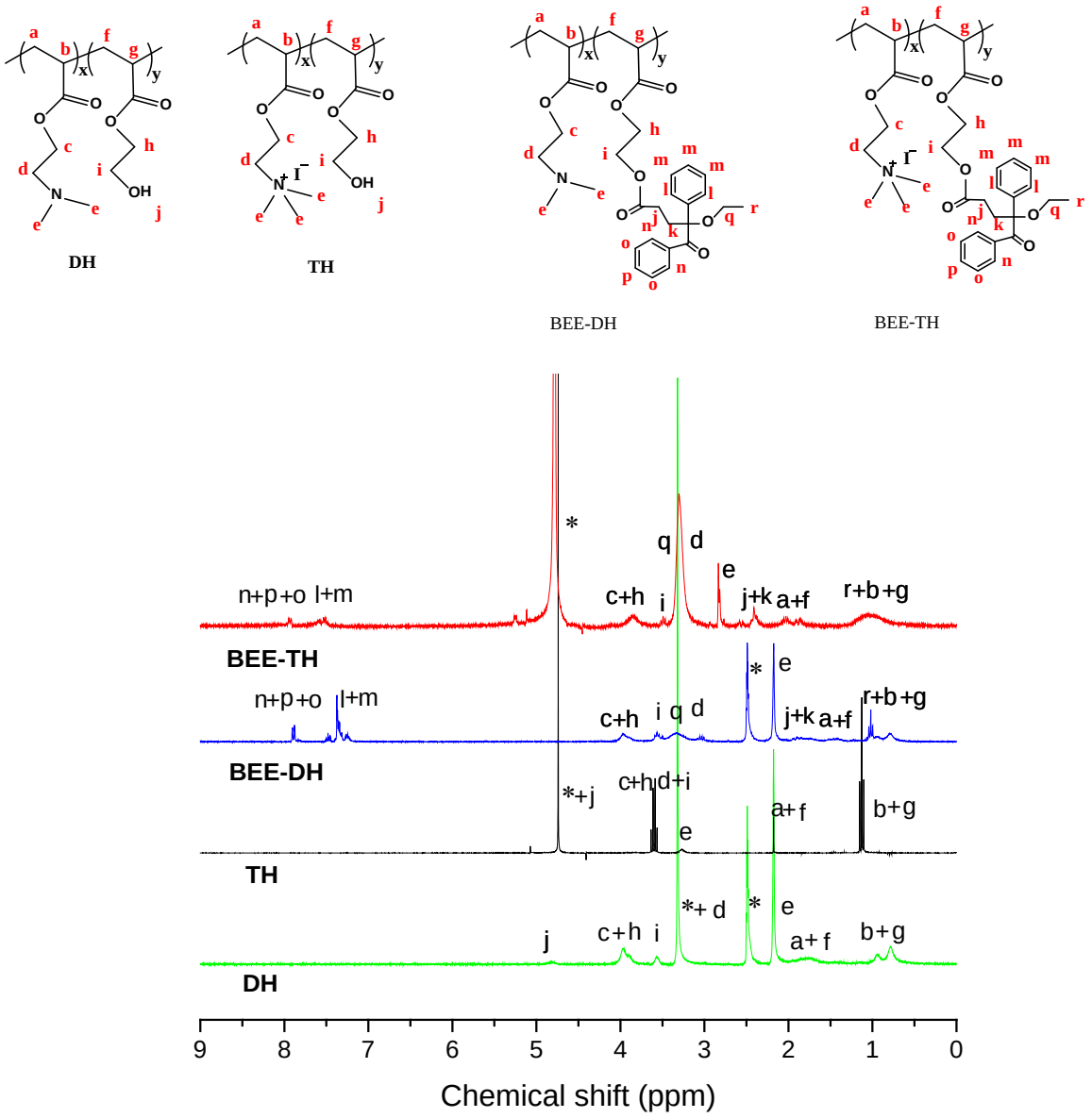

Figure 4.32. ^{1}H NMR spectra of DH (bottom, DMSO-d_6 as solvent), TH (lower middle, D_2O as solvent), BEE-DH (upper middle, DMSO-d_6 as solvent) and BEE-TH (top, D_2O as solvent). The corresponding structures and proton assignments are given in the figure. * indicates resonances from solvents.

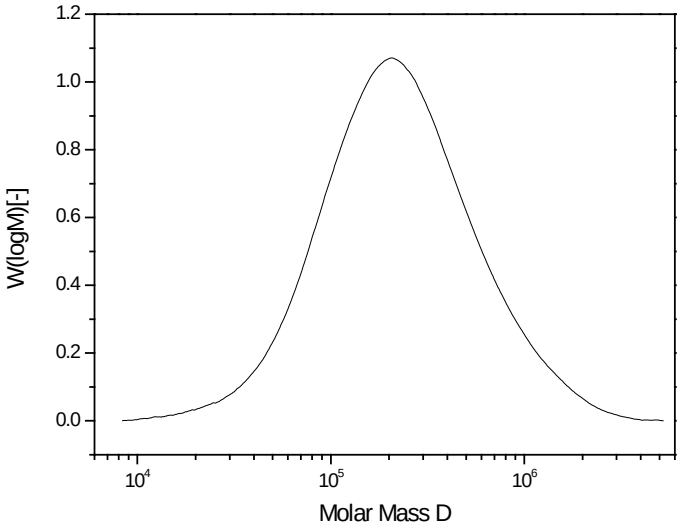

Figure 4.33. GPC curve of DH.

4.4 Membrane surface modification

In this section, results obtained from surface modification of NF membrane by photo grafting polymerization are presented. The base membranes NF270 and NTR7450 were used to investigate membrane surface chemistry on functionalization as well as surface charge, surface hydrophilicity and membrane performance.

4.4.1 Membrane chemistry

The membranes were characterized with ATR−IR spectroscopy to verify their chemical structure and also quantify functionalization. The pristine, BEE-TH premodified and modified membranes in dry state had been analyzed by FT-IR spectra (**Figure 4.34**). Typical polysulfone bands of the membrane were observed at 1487 cm^{-1} and 1584 cm^{-1}. The ester carbonyl peaks at 1720 cm^{-1} in premodified and modified membranes confirmed successful macroinitiator adsorption on surface and the grafted polyPEGMEMA gel from the macroinitiator modified surfaces. The intensity of those bands changed with varying modification conditions. These changes were quantified using

equation 3.8 and 3.9 to obtain the amount of grafted layer on membrane; the results are presented in section 4.4.2.

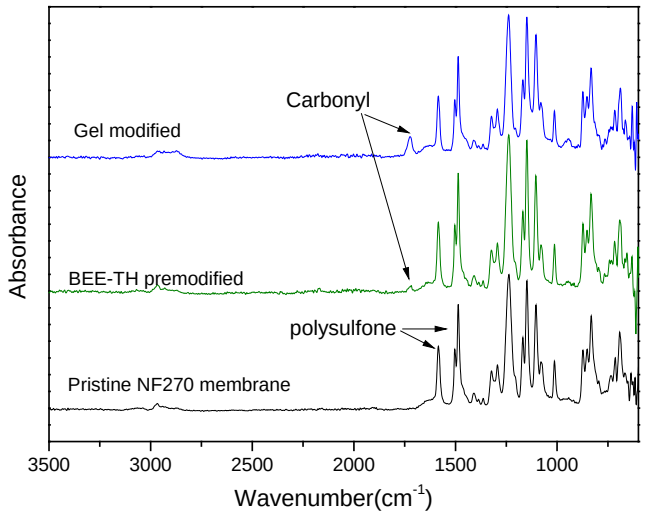

(a)

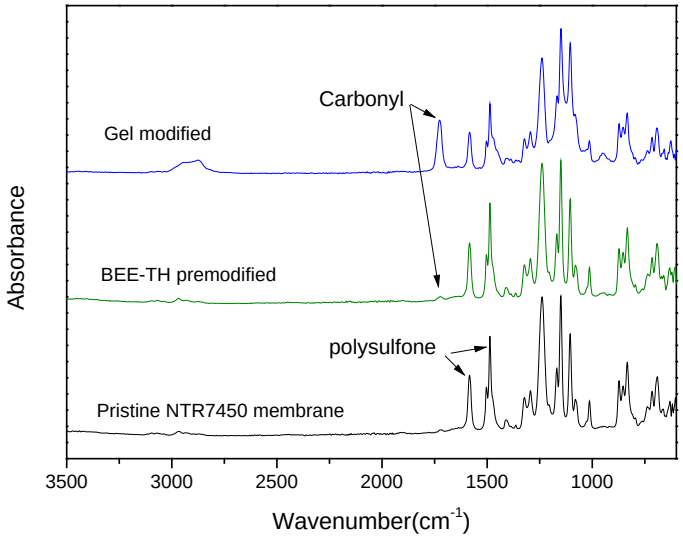

(b)

Figure 4.34. FT-IR spectra of the pristine, BEE-TH premodified and gel modified (a) NF270 and (b) NTR7450 membranes. Premodification using 10 mmol·L^{-1} HEMA units of BEE-TH, modification prepared at 0.5 mol·L^{-1} PEGMEMA400, EGDMA : PEGMEMA400 = 12.6 mol% and 20 min UV irradiation.

4.4.2 Degree of grafting and surface hydrophilicity

Degree of grafting was determined by gravimetry and IR spectra to characterize the amount of grafted layer on the membrane surface. The surface hydrophilicity of the membranes was characterized by water contact angle measurements. The contact angle of modified membrane is affected by the base membrane, the degree of surface coverage related to DG, and the structure of the grafted polymer. If the membrane surface has been completely covered by the grafted polymer, then the contact angle will mainly depend on the hydrophilicity/hydrophobicity balance of this polymer. For a membrane with incomplete surface coverage, both the base material and grafted polymer will contribute to contact angle [14].

NF270 membrane

Effect of macroinitiator concentration

The cationic photoreactive macroinitiators were electrostatically adsorbed onto membrane surface and subsequently used for initiating photo-grafting of polyPEGMEMA gels (**Figure 4.35)**. The amount of grafted polymer on the NF270 membrane was measured for premodification (**Figures 4.36**). The preDG only slightly increased with increasing copolymer concentration. Therefore, the following experiments were conducted using a copolymer concentration of 10 $mmol \cdot L^{-1}$ (based on HEMA units). Moreover, quaternized copolymers TH and BEE-TH which have strong ion exchange groups showed a higher preDG than copolymers DH and BEE-DH which have weak ion exchange group.

On the other hand, the immobilization behavior of macroinitiator BEE-TH on aromatic polyamide was monitored using QCM-D (Quartz Crystal Microbalance with Dissipation monitoring) technique by our collaborator Roni Kasher from Ben-Gurion University. Aromatic polyamide layer was prepared on gold coated quartz sensors to mimic the surface chemistry of polyamide membranes [160]. The results (unpublished) showed that the amount of BEE-TH immobilized on the model surface of polyamide membrane is identical with injected BEE-TH

with HEMA units concentrations ranging from 0.007 mmol·L^{-1} to 0.7 mmol·L^{-1}. It demonstrates that cationic groups of BEE-TH interact strongly with the negatively charged carboxylic groups on the membrane-mimetic surface and result in a very thin and rigid layer of BTH.

Figure 4.37 presents the relationship between the amount of grafted gel (DG_W value) on modified membrane and copolymer concentration used in premodification process. The amount of grafted gel only had a slow increase with the copolymer concentration used, and did not show a pronounced difference.

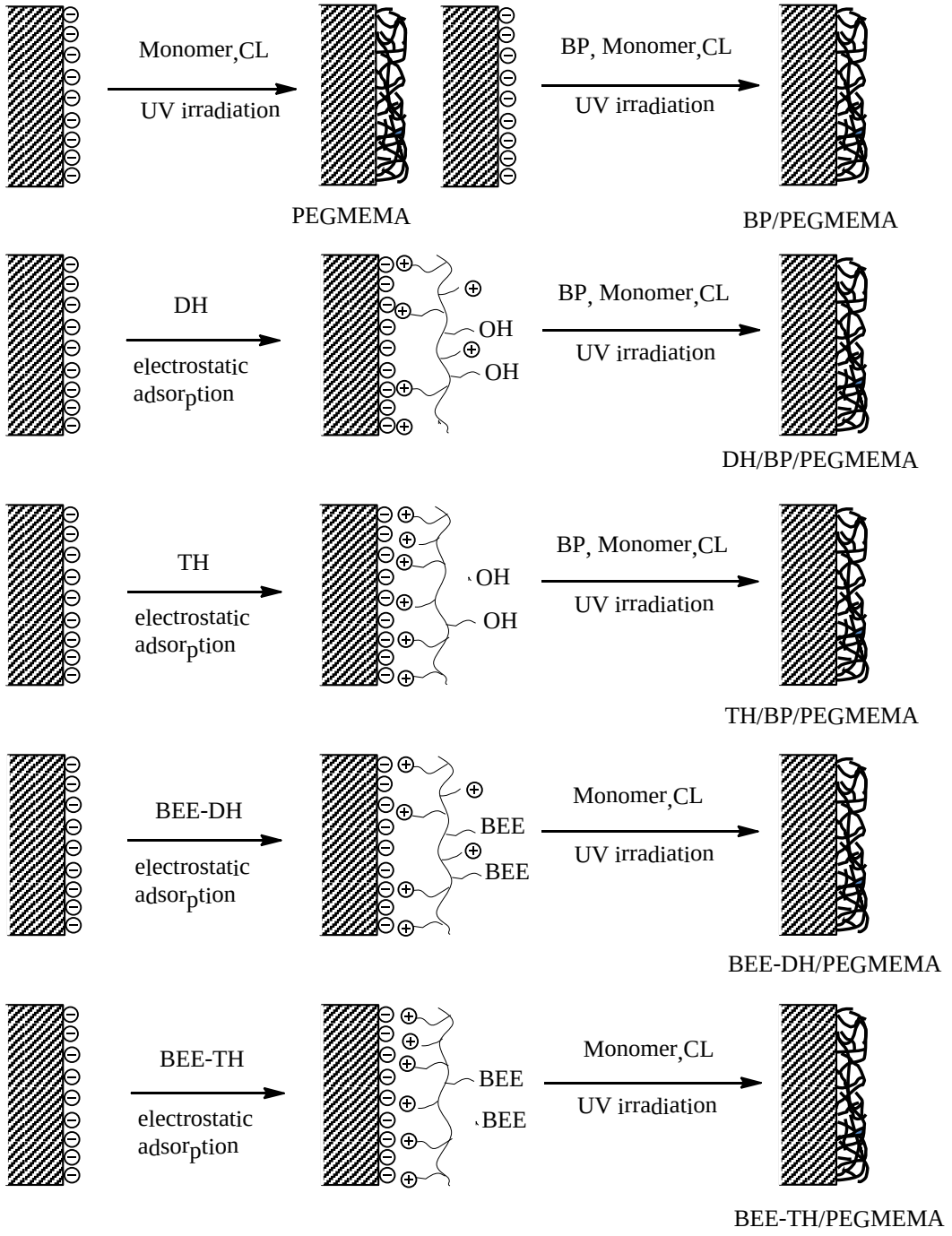

Figure 4.35. Experimental steps depicting the electrostatic adsorption of cationic photoreactive macroinitiators onto NF270 membrane surface and the subsequent photo-grafting of polyPEGMEMA gels.

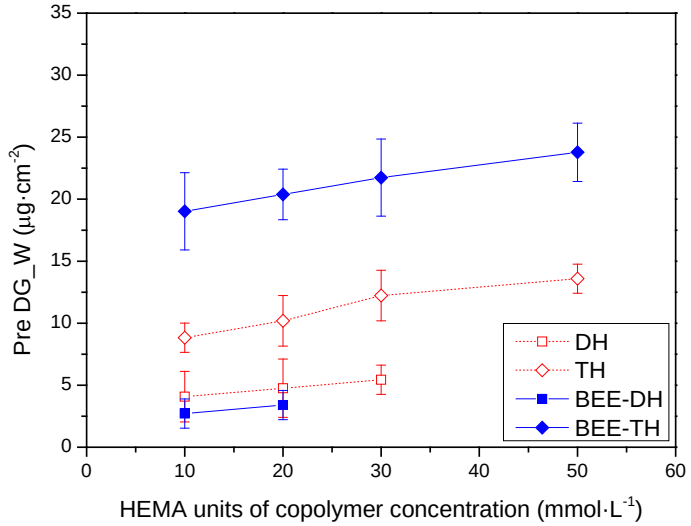

Figure 4.36. Effect of copolymer concentration in solution on adsorbed mass in premodified NF270 membrane.

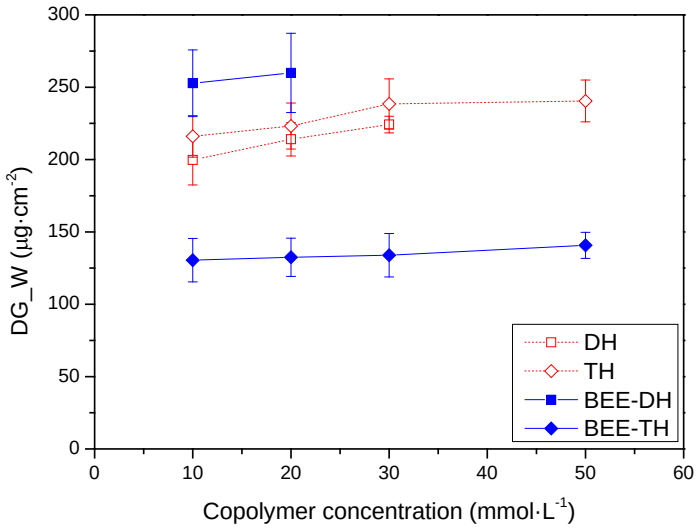

Figure 4.37. Effect of copolymer concentration on DG_W on gel modified NF270 membrane prepared at 0.5 mol·L^{-1} PEGMEMA400, EGDMA : PEGMEMA400 = 12.6 mol%, and 10 min UV irradiation.

As presented in **Figure 4.38**, all dried premodified membranes had a higher water contact angle values compare to pristine NF270 base membranes. The premodified NF270 membrane by adsorbed quaternized copolymer (TH, BEE-TH) had a lower contact angle than the one modified with their precursor (DH, BEE-DH) due to extra ionic groups and higher surface coverage. In addition, contact angle of BEE-TH premodified NF270 membrane slight increased with increasing BEE-TH concentration in the solution (**Figure 4.39**). It indicated that more hydrophilic cationic macroinitiator adsorbed on membrane surface. This correlates very well with the influence of macroinitiator concentration on the pre_DG and the QCM data (cf. above). On the other hand, the influence of UV irradiation on contact angle of BEE-DH and BEE-TH premodified membranes was also determined. First, these premodified membranes were immersed in 1 : 1 (v : v) mixture of ethanol and water, and then irradiated to UV for 20 min. The contact angle values of these membranes increased and became relatively closer (75.1 ± 2.7° for BEE-DH, 77.2 ± 2.4° for BEE-TH). After UV irradiation, the side segments with initiator of macroinitiator layers are anchored to surface, which means a less flexible hydrophilic side chain is immobilized on membrane surface.

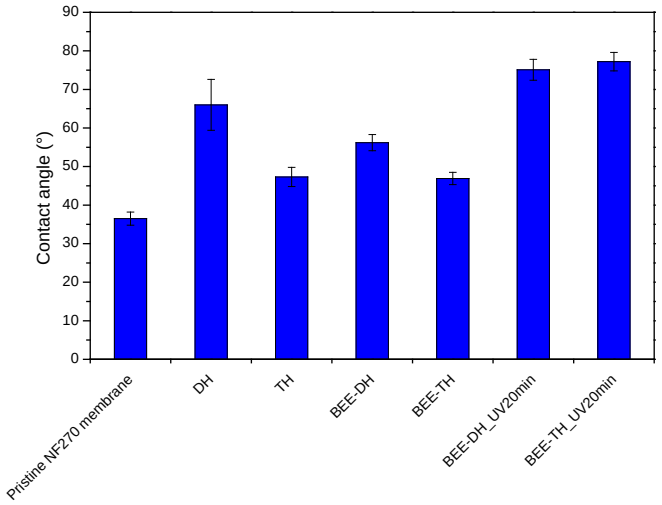

Figure 4.38. Effect of premodification on contact angle in premodified membrane prepared at 10 mmol·L^{-1} HEMA units of copolymer.

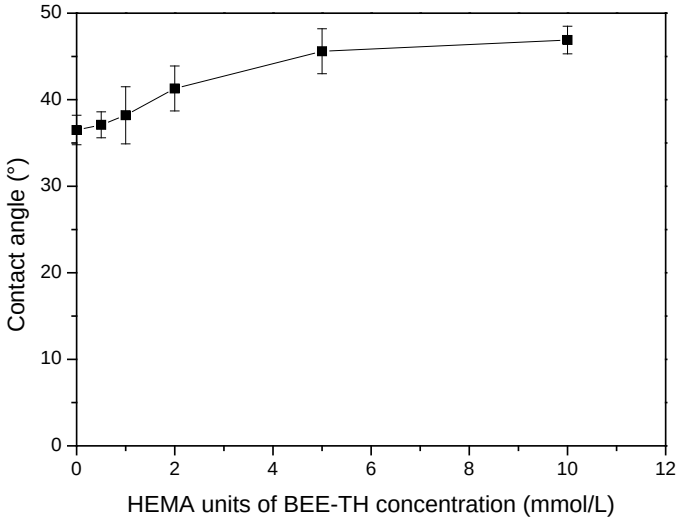

Figure 4.39. Effect of BEE-TH concentration on contact angle of premodified membrane.

Effect of UV irradiation and premodification

The effects of irradiation time and premodification on DG are presented in **Figure 4.40.** The DG increased with increasing UV time. With longer UV irradiation period, amount of free radicals in the grafting zone increased and more chains grew in gel network resulting in thicker grafted layer. Until 15 min irradiation, the DG_W values showed a similar tendency with DG_IR values. At longer irradiation time, the slope of the DG_IR plots was much lower than that of DG_W plots. Similar results were also observed in **Figure 4.42-4.44**. As the thickness of the grafted gel layer increases, the intensity of polysulfone bands of base membrane become weaker due to limited depth of light penetration [161]. It leads to a slow enhancement with DG_IR values. Therefore, determination of DG with higher value using gravimetry is more reasonable.

Modification with BP systems (BP/PEGMEMA, DH/BP/PEGMEMA, and TH/BP/ PEGMEMA; cf. Figure 4.35) yielded higher DG values than modification without BP systems (PEGMEMA, BEE-TH/PEGMEMA). In systems without BP, radicals are generated only from membrane solid surface and not from monomer or solvent. Apparently systems with BP have a higher reactivity.

The radicals can generate by hydrogen atom abstraction from the membrane surface membrane. And there is another possibility for hydrogen abstraction, i.e. from the solvent ethanol or the monomer. Moreover, modification using premodified membrane yielded lower DG values than modification using pristine membrane. During premodification, the copolymer was adsorbed onto the membrane surface. Radicals may trap in reactions with this copolymer layer and result in less efficient gel layer formation.

Interesting, for the same UV irradiation time, modification using BEE-DH premodified membrane with lower amount of grafted BEE-DH yielded highest DG. DLS data showed that BEE-DH existed as big aggregated particles in ethanol and water mixed solvent due to poor solubility (**Figure 4.41a)**. It leads to inhomogeneous adsorption (incompletely mussy coverage) on membrane surface. Consequently, more initiation sites will be preferably generated not only from BEE-DH and also from uncovered base membrane surface, and result in more polymer growth from surface. In contrast, small particle size and narrow size distribution of BEE-TH in solution indicated it is well dispersed in solvent (**Figure 4.41b**). This will form relatively completely coverage on membrane surface, and subsequently more homogeneous grafted polymerization.

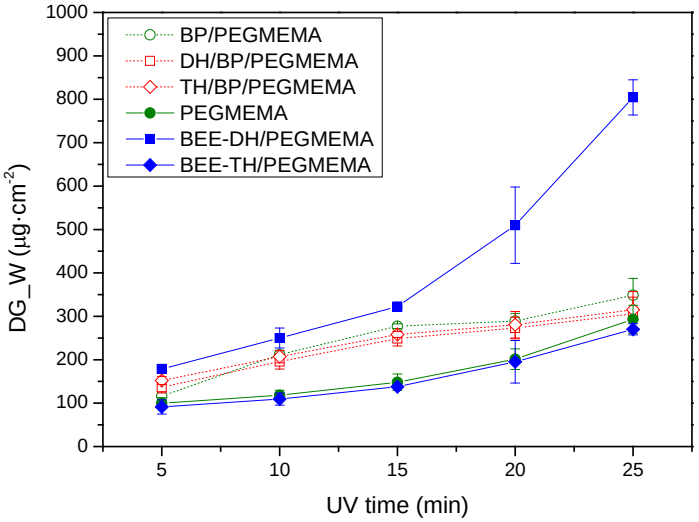

(a)

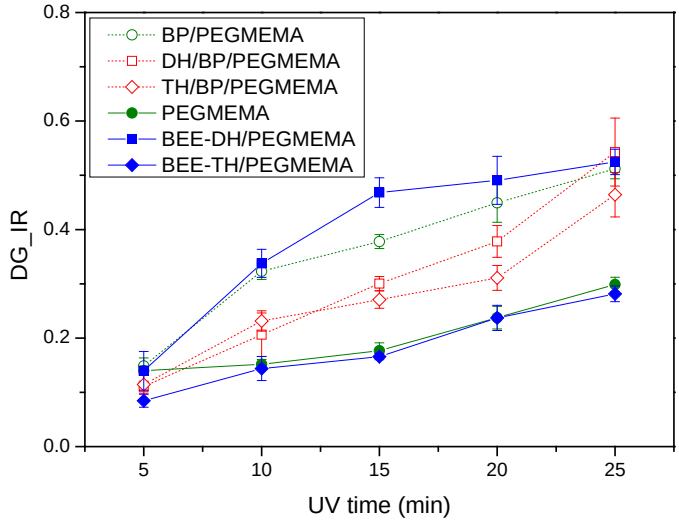

(b)

Figure 4.40. Effect of UV irradiation time and premodification on (a) DG_W and (b) DG_IR in gel modified NF270 membrane prepared at 0.5 mol·L^{-1} PEGMEMA400, EGDMA : PEGMEMA400 = 12.6 mol% and premodification using 10 mmol·L^{-1} HEMA units of copolymer.

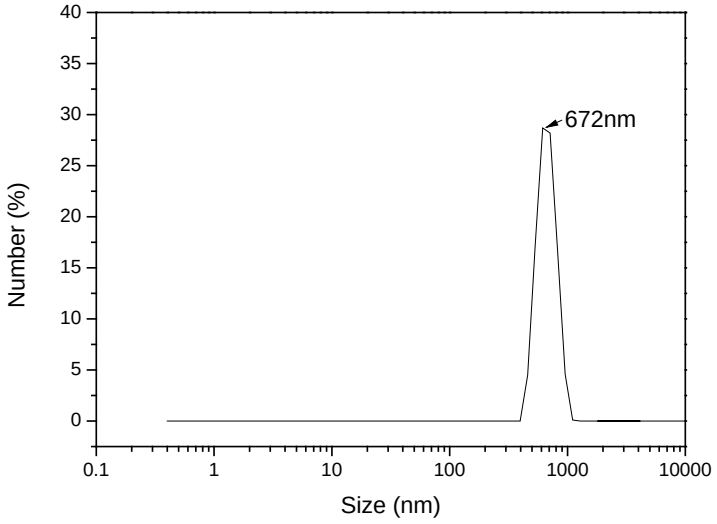

(a)

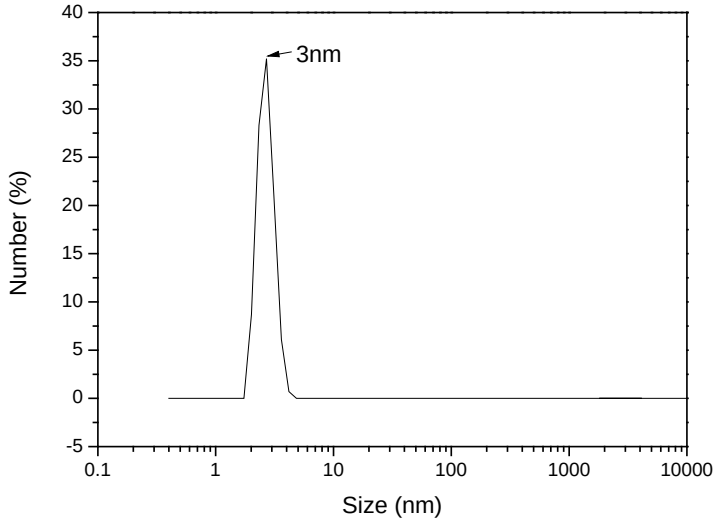

(b)

Figure 4.41. DLS data of 10 mmol·L^{-1} HEMA units in (a) BEE-DH (b) BEE-TH in 1 : 1 (v : v) mixture of ethanol and water.

Effect of crosslinker content and PEG side chain length

Figure 4.42 presents DG of membrane with varying crosslinker EGDMA content and PEG side chain length. As expected, the DG values increased with crosslinker content. Higher crosslinker content increases polymerization efficiency which is agreement with the results with bulk gel preparation (cf. Figure 4.4c in section 4.1.2). On the other hand, the DG for 12.6 mol% EGDMA increased with decreasing PEG side chain length. The membranes modified with short PEG side chain have a more efficient chain growth, which is correlated to the yield with bulk gel preparation obtained at low initiator content (cf. Figure 4.4b in section 4.1.2).

(a)

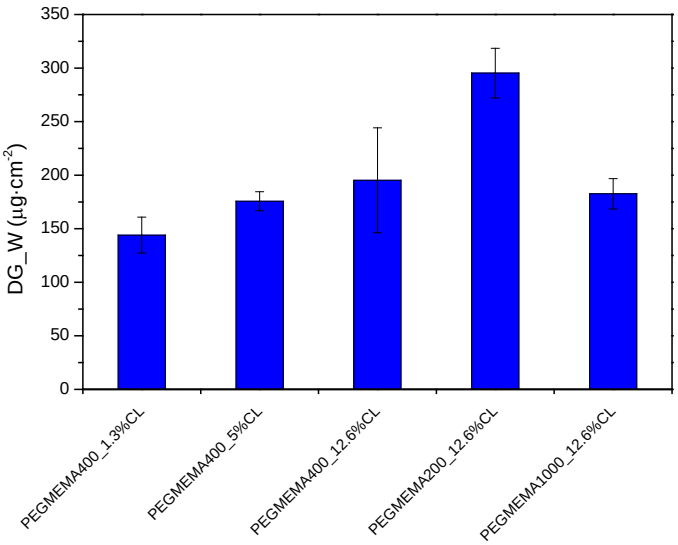

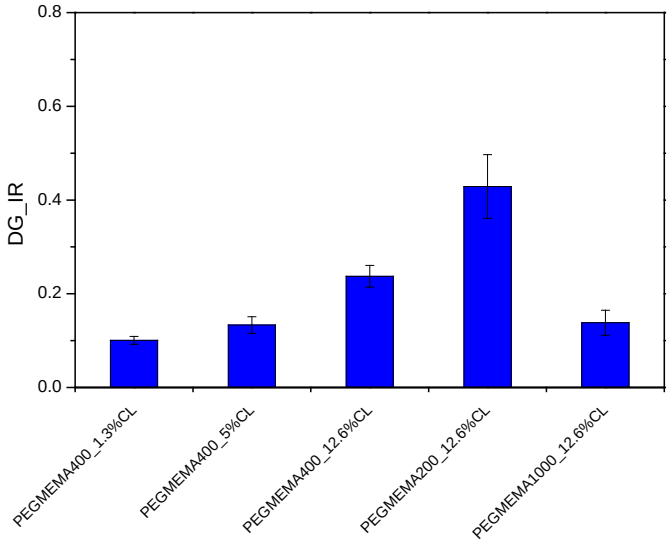

(b)

Figure 4.42. Effect of crosslinker content and PEG side chain length on (a) DG_W and (b) DG_IR in gel modified NF270 membrane prepared at 0.5 mol·L^{-1} PEGMEMA, 20 min UV irradiation and premodification using 10 mmol·L^{-1} HEMA units of BEE-TH.

The contact angles of gel modified NF270 membranes are presented in **Figure 4.43**. Generally, contact angle decreased with increasing DG due to more hydrophilic groups (PEG) on surface. **Figure 4.44** presents contact angles as function of crosslinker content and side PEG chain length. It can be seen that contact angle slightly decreased with decreasing crosslinker content probably due to the higher swelling degree of grafted gel layer in water. And longer hydrophilic PEG chains showed a lower contact angle value. This is because longer PEG chains have higher ethylene oxide content and, therefore, the resulting polymerized PEGMEMA has a relatively higher content of hydrophilic ethylene oxide units and a lower content of hydrophobic acrylate backbone units.

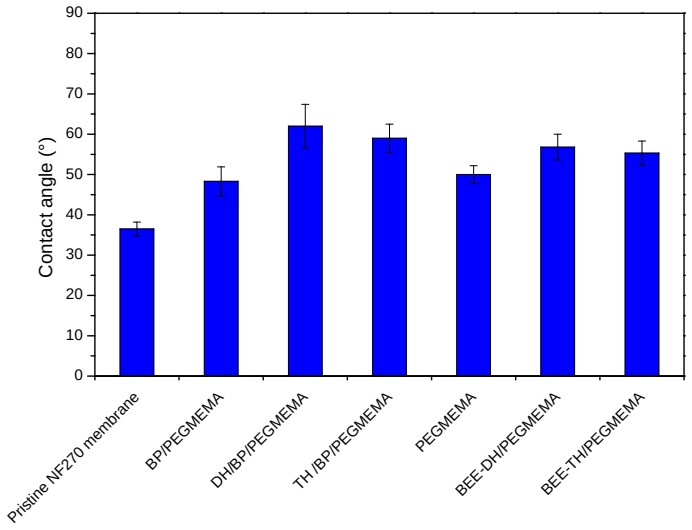

Figure 4.43. Effect of premodification on contact angle of gel modified NF270 membrane prepared at 0.5 mol·L^{-1} PEGMEMA400, EGDMA : PEGMEMA400 = 12.6 mol%, 20 min UV irradiation and premodification using 10 mmol·L^{-1} HEMA units of copolymer.

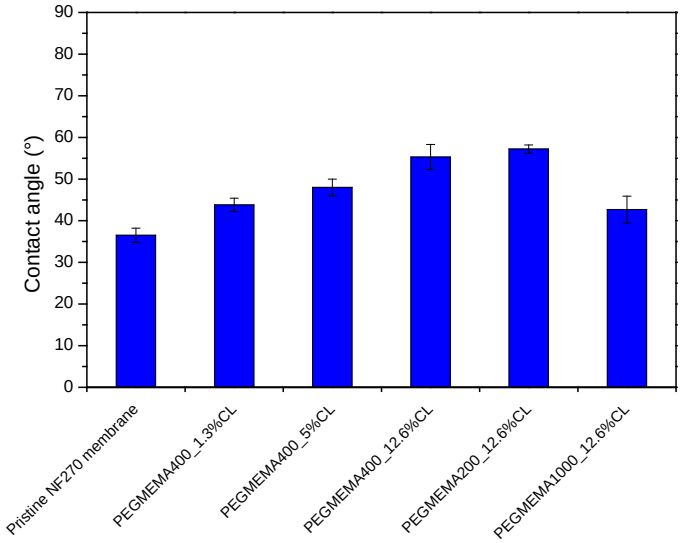

Figure 4.44. Effect of crosslinker content and PEG side chain length on contact angle in gel modified NF270 membrane prepared at 0.5 mol·L^{-1} PEGMEMA, 20 min UV irradiation and premodification using 10 mmol·L^{-1} HEMA units of BEE-TH.

NTR7450 membrane

Functionalization of NTR7450 membranes is presented in **Figure 4.45.** The amount of BEE-TH absorbed on NTR7450 membrane (~ 15 μg·cm^{-2}) was lower than that on NF270 membrane (~ 20 μg·cm^{-2}). NTR7450 membrane has much less density of negative charged groups on surface than NF270 membrane at the same pH [162, 163], it leads to less cationic groups of BEE-TH are electrostatically associating with negative charged group of NTR7450 membrane. Further, for the identical modification condition, the same concentration and UV irradiation time, NTR7450 membranes had a much higher DG. Evidently, under UV irradiation polyethersulfone backbone on top layer of NTR7450 membrane gave more starter radical than polyamide on top layer of NF270 membrane [164, 165].

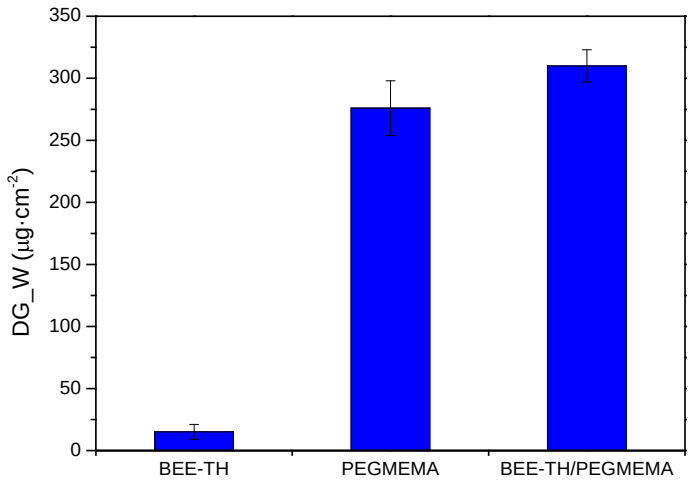

(a)

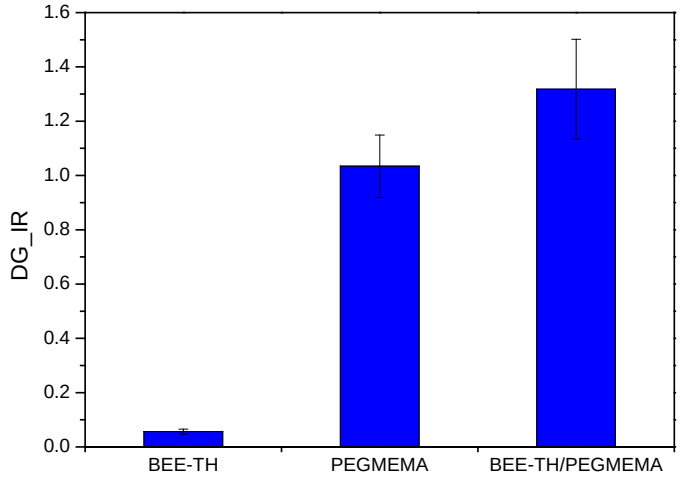

(b)

Figure 4.45. Effect of premodification on (a) DG_W and (b) DG_IR in premodified and gel modified NTR7450 membrane prepared at 0.5 mol·L^{-1} PEGMEMA, 20 min UV irradiation and premodification using 10 mmol·L^{-1} HEMA units of BEE-TH.

The contact angles of pristine, premodified and modified NTR7450 membranes are presented in **Figure 4.46**. The contact angles of NTR7450 membrane slightly decreased from 69.1 ± 2.7° to 66.0 ± 2.5° by adsorbed hydrophilic cationic BEE-TH. The influence of UV irradiation on contact angle of BEE-TH premodified NTR7450 membranes are investigated using the same procedures as with NF270 membrane. After UV irradiation this cationic reactive macroinitiator is anchored to membrane surface. Relatively similar values were observed for that of NTR7450 membrane and NF270 membrane. It indicates that macroinitiator immobilization with UV irradiation are independent on membrane chemistry. Moreover, gel modified NTR7450 have a slightly lower contact angle than gel modified NF270 membrane due to higher DG.

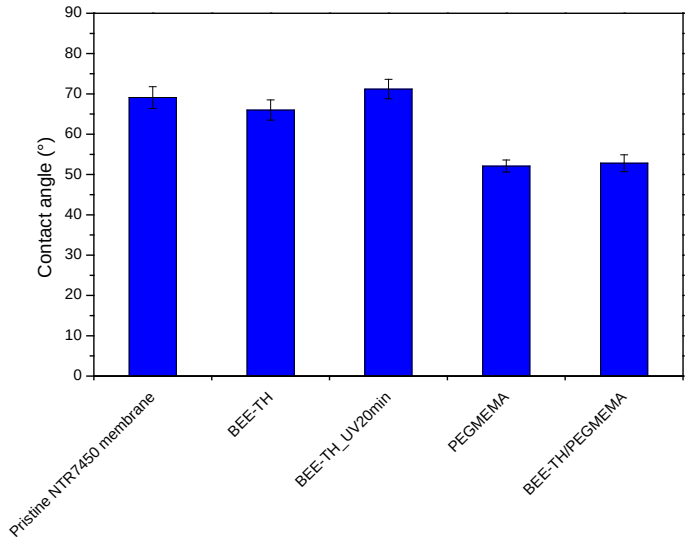

Figure 4.46. Effect of premodification on contact angle in premodified and gel modified NTR7450 membrane prepared at 0.5 mol·L^{-1} PEGMEMA, 20 min UV irradiation and premodification using 10 mmol·L^{-1} HEMA units of BEE-TH.

4.4.3 Surface charge

One of the aims of this study was to synthesize antibiofouling polymer hydrogel grafted membrane. Surface charge plays an important role in biofouling, cf. section 2.3.2. Therefore, it is important to know the membrane surface charge. The surface charge of membrane was investigated by zeta potential.

NF270 membrane

Effect of premodification

Figure 4.47 presents the zeta potential of pristine and premodified membrane. As clearly seen, the zeta potential of the pristine NF270 membrane was negative at high pH and became less negative as pH decreased, and the isoelectric point (IEP) was observed at approximately pH 3.7.

These results are in agreement with carboxylic groups ($–COO^-$) on polyamide membranes which are weakly acidic and will not be dissociated at a low pH.

Indeed, the effective surface charge of the NF270 base membrane changed to less negative and even became positive by adsorbed copolymer. IEP of membranes premodified with quaternized copolymer (TH, BEE-TH) is at pH 5.7. The strong cationic groups ($-(CH_3)_3N^+$) are completely electrostatically associating with weak acidic groups ($–COO^-$) on membrane. In contrast, IEP of membranes premodified with not quaternized copolymer DH and BEE-DH are 8.0 and 7.2 respectively. The weak cationic groups ($-(CH_3)_2N$) are incompletely associating with negative groups on membrane, part of the positive groups are exposed on surface yielding positive zeta potentials with DH and BEE-DH premodified membrane at pH 7. Schematic depiction of copolymer adsorptions was presented in **Figure 4.35**.

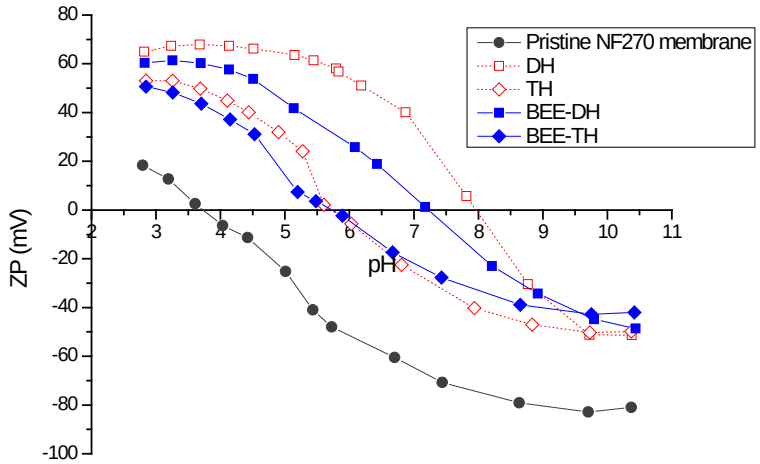

Figure 4.47. Effect of premodification on zeta potential in premodified NF270 membrane prepared at 10 $mmol \cdot L^{-1}$ HEMA units of copolymer.

Effect of photo modification

The effective surface charge of the NF270 membrane had been decreased toward neutral by grafted polymer hydrogel layers compared to base premodified membrane (**Figure 4.48**), a

promising feature for potential fouling-resistant membrane [166]. The zeta potentials became less negative with increasing DG (e.g. compare PEGMEMA ~ 201 μg/cm^2 and BP/PEGMEMA ~ 279 μg/cm^2) which is also related to increasing UV time (**Figure 4.49**). The higher DG will diminish higher surface charge. This phenomenon agrees with previously reported ZP of photo grafted polyamide membrane where absolute value decreases with increasing DG of gel layer [15].

Figure 4.50 presents zeta potential of membranes as functions of crosslinker EGDMA content and PEG side chain length. The IEP of modified membrane increased with increasing crosslinker content. The lower crosslinker content in the gel layer increases the thickness of the swelling layers, which leads to a shear plane shifted towards the solution bulk and results in a lower zeta potential [167]. Conflicting with the above results, membrane modified using PEGMEMA200 which had a higher DG showed a higher surface charge, it is probably due to positively charged segments of macroinitiator which had diffused to the interface.

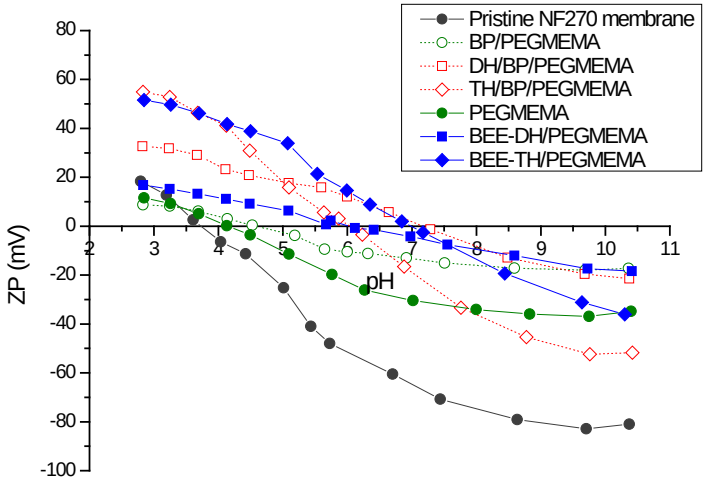

Figure 4.48. Effect of premodification on zeta potential of gel modified NF270 membrane prepared at 0.5 mol·L^{-1} PEGMEMA400, EGDMA : PEGMEMA400 = 12.6 mol%, 20 min UV irradiation and premodification using 10 mmol·L^{-1} HEMA units of copolymer.

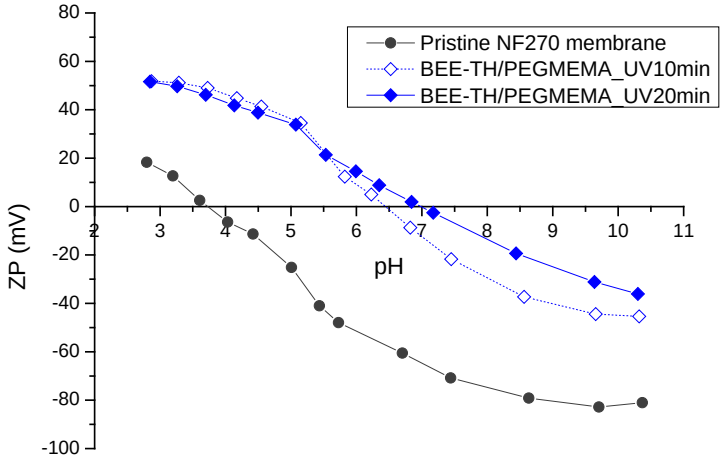

Figure 4.49. Effect of UV irradiation time on zeta potential in gel modified NF270 membrane prepared at 0.5 mol·L^{-1} PEGMEMA400, EGDMA: PEGMEMA400 = 12.6 mol%, and premodification using 10 mmol·L^{-1} HEMA units of BEE-TH.

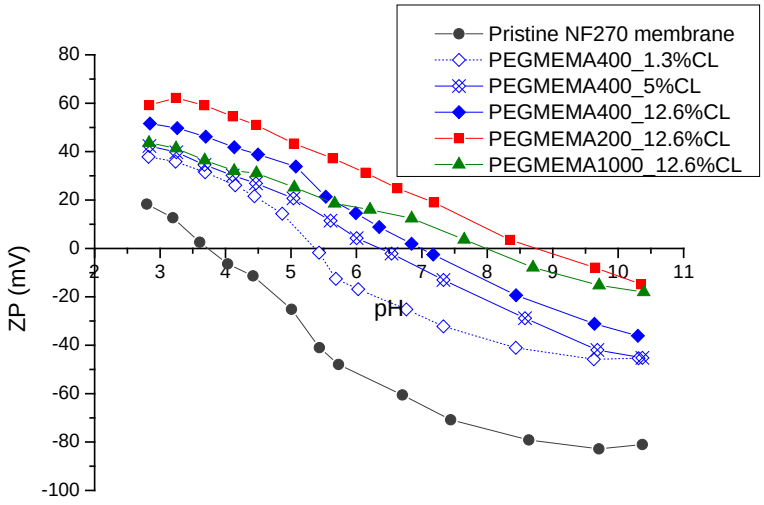

Figure 4.50. Effect of crosslinker content and PEG side chain length on zeta potential in gel modified NF270 membrane prepared at 0.5 mol·L^{-1} PEGMEMA, 20 min UV irradiation and premodification using 10 mmol·L^{-1} HEMA units of BEE-TH.

NTR7450 membrane

Figure 4.51 presents the zeta potential of pristine, premodified and modified NTR7450 membranes. The surface of pristine NTR7450 membranes had a negative charge over the entire pH range studied, and the absolute values decreased to acidic pH values. Sulfonic acid groups ($-SO_3^-$) on NTR 7450 membrane surface are strongly acidic and are completely dissociated over nearly the entire pH range. The IEP of BEE-TH premodified membrane is at pH 7.6. According to the theory of Lewis acids and bases, the strong positive groups ($-(CH_3)_3N^+$) are incompletely electrostatic associating with strong acidic groups ($-SO_3^-$) on membrane, part of positive group are exposed on surface to exhibit positive zeta potentials at pH 7. The ZP curve of gel modified membrane showed a same tendency with base membrane, different with premodified membrane. It reflects that the surface behaviors are also dependent on raw base membrane. Furthermore, the effective surface charge became lower with increasing DG (compare PEGMEMA ~ 276 $\mu g \cdot cm^{-2}$ and BEE-TH_/PEGMEMA ~ 310 $\mu g \cdot cm^{-2}$). This phenomenon has also been reported by Susanto et al. with photo grafted polyethersulfone membrane [14].

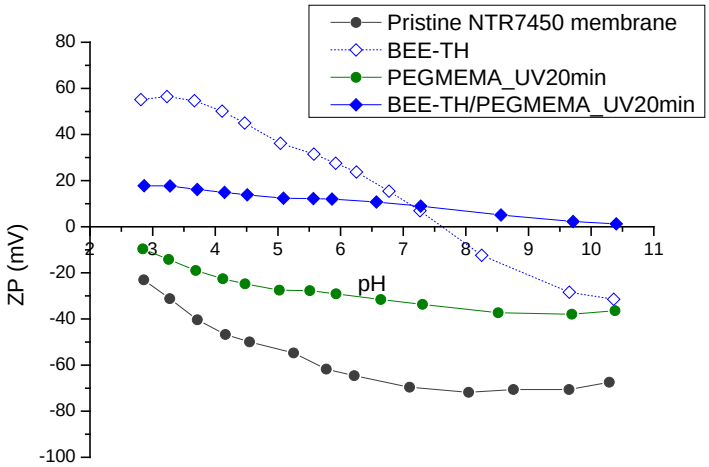

Figure 4.51. Effect of premodification on zeta potential in premodified and gel modified NTR7450 membrane prepared at 0.5 $mol \cdot L^{-1}$ PEGMEMA400**,** 20 min UV irradiation and premodification using 10 $mmol \cdot L^{-1}$ HEMA units of BEE-TH.

4.4.4 Water permeability and salt rejection

Performance of NF270 membrane

Effect of premodification

As seen in **Figure 4.52**, the water permeability of the premodified NF270 membranes decreased, while its salts rejection increased. Lower water flux is typically accompanied by increased NaCl rejection due to the inverse relationship between permeability and selectivity [163, 164].

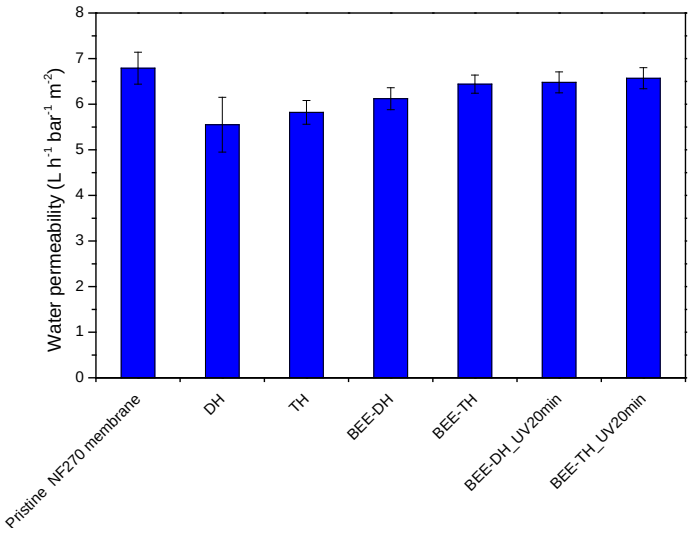

(a)

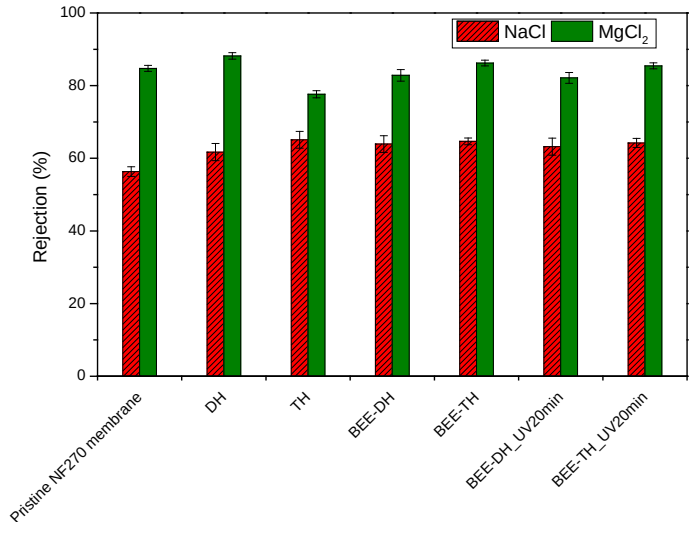

(b)

Figure 4.52. Effect of premodification on (a) water permeability and (b) salt rejection in premodified NF270 membrane prepared at 10 mmol·L^{-1} HEMA units of copolymer.

Effect of photo modification

The water permeability and salts rejection of NF270 membranes modified with 20 min UV irradiation are presented in **Figure 4.53**. Modification using BEE-TH premodified membrane caused a 46% relative decrease in water permeability, 17% relative increase in NaCl rejection and 7% relative increase $MgCl_2$ rejection, while modifaction with PEGMEMA produced a modified membrane with 55% lower water permeability, 41% relative higher NaCl rejection and 13% relative higher than $MgCl_2$ rejection than the pristine membrane. Modification using BEE-DH premodified membrane resulted in a larger decrease in water permeability and increase in salt rejection than that obtained with the BEE-TH premodified membrane. Modification with BP system resulted in 74 – 85% relative decrease in water permeability, 11% – 29% relative increase in NaCl rejection and 2% – 7% relative increase in $MgCl_2$ rejection. Surface modifications causing decreases in water permeability similar to those results also observed in previous studies. For example, Sagle et al. reported 35 – 40% relative decrease in water permeability observed for PEG based hydrogel coated membranes [15], Bernstein et al. reported 20 – 40% relative decrease in water permeability observed for polyHEMA-grafted membranes [168], Belfer et al. reported up to 25% relative decrease in water permeability for polyamide membranes grafted with polyPEGMA) [66], Louie et al. reported up to an 80% relative decrease in water permeability for polyamide membranes coated with polyether–polyamide [151] and Mickols reported 68 – 84 % relative decrease in water permeability for polyamide membranes chemically grafted with PEG diepoxide [169]. Moreover surface modifications that reduce flux often increase rejection [15, 66, 151, 169], so the increase in rejection accompanying surface modification with polyPEGMEMA gel is reasonable. Increasing rejection could be explained as the result of plugging surface defects in the polyamide membrane by gel layer, or possibly as the result of gel layer interacting with and influencing the chemistry and transport properties of the polyamide membrane [15, 65, 66]. Polyamide membranes contains low levels of defects [65], the

grafted hydrogel layer may seal these defects and decrease salts penetration through the membrane. On the other hand, due to less effective charge on the modified membrane compared to pristine membrane, less amounts of salt can be accumulated on the modified membrane surface, which means a lower concentration polarization. In addition, the decrease in water permeability typically decreases concentration polarization. Decreasing concentration polarization will result in increasing salt rejection [170].

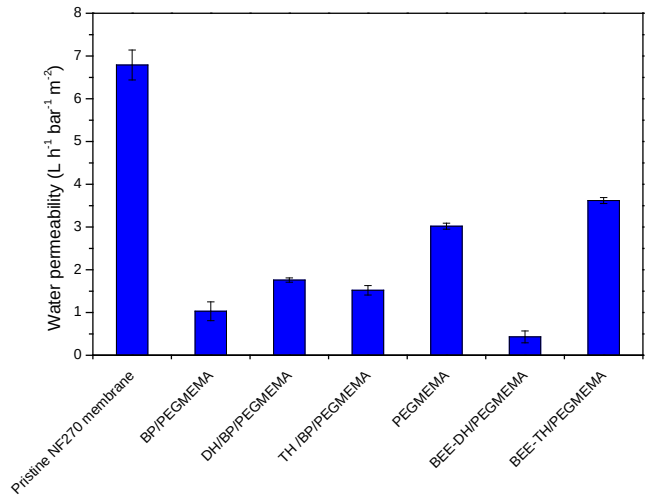

(a)

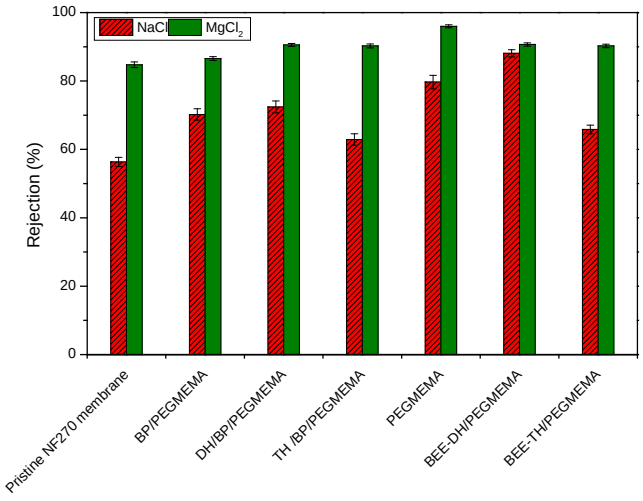

(b)

Figure 4.53. Effect of premodification on (a) water permeability and (b) salt rejection in gel modified NF270 membrane prepared at 0.5 mol·L^{-1} PEGMEMA400, EGDMA : PEGMEMA400 = 12.6 mol%, 20 min UV irradiation and premodification using 10 mmol·L^{-1} HEMA units of copolymer.

The performances of membrane modified with 10 min UV irradiation are presented in **Figure 4.54**. Surface modification with 10 min UV irradiation showed a less decrease in water permeability and increase in salts rejection than that obtained with 20 min irradiation. It could be also explained by plugging surface defects and the effect of concentration polarization. Lower amount of gel layer on membrane could less effectively plug defects and have a higher concentration polarization on membrane surface; these factors could contribute to a lower decrease in water permeability and increase in salts rejection.

The influences of crosslinker content and PEG chain length on membrane performances are presented in **Figure 4.55**. It is clearly seen that modification with lower crosslinker content which had a lower DG had less impact on membrane performances. This phenomenon had also been observed by other authors [14]. In addition, modification with shorter PEG chain which had a higher DG exhibited lower water permeability and higher salt rejection than that obtained with longer PEG chain. These results indicate that higher DG has a larger influence on membrane performance.

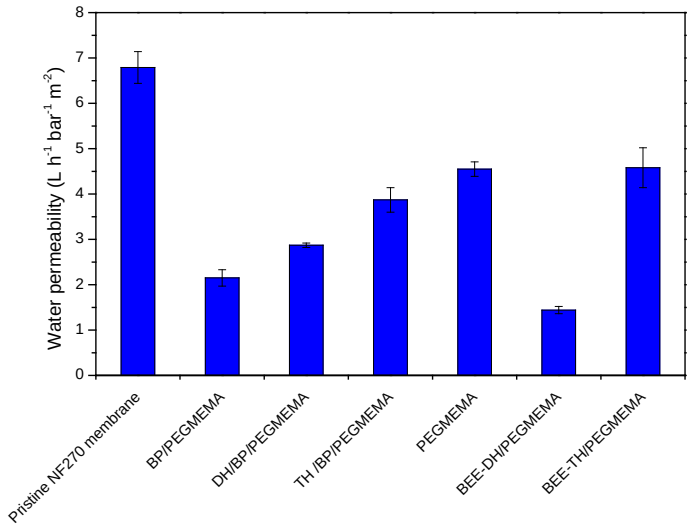

(a)

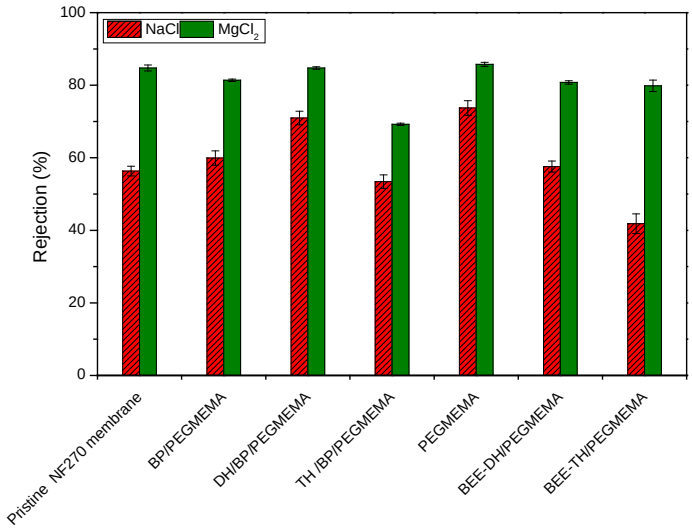

(b)

Figure 4.54. Effect of premodification on (a) water permeability and (b) salt rejection in gel modified NF270 membrane prepared at 0.5 mol·L^{-1} PEGMEMA400, EGDMA : PEGMEMA400 = 12.6 mol%, 10 min UV irradiation and premodification using 10 mmol·L^{-1} HEMA units of copolymer.

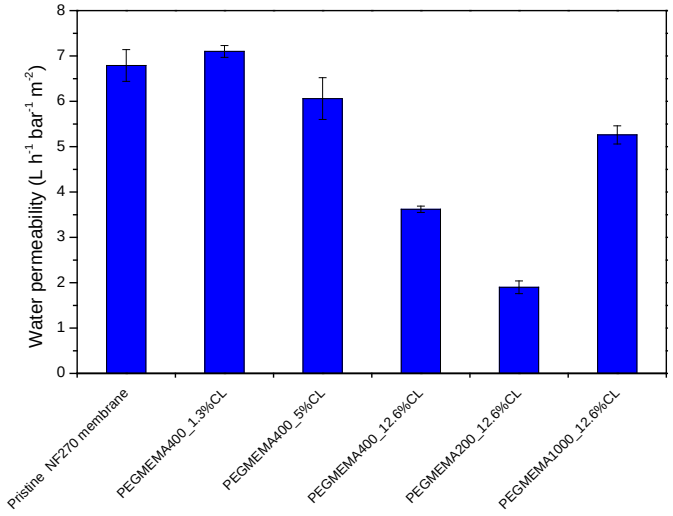

(a)

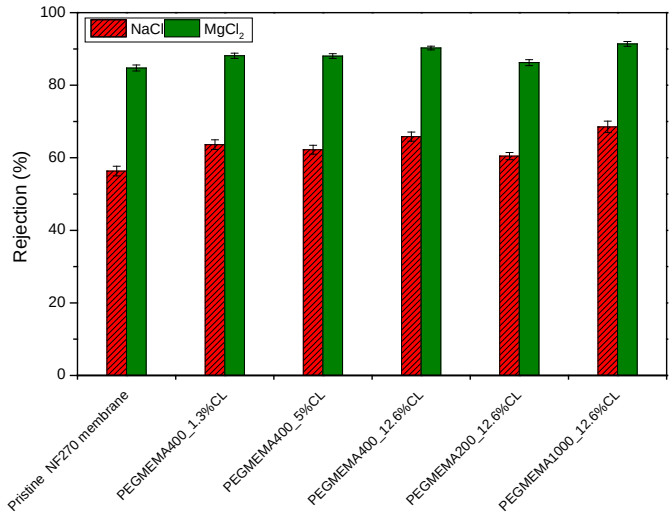

(b)

Figure 4.55. Effect of crosslinker content and PEG side chain length on (a) water permeability and (b) salt rejection in gel modified NF270 membrane prepared at 0.5 mol·L^{-1} PEGMEMA, 20 min UV irradiation and premodification using 10 mmol·L^{-1} HEMA units of BEE-TH.

Performance of NTR7450 membrane

The performances of pristine, premodified and modified NTR7450 membranes are presented in **Figure 4.56**. Compared to NF270 membrane, the water permeability and salt rejection of NTR7450 membrane largely decreased by absorbed BEE-TH. The particle sizes of BEE-TH in solution are ranging from 2 nm to 4 nm, cf. Figure 4.41.. Some segments of small particles can diffuse into or block the pores of active layer on NTR7450 membrane with large pores of 1.4 nm diameter [163] while have a less effect on that of NF 270 membrane with small pores of 0.7 nm [163]. And it results in a decrease in water permeability companying with an increase in $MgCl_2$ rejection. However NaCl rejection decreased due to less Donnan exclusion with reduction of the electrostatic repulsion between monovalent Cl^- and less charged modified membrane surface, cf. section 2.1. Nevertheless, this repulsion is less worth considerable with existing divalent Mg^{2+}. Moreover, the water permeability of membrane modified with UV irradiation became nearly invisible. Because photodegraded polyethersulfone backbone on the top active layer of NTR7450 membrane in combination with macroinitiator produces a highly crosslinked barrier layer is loses its desired function. However, there was minimal change in salt rejection. It indicates that this denser layer do not support to improve salt rejection. Because the very low permeability, further fouling studies were not performed.

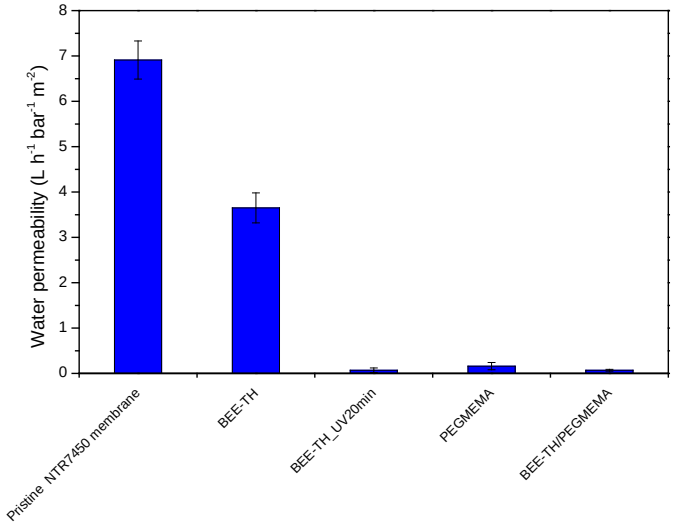

(a)

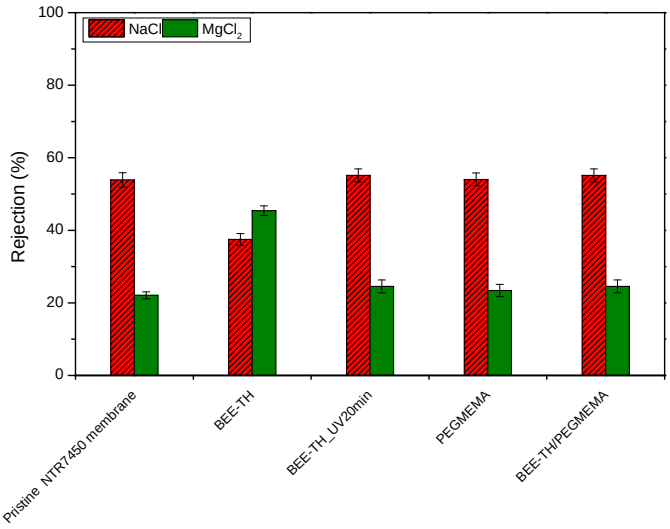

(b)

Figure 4.56. Effect of premodification on (a) water permeability and (b) salt rejection in premodified and gel modified NTR7450 membrane prepared at 0.5 mol·L^{-1} PEGMEMA, 20 min UV irradiation and premodification using 10 mmol·L^{-1} HEMA units of BEE-TH.

4.5 Fouling performance of membranes

As mentioned in section 2.1, fouling on membrane results in declined permeate flux and selectivity. Protein fouling of membranes can be affected by the membrane material, its pore size and pore size distribution. NF and RO membranes are fouled by accumulating foulant cake layer [171], its fouling mechanism is related to membrane physical-chemical properties, i.e. smoother and more hydrophilic surface and those with favorable electrostatic repulsion experienced less initial fouling [172]. Moreover, it is important to note that protein fouling is also highly dependent on solution chemistry (i.e. pH, ionic strength and solute [172-174]) and hydrodynamic conditions [172] .

Static protein sorption and dynamic filtration experiments were used to evaluate the water permeability of pristine, premodified and modified NF270 membranes, as presented in **Figure 4.57**. All premodified and gel modified membranes showed lower irreversible protein fouling than pristine membrane. In contrast, Lys showed a higher water permeability decrease than BSA, this result agrees well with previously reported study [173]. NF270 membrane has a negatively charged surface, which helps to attract positively charged Lys molecule at pH 7.4 (below the IEP 10.7 [175]) while less or no attractive electrostatic interactions occur with neutral BSA molecule at pH 4.8 (equal to IEP 4.8 [176]). Simultaneously, Lys with smaller size could facile permeate through grafted layer and thus foul the active layer of membrane.

It is also interesting to observe that the water permeability of premodified membranes were even increased in most case, which suggests that BEE-TH may partially detach from grafted layer during protein sorption and filtration and results in retrieving lost permeability due to covered layer. However, water permeability still reduced after static BSA sorption. Neutral BSA molecule with static sorption has a less impact on BEE-TH detachment. Furthermore, there was minimal change in water permeability with protein sorption observed between the unirradiated and UV irradiated premodified membrane, while treatment with protein filtration using unirradiated membrane produce a remarkable increase in water permeability. As mentioned in section 4.4,

BEE-TH was anchored to membrane surface by UV irradiation, and more stable on membrane surface than that without UV irradiation. This less stable BEE-TH layer on unirradiated membrane could be substantial detached and result in an increase in water permeability.

Small reductions in water permeability were observed for gel modified membranes. Hydrogel layer which is relatively hydrophilic and less charge (c.f. section 4.4) could deter significant hydrophobic and electrostatic interactions, which would cause adhesion of the protein to the membrane surface to fail. In addition, modification with 1.3% crosslinker had a relatively small decrease in water permeability than that obtained with 12.6% crosslinker. It refers to a loose network results in more protein permeating through gel layer and accumulating on membrane barrier layer surface.

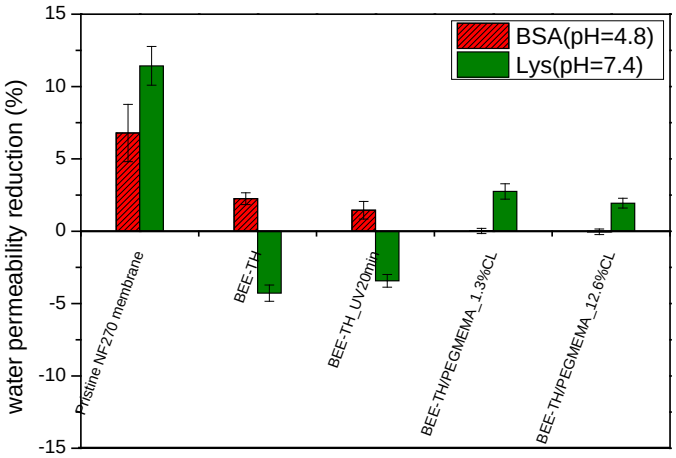

(a)

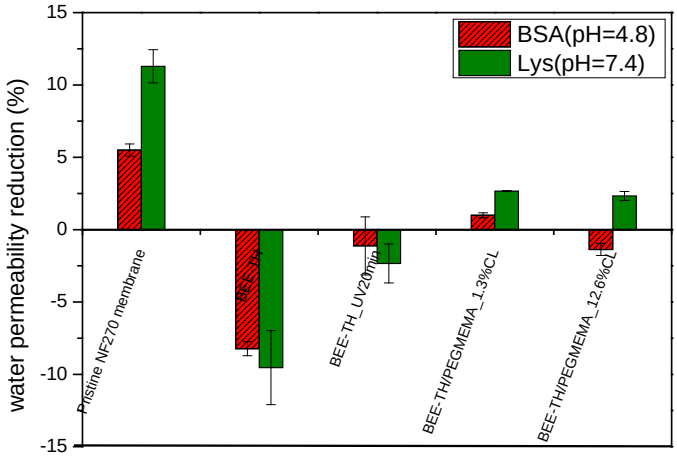

(b)

Figure 4.57. Fouling with (a) protein sorption and (b) protein filtration on water permeability reduction in premodified and gel modified NF270 membrane prepared at 0.5 mol·L^{-1} PEGMEMA, 20 min UV irradiation and premodification using 10 mmol·L^{-1} HEMA units of BEE-TH.

Figure 4.58 presents NaCl rejection relative reduction of pristine, premodified and modified NF270 membranes ranging from -13% and 6%. These changes on salt rejection are relatively small. Generally, NaCl rejection increased with decreasing water permeability, which is agreement with the results of section 4.4.4.

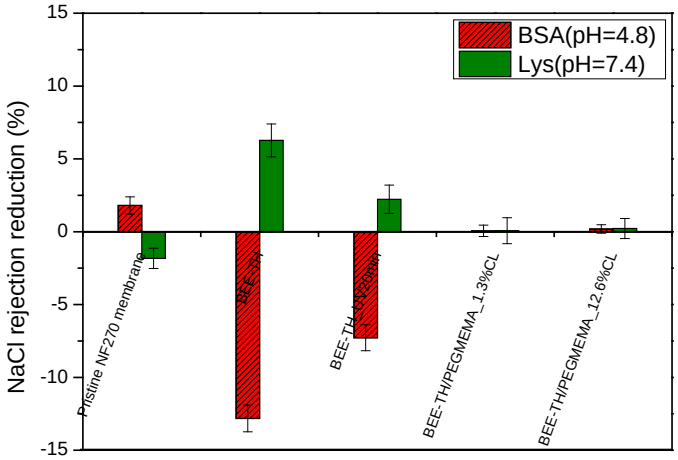

(a)

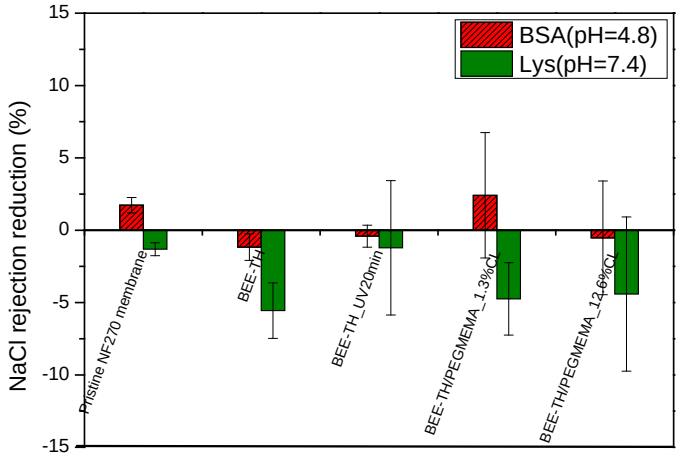

(b)

Figure 4.58. Fouling with (a) protein sorption and (b) protein filtration on NaCl rejection reduction in premodified and gel modified NF270 membrane prepared at 0.5 $mol \cdot L^{-1}$ PEGMEMA, 20 min UV irradiation and premodification using 10 $mmol \cdot L^{-1}$ HEMA units of BEE-TH.

Chapter 5 Conclusions

In this work, the use of hydrogels as coating materials for reducing biofouling in desalination membranes was explored. Preparation and characterization of bulk gel was firstly done; then examination of potential of reducing biofouling on surface anchored gel; and finally surface modification of desalination membrane.

A series of crosslinked polyPEGMEMA gels was prepared with three PEG side chain lengths and by varying monomer, crosslinker monomer and initiator concentrations. The chemical structure of the gels was characterized by FTIR spectroscopy and solid state NMR techniques. It was found that a small fraction of incompletely reacted crosslinker was present in all hydrogels. The gels containing a longer PEG side group showed less complete reaction. Nevertheless, the content of resulting dangling double bonds (estimated to be less than 5 mol% for the typical preparations) was low enough and could be ignored in calculations of mesh size from swelling data.

The swelling measurements indicated that the monomer and crosslinker concentrations are two parameters that have a dominant influence on the swelling degree of polyPEGMEMA200 and 400 gels at high monomer conversion. The equilibrium gel swelling properties were dependent on the internal network structure. The gels that had higher crosslinker content showed lower swelling. Comparison of two estimates of network mesh size based on gel swelling and rheological behavior showed that the mesh sizes estimated from rheology were about 4 times higher, but a good correlation between both sets of data was observed for polyPEGMEMA200 and 400 gels for different crosslinker contents. Because of the very high swelling, the rubber elasticity model used for calculations of mesh size from G' values seemed not to be applicable. For the same preparation conditions, polyPEGMEMA400 had the largest mesh size, which was apparently related to the higher water uptake per monomer unit due to longer PEG side chain than for polyPEGMEMA200. However, for polyPEGMEMA1000 both swelling and rheology data indicated that physical crosslinks, presumably originating from side chain entanglement,

produced an additional cross-linking effect that was significantly more pronounced than for the other two monomers. These interpretations had been confirmed by the partition coefficients for three model proteins with different size. Size exclusion, as quantified by the protein partitioning coefficient, was well correlated with the degree of chemical crosslinking and protein size for polyPEGMEMA200 and polyPEGMEMA400 while the protein partitioning for polyPEGMEMA1000 was smaller and almost independent of chemical crosslinking. On the other hand, good correlation between protein partitioning and G' had been observed because both data are directly reflecting the influences of chemical as well as physical crosslinking.

Gel films were anchored to glass slides by modifying glass with methacrylate-capped alkoxy-silane prior to gel layer synthesis. The gel thickness was controlled by preparing the gel in a thin gap between two slides. Contact angle measurements indicated that the gel surfaces are hydrophilic, which could be potentially useful for making antibiofouling surfaces. Bacterial deposition was significantly reduced on polyPEGMEMA gel surface. Biofilm growth occurred only on glass used as a reference material, while just very few bacteria were observed on the gel samples. Moreover, the gels containing a longer PEG side group showed a stronger resistance toward bacterial deposition.

Cationic and photoreactive macroinitiator had been designed that can be readily adsorbed onto negatively charged membrane though electrostatic interaction and subsequently used to anchor gel layer to membrane surface. Cationic and nonionic copolymer were synthesized from DMAEMA and HEMA copolymerization with high conversions, as determined by ^{1}H NMR spectroscopy. Macroinitiator immobilization and surface initiated grafting of gel layer on membrane was confirmed by observable change in ATR−IR spectra after modification. The conditions for copolymer immobilization had been optimized. Macroinitiator immobilization was significantly affected by its charge, where higher amount of quaternized copolymer are immobilized on membrane through stable and strong electrostatic interaction. Moreover NTR7450 membrane showed a lower BEE-TH adsorption due to less negatively charged groups

on the top layer compared to NF270 membrane. Various factors affecting photo-grafting efficiency, surface-selectivity and grafting controllability such as premodification conditions with macroinitiator, UV irradiation time, crosslinker content, PEG side chain length, and membrane chemistry have been investigated in detail. The copolymer layer adsorbed on NF270 membrane surface can trap UV-generated radicals and results in less DG. Longer UV time, higher crosslinker content and shorter PEG chain length increased DG which is due to to more effectively polymerization. Results obtained from modification of NTR7450 membrane suggest that radicals of polyethersulfone by obtained by direct UV excitation reacted with added compound which was essential to disable the function of barrier layer. The modifications could also change the membrane characteristics with respect to the membrane surface charge, surface hydrophilicity, and performance. The ZP data indicated that all premodified and modified membranes were less negative charged, and it supports the interpretation of contact angle data with respect to coverage of the outer membrane surface. Grafted gel layer changed the chemistry and transport properties of modified membrane, the latter probably by plugging surface defects with gel layer. The tests of membrane performance observed the decrease water permeability which is related to DG and the increase in salt rejection with modification. It could be explained as the result of plugging surface defects on membrane surface with gel layer and changing chemistry and transport properties of membrane by grafted gel layer. All gel modified NF270 membranes demonstrated lower protein fouling tendencies than the pristine membrane. However, biofoulign studies with the membranes are still to be done.

Overall, these works provide the basis for the development of the anchored photo-grafting antibiofouling hydrogel coatings on membranes and other materials.

References

[1] H. C. Flemming, *Biofouling in water systems – cases, causes and countermeasures.* Applied Microbiology and Biotechnology, 2002, 59, 629-640.

[2] H. Ivnitsky, I. Katz, D. Minz, G. Volvovic, E. Shimoni, E. Kesselman, R. Semiat, and C.G. Dosoretz, *Bacterial community composition and structure of biofilms developing on nanofiltration membranes applied to wastewater treatment.* Water Research, 2007, 41, 3924-3935.

[3] H. Kobayashi and Y. Ikacia, *Corneal cell adhesion and proliferation on hydrogel sheets bound with cell-adhesive proteins.* Current Eye Research, 1991, 10, 899-908.

[4] Y. Tatekawa, Y. Ikada, H. Komuro, and M. Kaneko, *Experimental repair of tracheal defect using a bioabsorbable copolymer.* Journal of Surgical Research, 2010, 160, 114-121.

[5] M. Herzberg and M. Elimelech, *Biofouling of reverse osmosis membranes: Role of biofilm-enhanced osmotic pressure.* Journal of Membrane Science, 2007, 295, 11-20.

[6] R. P. Schneider, L. M. Ferreira, P. Binder, E. M. Bejarano, K. P. Góes, E. Slongo, C. R. Machado, and G. M. Z. Rosa, *Dynamics of organic carbon and of bacterial populations in a conventional pretreatment train of a reverse osmosis unit experiencing severe biofouling.* Journal of Membrane Science, 2005, 266, 18-29.

[7] E. Kujundzic, A. Cristina Fonseca, E. A. Evans, M. Peterson, A. R. Greenberg, and M. Hernandez, *Ultrasonic monitoring of earlystage biofilm growth on polymeric surfaces.* Journal of Microbiological Methods, 2007, 68, 458-467.

[8] J. S. Vrouwenvelder, M. C. M. van Loosdrecht, and J. C. Kruithof, *Early warning of biofouling in spiral wound nanofiltration and reverse osmosis membranes.* Desalination, 2011, 265, 206-212.

[9] A. Al-Amoudi and R. W. Lovitt, *Fouling strategies and the cleaning system of NF membranes and factors affecting cleaning efficiency.* Journal of Membrane Science, 2007, 303, 4-28.

[10] A. Rosenhahn, S. Schilp, H. J. Kreuzer, and M. Grunze, *The role of 'inert' surface chemistry in marine biofouling prevention.* Physical Chemistry Chemical Physics, 2010, 12, 4275-4286.

[11] E. Ostuni, R. G. Chapman, R. E. Holmlin, S. Takayama, and G. M. Whitesides, *A survey of structure−property relationships of surfaces that resist the adsorption of protein.* Langmuir, 2001, 17, 5605-5620.

[12] E. Ostuni, R. G. Chapman, M. N. Liang, G. Meluleni, G. Pier, D. E. Ingber, and G. M. Whitesides, *Self-assembled monolayers that resist the adsorption of proteins and the adhesion of bacterial and mammalian cells.* Langmuir, 2001, 17, 6336-6343.

[13] G. Kang, M. Liu, B. Lin, Y. Cao, and Q. Yuan, *A novel method of surface modification on thin-film composite reverse osmosis membrane by grafting poly(ethylene glycol).* Polymer, 2007, 48, 1165-1170.

[14] H. Susanto and M. Ulbricht, *Photografted thin polymer hydrogel layers on pes ultrafiltration membranes: Characterization, stability, and influence on separation performance.* Langmuir, 2007, 23, 7818-7830.

[15] A. C. Sagle, E. M. Van Wagner, H. Ju, B. D. McCloskey, B. D. Freeman, and M. M. Sharma, *PEG-coated reverse osmosis membranes: Desalination properties and fouling resistance.* Journal of Membrane Science, 2009, 340, 92-108.

[16] E. Kulik and Y. Ikada, *In vitro platelet adhesion to nonionic and ionic hydrogels with different water contents.* Journal of Biomedical Materials Research, 1996, 30, 295-304.

[17] J. D. Mendelsohn, S. Y. Yang, J. A. Hiller, A. I. Hochbaum, and M. F. Rubner, *Rational design of cytophilic and cytophobic polyelectrolyte multilayer thin films.* Biomacromolecules, 2002, 4, 96-106.

[18] T. Ekblad, G. Bergstrolm, T. Ederth, S. L. Conlan, R. Mutton, A. S. Clare, S. Wang, Y. Liu, Q. Zhao, F. DaSouza, G. T. Donnelly, P. R. Willemsen, M. E. Pettitt, M. E. Callow, J. A. Callow, and B. Liedberg, *Poly(ethylene glycol)-containing hydrogel surfaces for antifouling applications in marine and freshwater environments.* Biomacromolecules, 2008, 9, 2775-2783.

[19] Q. Yang, N. Adrus, F. Tomicki, and M. Ulbricht, *Composites of functional polymeric hydrogels and porous membranes.* Journal of Materials Chemistry, 2011, 21, 2783-2811.

[20] H. Ju, B. D. McCloskey, A. C. Sagle, V. A. Kusuma, and B. D. Freeman, *Preparation and characterization of crosslinked poly(ethylene glycol) diacrylate hydrogels as fouling-resistant membrane coating materials.* Journal of Membrane Science, 2009, 330, 180-188.

[21] L. F. Greenlee, D. F. Lawler, B. D. Freeman, B. Marrot, and P. Moulin, *Reverse osmosis desalination: Water sources, technology, and today's challenges.* Water Research, 2009, 43, 2317-2348.

[22] R. J. Petersen, *Composite reverse osmosis and nanofiltration membranes.* Journal of Membrane Science, 1993, 83, 81-150.

[23] C. Y. Tang, Y. N. Kwon, and J. O. Leckie, *Effect of membrane chemistry and coating layer on physiochemical properties of thin film composite polyamide RO and NF membranes: I. FTIR and XPS characterization of polyamide and coating layer chemistry.* Desalination, 2009, 242, 149-167.

[24] K. Wang, J. P. Chen, Y.T. Hung, N. K. Shammas, *Membrane and desalination technologies.* 2011, New York, Springer.

[25] M. C. Porter, *Handbook of industrial membrane technology*. 1988, New Jersey, Noyes.

[26] J. Wagner, *Membrane filtration handbook practical tips and hints*. 2001, Osmonics, Inc.

[27] M. Mulder, *Basic principles of membrane technology*. second edition. 1996, Netherlands, Kluwer academic publishers.

[28] W. R. Bowen and H. Mukhtar, *Characterisation and prediction of separation performance of nanofiltration membranes.* Journal of Membrane Science, 1996, 112, 263-274.

[29] R. Levenstein, D. Hasson, and R. Semiat, *Utilization of the donnan effect for improving electrolyte separation with nanofiltration membranes.* Journal of Membrane Science, 1996, 116, 77-92.

[30] W. J. Koros, Y. H. Ma, and T. Shimidzu, *Terminology for membranes and membrane processes* Journal of Membrane Science, 1996, 120, 149-159.

[31] H. S. Vrouwenvelder, J. A. M. van Paassen, H. C. Folmer, J. A. M. H. Hofman, M. M. Nederlof, and D. van der Kooij, *Biofouling of membranes for drinking water production.* Desalination, 1998, 118, 157-166.

[32] J. S. Vrouwenvelder, J. W. N. M. Kappelhof, S. G. J. Heijrnan, J. C. Schippers, and D. van der Kooija, *Tools for fouling diagnosis of NF and RO membranes and assessment of the fouling potential of feed water.* Desalination, 2003, 157, 361-365.

[33] C. Jarusutthirak, S. Mattaraj, and R. Jiraratananon, *Influence of inorganic scalants and natural organic matter on nanofiltration membrane fouling.* Journal of Membrane Science, 2007, 287, 138-145.

[34] B. Van der Bruggen, L. Braeken, and C. Vandecasteele, *Flux decline in nanofiltration due to adsorption of organic compounds.* Separation and Purification Technology, 2002, 29, 23-31.

[35] A. S. Al-Amoudi and A. M. Farooque, *Performance restoration and autopsy of NF membranes used in seawater pretreatment.* Desalination, 2005, 178, 261-271.

[36] H. Huiting, J. W. N. M. Kappelhof, and T. G. J. Bosklopper, *Operation of NF/RO plants: From reactive to proactive.* Desalination, 2001, 139, 183-189.

[37] A. E. Williams, L. J. Lund, J. A. Johnson, and Z. J. Kabala, *Natural and anthropogenic nitrate contamination of groundwater in a rural community, california*. Environmental Science & Technology, 1998, 32, 32-39.

[38] B. Gottenbos, H. C. van der Mei, and H. J. Busscher, *Models for studying initial adhesion and surface growth in biofilm formation on surfaces*, in *Methods in enzymology*, J.D. Ron, 1999, Academic Press. 523-534.

[39] A. Roosjen, W. Norde, H. van der Mei, and H. Busscher, *The use of positively charged or low surface free energy coatings versus polymer brushes in controlling biofilm.* Progress in Colloid and Polymer Science, 2006, 132, 138-144.

[40] Y. H. An and R. J. Friedman, *Concise review of mechanisms of bacterial adhesion to biomaterial surfaces.* Journal of Biomedical Materials Research, 1998, 43, 338-348.

[41] M. Shen, M. S. Wagner, D. G. Castner, B. D. Ratner, and T. A. Horbett, *Multivariate surface analysis of plasma-deposited tetraglyme for reduction of protein adsorption and monocyte adhesion†.* Langmuir, 2003, 19, 1692-1699.

[42] M. W. A. Skoda, F. Schreiber, R. M. J. Jacobs, J. R. P. Webster, M. Wolff, R. Dahint, D. Schwendel, and M. Grunze, *Protein density profile at the interface of water with oligo(ethylene glycol) self-assembled monolayers.* Langmuir, 2009, 25, 4056-4064.

[43] M. C. van Loosdrecht, J. Lyklema, W. Norde, and A. J. Zehnder, *Bacterial adhesion: A physicochemical approach.* Microbial Ecology, 1989, 17, 1-15.

[44] M. C. van Loosdrecht, J. Lyklema, W. Norde, G. Schraa, and A. J. Zehnder, *Electrophoretic mobility and hydrophobicity as a measured to predict the initial steps of bacterial adhesion.* Applied and Environmental Microbiology, 1987, 53, 1898-1901.

[45] A. M. B. J. Vitte, A. Pierres and P. Bongrand, *Is there a predictable relationship between surface physical-chemical properties and cell behaviour at the interface?* European Cells and Material, 2004, 7, 52-63.

[46] H. H. M. Rijnaarts, W. Norde, E. J. Bouwer, J. Lyklema, and A. J. B. Zehnder, *Reversibility and mechanism of bacterial adhesion.* Colloids and Surfaces B: Biointerfaces, 1995, 4, 5-22.

[47] L. Hall-Stoodley, J. W. Costerton, and P. Stoodley, *Bacterial biofilms: From the natural environment to infectious diseases.* Nature Reviews Microbiology, 2004, 2, 95-108.

[48] J. Palmer, S. Flint, and J. Brooks, *Bacterial cell attachment, the beginning of a biofilm.* Journal of Industrial Microbiology & Biotechnology, 2007, 34, 577-588.

[49] J. S. Vrouwenvelder, J. A. M. van Paassen, J. M. C. van Agtmaal, M.C.M. van Loosdrecht, and J. C. Kruithof, *A critical flux to avoid biofouling of spiral wound nanofiltration and reverse osmosis membranes: Fact or fiction?* Journal of Membrane Science, 2009, 326, 36-44.

[50] A. Brehant, V. Bonnelye, and M. Perez, *Comparison of MF/UF pretreatment with conventional filtration prior to ro membranes for surface seawater desalination.* Desalination, 2002, 144, 353-360.

[51] C.K. Teng, M. N. A. Hawlader, and A. Malek, *An experiment with different pretreatment methods.* Desalination, 2003, 156, 51-58.

[52] H. Ivnitsky, I. Katz, D. Minz, E. Shimoni, Y. Chen, J. Tarchitzky, R. Semiat, and C.G. Dosoretz, *Characterization of membrane biofouling in nanofiltration processes of wastewater treatment.* Desalination, 2005, 185, 255-268.

[53] J. S. Baker and L. Y. Dudley, *Biofouling in membrane systems — a review.* Desalination, 1998, 118, 81-89.

[54] D. Kim, S. Jung, J. Sohn, H. Kim, and S. Lee, *Biocide application for controlling biofouling of swro membranes — an overview.* Desalination, 2009, 238, 43-52.

[55] J. M. Ruiz, G. Bachelet, P. Caumette, and O. F. X. Donard, *Three decades of tributyltin in the coastal environment with emphasis on arcachon bay, france.* Environmental Pollution, 1996, 93, 195-203.

[56] H. C. Flemming, *Reverse osmosis membrane biofouling.* Experimental Thermal and Fluid Science, 1997, 14, 382-391.

[57] H. C. Flemming and G. Schaule, *Biofouling on membranes - a microbiological approach.* Desalination, 1988, 70, 95-119.

[58] M. Ulbricht, *Advanced functional polymer membranes.* Polymer, 2006, 47, 2217-2262.

[59] Y. Zhou, S. Yu, C. Gao, and X. Feng, *Surface modification of thin film composite polyamide membranes by electrostatic self deposition of polycations for improved fouling resistance.* Separation and Purification Technology, 2009, 66, 287-294.

[60] S. Pal, S. K. Ghatak, S. De, and S. DasGupta, *Characterization of CO_2 plasma treated polymeric membranes and quantification of flux enhancement.* Journal of Membrane Science, 2008, 323, 1-10.

[61] E. S. Kim, Q. Yu, and B. Deng, *Plasma surface modification of nanofiltration (NF) thin-film composite (TFC) membranes to improve anti organic fouling.* Applied Surface Science, 2011, 257, 9863-9871.

[62] G. Belfort and M. Ulbricht, *Surface modification of ultrafiltration membranes by low temperature plasma. I. Treatment of polyacrylonitrile.* Journal of Applied Polymer Science, 1995, 56, 325-343.

[63] E. M. Van Wagner, A. C. Sagle, M. M. Sharma, Y. H. La, and B. D. Freeman, *Surface modification of commercial polyamide desalination membranes using poly(ethylene glycol) diglycidyl ether to enhance membrane fouling resistance.* Journal of Membrane Science, 2011, 367, 273-287.

[64] X. Wei, Z. Wang, J. Chen, J. Wang, and S. Wang, *A novel method of surface modification on thin-film-composite reverse osmosis membrane by grafting hydantoin derivative.* Journal of Membrane Science, 2010, 346, 152-162.

[65] V. Freger, J. Gilron, and S. Belfer, *TFC polyamide membranes modified by grafting of hydrophilic polymers: An FT-IR/AFM/TEM study*. Journal of Membrane Science, 2002, 209, 283-292.

[66] J. Gilron, S. Belfer, P. Väisänen, and M. Nyström, *Effects of surface modification on antifouling and performance properties of reverse osmosis membranes.* Desalination, 2001, 140, 167-179.

[67] S. Belfer, R. Fainshtain, Y. Purinson, J. Gilron, M. Nyström, and M. Mänttäri, *Modification of NF membrane properties by in situ redox initiated graft polymerization with hydrophilic monomers.* Journal of Membrane Science, 2004, 239, 55-64.

[68] J. H. Kim, P. K. Park, C. H. Lee, and H. H. Kwon, *Surface modification of nanofiltration membranes to improve the removal of organic micro-pollutants (EDCs and PhACs) in drinking water treatment: Graft polymerization and cross-linking followed by functional group substitution.* Journal of Membrane Science, 2008, 321, 190-198.

[69] S. Saha, M. L. Bruening and G. L. Baker, Effect of substrate in surface ATRP.. Polymer Preprints, 2008, 49, 96.

[70] K. Matyjaszewski, P. J. Miller, N. Shukla, B. Immaraporn, A. Gelman, B. B. Luokala, T.M. Siclovan, G. Kickelbick, T. Vallant, H. Hoffmann, and T. Pakula, *Polymers at interfaces: Using atom transfer radical polymerization in the controlled growth of homopolymers and block copolymers from silicon surfaces in the absence of untethered sacrificial initiator.* Macromolecules, 1999, 32, 8716-8724.

[71] W. Huang, J. B. Kim, M. L. Bruening, and G. L. Baker, *Functionalization of surfaces by water-accelerated atom-transfer radical polymerization of hydroxyethyl methacrylate and subsequent derivatization.* Macromolecules, 2002, 35, 1175-1179.

[72] M. L. Bruening, D. M. Dotzauer, P. Jain, L. Ouyang, and G. L. Baker, *Creation of functional membranes using polyelectrolyte multilayers and polymer brushes.* Langmuir, 2008, 24, 7663-7673.

[73] S. Edmondson, C. D. Vo, S. P. Armes, and G. F. Unali, *Surface polymerization from planar surfaces by atom transfer radical polymerization using polyelectrolytic macroinitiators.* Macromolecules, 2007, 40, 5271-5278.

[74] X. Chen and S. P. Armes, *Surface polymerization of hydrophilic methacrylates from ultrafine silica sols in protic media at ambient temperature: A novel approach to surface functionalization using a polyelectrolytic macroinitiator.* Advanced Materials, 2003, 15, 1558-1562.

[75] X. Y. Chen, S. P. Armes, S. J. Greaves, and J. F. Watts, *Synthesis of hydrophilic polymer-grafted ultrafine inorganic oxide particles in protic media at ambient temperature via atom transfer radical polymerization: Use of an electrostatically adsorbed polyelectrolytic macroinitiator.* Langmuir, 2004, 20, 587-595.

[76] T. M. Fulghum, D. L. Patton, and R. C. Advincula, *Fuzzy ternary particle systems by surface-initiated atom transfer radical polymerization from layer-by-layer colloidal core−shell macroinitiator particles.* Langmuir, 2006, 22, 8397-8402.

[77] P. Jain, J. Dai, S. Grajales, S. Saha, G. L. Baker, and M. L. Bruening, *Completely aqueous procedure for the growth of polymer brushes on polymeric substrates.* Langmuir, 2007, 23, 11360-11365.

[78] M. Ulbricht, A. Oechel, C. Lehmann, G. Tomaschewski, and H. G. Hicke, *Gas-phase photoinduced graft polymerization of acrylic acid onto polyacrylonitrile ultrafiltration membranes.* Journal of Applied Polymer Science, 1995, 55, 1707-1723.

[79] M. Ulbricht, *Photograft-polymer-modified microporous membranes with environment-sensitive permeabilities.* Reactive and Functional Polymers, 1996, 31, 165-177.

[80] C. Geismann and M. Ulbricht, *Photoreactive functionalization of poly(ethylene terephthalate) track-etched pore surfaces with "smart" polymer systems.* Macromolecular Chemistry and Physics, 2005, 206, 268-281.

[81] M. Ulbricht and H. Yang, *Porous polypropylene membranes with different carboxyl polymer brush layers for reversible protein binding via surface-initiated graft copolymerization.* Chemistry of Materials, 2005, 17, 2622-2631.

[82] D. He, H. Susanto, and M. Ulbricht, *Photo-irradiation for preparation, modification and stimulation of polymeric membranes.* Progress in Polymer Science, 2009, 34, 62-98.

[83] G. B. Sigal, M. Mrksich, and G. M. Whitesides, *Effect of surface wettability on the adsorption of proteins and detergents.* Journal of the American Chemical Society, 1998, 120, 3464-3473.

[84] A. Sethuraman, M. Han, R. S. Kane, and G. Belfort, *Effect of surface wettability on the adhesion of proteins.* Langmuir, 2004, 20, 7779-7788.

[85] V. Vadillo-Rodríguez and B. E. Logan, *Localized attraction correlates with bacterial adhesion to glass and metal oxide substrata.* Environmental Science & Technology, 2006, 40, 2983-2988.

[86] M. Pasmore, P. Todd, S. Smith, D. Baker, J. Silverstein, D. Coons, and C. N. Bowman, *Effects of ultrafiltration membrane surface properties on pseudomonas aeruginosa biofilm initiation for the purpose of reducing biofouling.* Journal of Membrane Science, 2001, 194, 15-32.

[87] J. Skvarla, *A physico-chemical model of microbial adhesion.* Journal of the Chemical Society, Faraday Transactions, 1993, 89, 2913-2921.

[88] R. L. Taylor, J. Verran, G. C. Lees, and A. J. P. Ward, *The influence of substratum topography on bacterial adhesion to polymethyl methacrylate.* Journal of Materials Science: Materials in Medicine, 1998, 9, 17-22.

[89] Q. Li, Z. Xu, and I. Pinnau, *Fouling of reverse osmosis membranes by biopolymers in wastewater secondary effluent: Role of membrane surface properties and initial permeate flux.* Journal of Membrane Science, 2007, 290, 173-181.

[90] X. P. Zou, E. T. Kang, and K. G. Neoh, *Plasma-induced graft polymerization of poly(ethylene glycol) methyl ether methacrylate on Si(100) surfaces for reduction in protein adsorption and platelet adhesion.* Plasmas and Polymers, 2002, 7, 151-170.

[91] R. Michel, S. Pasche, M. Textor, and D. G. Castner, *Influence of PEG architecture on protein adsorption and conformation.* Langmuir, 2005, 21, 12327-12332.

[92] K. D. Park, Y. S. Kim, D. K. Han, Y. H. Kim, E. H. B. Lee, H. Suh, and K. S. Choi, *Bacterial adhesion on PEG modified polyurethane surfaces.* Biomaterials, 1998, 19, 851-859.

[93] C. S. Gudipati, J. A. Finlay, J. A. Callow, M. E. Callow, and K. L. Wooley, *The antifouling and fouling-release perfomance of hyperbranched fluoropolymer (HBFP) poly(ethylene glycol) (PEG) composite coatings evaluated by adsorption of biomacromolecules and the green fouling alga ulva.* Langmuir, 2005, 21, 3044-3053.

[94] P. Hamilton-Brown, T. Gengenbach, H. J. Griesser, and L. Meagher, *End terminal, poly(ethylene oxide) graft layers: Surface forces and protein adsorption.* Langmuir, 2009, 25, 9149-9156.

[95] S. I. Jeon, J. H. Lee, J. D. Andrade, and P. G. De Gennes, *Protein—surface interactions in the presence of polyethylene oxide: I. Simplified theory.* Journal of Colloid and Interface Science, 1991, 142, 149-158.

[96] A. Roosjen, H. C. van der Mei, H. J. Busscher, and W. Norde, *Microbial adhesion to poly(ethylene oxide) brushes: Influence of polymer chain length and temperature.* Langmuir, 2004, 20, 10949-10955.

[97] J. N. Kizhakkedathu, J. Janzen, Y. Le, R. K. Kainthan, and D. E. Brooks, *Poly(oligo(ethylene glycol)acrylamide) brushes by surface initiated polymerization: Effect of macromonomer chain length on brush growth and protein adsorption from blood plasma.* Langmuir, 2009, 25, 3794-3801.

[98] D. Lazos, S. Franzka, and M. Ulbricht, *Size-selective protein adsorption to polystyrene surfaces by self-assembled grafted poly(ethylene glycols) with varied chain lengths.* Langmuir, 2005, 21, 8774-8784.

[99] K. Ishihara, H. Miyazaki, T. Kurosaki, and N. Nakabayashi, *Improvement of blood compatibility on cellulose dialysis membrane. III. Synthesis and performance of water-soluble cellulose grafted with phospholipid polymer as coating material on cellulose dialysis membrane.* Journal of Biomedical Materials Research, 1995, 29, 181-188.

[100] Z. K. Xu, Q. W. Dai, J. Wu, X. J. Huang, and Q. Yang, *Covalent attachment of phospholipid analogous polymers to modify a polymeric membrane surface: A novel approach.* Langmuir, 2004, 20, 1481-1488.

[101] W. Feng, S. Zhu, K. Ishihara, and J. L. Brash, *Adsorption of fibrinogen and lysozyme on silicon grafted with poly(2-methacryloyloxyethyl phosphorylcholine) via surface-initiated atom transfer radical polymerization.* Langmuir, 2005, 21, 5980-5987.

[102] N. B. Holland, Y. Qiu, M. Ruegsegger, and R. E. Marchant, *Biomimetic engineering of non-adhesive glycocalyx-like surfaces using oligosaccharide surfactant polymers.* Nature, 1998, 392, 799-801.

[103] S. Chen, Z. Cao, and S. Jiang, *Ultra-low fouling peptide surfaces derived from natural amino acids.* Biomaterials, 2009, 30, 5892-5896.

[104] N. A. Peppas, *Hydrogels in medicine and pharmacy*. Fundamentals. Vol. 1. 1986, Boca Raton, Florida, USA, CRC Press.

[105] N. A. Peppas, J. Z. Hilt, A. Khademhosseini, and R. Langer, *Hydrogels in biology and medicine: From molecular principles to bionanotechnology.* Advanced Materials, 2006, 18, 1345-1360.

[106] L. Faxälv, T. Ekblad, B. Liedberg, and T. L. Lindahl, *Blood compatibility of photografted hydrogel coatings.* Acta Biomaterialia, 2010, 6, 2599-2608.

[107] D. G. Ahearn, D. T. Grace, M. J. Jennings, R. N. Borazjani, K. J. Boles, L. J. Rose, R. B. Simmons, and E. N. Ahanotu, *Effects of hydrogel/silver coatings on in vitro adhesion to catheters of bacteria associated with urinary tract infections.* Current Microbiology, 2000, 41, 120-125.

[108] T. Murosaki, T. Noguchi, K. Hashimoto, A. Kakugo, T. Kurokawa, J. Saito, Y. M. Chen, H. Furukawa, and J. P. Gong, *Antifouling properties of tough gels against barnacles in a long-term marine environment experiment.* Biofouling, 2009, 25, 657-666.

[109] G. Odian, *Principles of polymerization*. Fourth edition. 2004, Wiley.

[110] K. Pal, A. K. Banthia, and D. K. Majumdar, *Polymeric hydrogels: Characterization and biomedical applications - a mini review.* Designed Monomers and Polymers, 2009, 12, 197-220.

[111] C. Tiziana and A. P. Nikolaos, *Correlation between mesh size and equilibrium degree of swelling of polymeric networks.* Journal of Biomedical Materials Research, 1989, 23, 1183-1193.

[112] J. P. Munch, S. Candau, J. Herz, and G. Hild, *Inelastic light scattering by gel modes in semi-dilute polymer solutions and permanent networks at equilibrium swollen state.* Journal de physique archives, 1977, 38, 971-976.

[113] F. Yañez, J. L. Gomez-Amoza, B. Magariños, A. Concheiro, and C. Alvarez-Lorenzo, *Hydrogels porosity and bacteria penetration: Where is the pore size threshold?* Journal of Membrane Science, In Press, Corrected Proof.

[114] J. Zhang and N. A. Peppas, *Morphology of poly(methacrylic acid)/poly(n-isopropyl acrylamide) interpenetrating polymeric networks.* Journal of Biomaterials Science, Polymer Edition, 2002, 13, 511-525.

[115] S. Orsi, D. Guarnieri, and P. Netti, *Design of novel 3D gene activated PEG scaffolds with ordered pore structure.* Journal of Materials Science: Materials in Medicine, 2010, 21, 1013-1020.

[116] M. M. Chui, R. J. Phillips, and M. J. McCarthy, *Measurement of the porous microstructure of hydrogels by nuclear magnetic resonance.* Journal of Colloid and Interface Science, 1995, 174, 336-344.

[117] J. Hradil and E. Králová, *Styrene–divinylbenzene copolymers post-crosslinked with tetrachloromethane.* Polymer, 1998, 39, 6041-6048.

[118] A. K. Jha, R. A. Hule, T. Jiao, S. S. Teller, R. J. Clifton, R. L. Duncan, D. J. Pochan, and X. Jia, *Structural analysis and mechanical characterization of hyaluronic acid-based doubly cross-linked networks.* Macromolecules, 2009, 42, 537-546.

[119] C. Fanger, H. Wack, and M. Ulbricht, *Macroporous poly (n-isopropylacrylamide) hydrogels with adjustable size "cut-off" for the efficient and reversible immobilization of biomacromolecules.* Macromolecular Bioscience, 2006, 6, 393-402.

[120] I. Eshet, V. Freger, R. Kasher, M. Herzberg, J. Lei, and M. Ulbricht, *Chemical and physical factors in design of antibiofouling polymer coatings.* Biomacromolecules, 2011, 12, 2681-2685.

[121] N.A. Peppas, H. J. Moynihan, and L. M. Lucht, *The structure of highly crosslinked poly(2-hydroxyethyl methacrylate) hydrogels.* Journal of Biomedical Materials Research, 1985, 19, 397-411.

[122] M. Grassi, R. Lapasin, T. Coviello, P. Matricardi, C. Di Meo, and F. Alhaique, *Scleroglucan/borax/drug hydrogels: Structure characterisation by means of rheological and diffusion experiments.* Carbohydrate Polymers, 2009, 78, 377-383.

[123] J. Wang and V.M. Ugaz, *Using in situ rheology to characterize the microstructure in photopolymerized polyacrylarnide gels for DNA electrophoresis.* Electrophoresis, 2006, 27, 3349-3358.

[124] A. M. Lowman and N. A. Peppas, *Analysis of the complexation/decomplexation phenomena in graft copolymer networks.* Macromolecules, 1997, 30, 4959-4965.

[125] J. Brandrup, E. H. Immergut, and E. A. Grulke, Polymer handbook. Fourth edition. 1999, USA, John Wiley & Sons, Inc.

[126] N. Hisano, H. Iwata, Y. Teramura, H. Chen, and Y. Ikada, *Kinetic analyses of disulfide formation between thiol groups attached to linear poly(acrylamide).* Journal of Polymer Science Part A: Polymer Chemistry, 2011, 49, 671-679.

[127] E. E. Chang, Y. C. Chang, C. H. Liang, C. P. Huang, and P. C. Chiang, *Identifying the rejection mechanism for nanofiltration membranes fouled by humic acid and calcium ions exemplified by acetaminophen, sulfamethoxazole, and triclosan.* Journal of Hazardous Materials, 2012, 221–222, 19-27.

[128] A. Heydorn, B. K. Ersbøll, M. Hentzer, M. R. Parsek, M. Givskov, and S. Molin, *Experimental reproducibility in flow-chamber biofilms.* Microbiology, 2000, 146, 2409-2415.

[129] A. Heydorn, A. T. Nielsen, M. Hentzer, C. Sternberg, M. Givskov, B. K. Ersbøll, and S. Molin, *Quantification of biofilm structures by the novel computer program comstat.* Microbiology, 2000, 146, 2395-2407.

[130] S. Schwark and M. Ulbricht, *Toward protein-selective membrane adsorbers: A novel surface-selective photo-grafting method.* European Polymer Journal, 2012, 48, 1914-1922.

[131] N. J. Harrick, *Total internal reflection and its application to surface studies.* Annals of the New York Academy of Sciences, 1963, 101, 928-959.

[132] G. Bodenhausen and D. J. Ruben, *Natural abundance nitrogen-15 NMR by enhanced heteronuclear spectroscopy.* Chemical Physics Letters, 1980, 69, 185-189.

[133] J. Keeler, *Understanding NMR spectroscopy*. Second edition. 2010, Wiley.

[134] M. Kucharski and R. Lubczak, *Copolymerization of hydroxyalkyl methacrylates with acrylamide and methacrylamide I. Determination of reactivity ratios.* Journal of Applied Polymer Science, 1997, 64, 1259-1265.

[135] H. H. Winter and F. Chambon, *Analysis of linear viscoelasticity of a crosslinking polymer at the gel point.* Journal of Rheology, 1986, 30, 367-382.

[136] X. Hu, L. Ma, C. Wang, and C. Gao, *Gelatin hydrogel prepared by photo-initiated polymerization and loaded with TGF-β1 for cartilage tissue engineering.* Macromolecular Bioscience, 2009, 9, 1194-1201.

[137] S. P. Zustiak and J. B. Leach, *Hydrolytically degradable poly(ethylene glycol) hydrogel scaffolds with tunable degradation and mechanical properties.* Biomacromolecules, 2010, 11, 1348-1357.

[138] S. A. Meenach, K. W. Anderson, and J. Z. Hilt, *Synthesis and characterization of thermoresponsive poly(ethylene glycol)-based hydrogels and their magnetic nanocomposites.* Journal of Polymer Science Part A: Polymer Chemistry, 2010, 48, 3229-3235.

[139] D. Imren, M. Gümüsderelioglu, and A. Güner, *In vitro release kinetics of bovine serum albumin from highly swellable dextran hydrogels.* Journal of Applied Polymer Science, 2009, 115, 740-747.

[140] J. R. Colvin, *The size and shape of lysozyme.* Canadian Journal of Chemistry, 1952, 30, 831-834.

[141] L. Bachmann, W. W. Schmitt-Fumain, R. Hammel, and K. Lederer, *Size and shape of fibrinogen, 1. Electron microscopy of the hydrated molecule.* Die Makromolekulare Chemie, 1975, 176, 2603-2618.

[142] K. L. Prime and G. M. Whitesides, *Adsorption of proteins onto surfaces containing end-attached oligo(ethylene oxide): A model system using self-assembled monolayers.* Journal of the American Chemical Society, 1993, 115, 10714-10721.

[143] C. L. Bell and N. A. Peppas, *Water, solute and protein diffusion in physiologically responsive hydrogels of poly(methacrylic acid-g-ethylene glycol).* Biomaterials, 1996, 17, 1203-1218.

[144] S. I. Jeon and J. D. Andrade, *Protein—surface interactions in the presence of polyethylene oxide: II. Effect of protein size.* Journal of Colloid and Interface Science, 1991, 142, 159-166.

[145] L. R. G. Treloar, *The physics of rubber elasticity*. Third edition. 1975, Oxford University Press.

[146] F. Xu, C. E. Flanagan, A. Ruiz, W. C. Crone, and K. S. Masters, *Polyurethane/dermatan sulfate copolymers as hemocompatible, non-biofouling materials.* Macromolecular Bioscience, 2011, 11, 257-266.

[147] B. Purevdorj, J. W. Costerton, and P. Stoodley, *Influence of hydrodynamics and cell signaling on the structure and behavior of pseudomonas aeruginosa biofilms.* Applied and Environmental Microbiology, 2002, 68, 4457-4464.

[148] G. Chen, D. E. Beving, R. S. Bedi, Y. S. Yan, and S. L. Walker, *Initial bacterial deposition on bare and zeolite-coated aluminum alloy and stainless steel.* Langmuir, 2009, 25, 1620-1626.

[149] N. Park, B. Kwon, I. S. Kim, and J. Cho, *Biofouling potential of various nf membranes with respect to bacteria and their soluble microbial products (SMP): Characterizations, flux decline, and transport parameters.* Journal of Membrane Science, 2005, 258, 43-54.

[150] Y. H. Zhao, X. Y. Zhu, K. H. Wee, and R. Bai, *Achieving highly effective non-biofouling performance for polypropylene membranes modified by UV-induced surface graft polymerization of two oppositely charged monomers.* The Journal of Physical Chemistry B, 2010, 114, 2422-2429.

[151] J. S. Louie, I. Pinnau, I. Ciobanu, K. P. Ishida, A. Ng, and M. Reinhard, *Effects of polyether–polyamide block copolymer coating on performance and fouling of reverse osmosis membranes.* Journal of Membrane Science, 2006, 280, 762-770.

[152] J. A. Redman, S. L. Walker, and M. Elimelech, *Bacterial adhesion and transport in porous media: Role of the secondary energy minimum.* Environmental Science & Technology, 2004, 38, 1777-1785.

[153] W. Lee, C. H. Ahn, S. Hong, S. Kim, S. Lee, Y. Baek, and J. Yoon, *Evaluation of surface properties of reverse osmosis membranes on the initial biofouling stages under no filtration condition.* Journal of Membrane Science, 2010, 351, 112-122.

[154] M. C. van Loosdrecht, J. Lyklema, W. Norde, G. Schraa, and A. J. Zehnder, *The role of bacterial cell wall hydrophobicity in adhesion.* Applied and Environmental Microbiology, 1987, 53, 1893-1897.

[155] M. Simões, M. O. Pereira, and M. J. Vieira, *Effect of mechanical stress on biofilms challenged by different chemicals.* Water Research, 2005, 39, 5142-5152.

[156] C. Díaz, R. C. Salvarezza, M. A. Fernández Lorenzo de Mele, and P. L. Schilardi, *Organization of pseudomonas fluorescens on chemically different nano/microstructured surfaces.* ACS Applied Materials & Interfaces, 2010, 2, 2530-2539.

[157] T. H. Chong, F. S. Wong, and A. G. Fane, *The effect of imposed flux on biofouling in reverse osmosis: Role of concentration polarisation and biofilm enhanced osmotic pressure phenomena*. Journal of Membrane Science, 2008, 325, 840-850.

[158] A. O. T. George and K. Roberto, *Initiation of biofilm formation in pseudomonas fluorescens WCS365 proceeds via multiple, convergent signalling pathways: A genetic analysis.* Molecular Microbiology, 1998, 28, 449-461.

[159] G. Chen, Y. Hong, and S. L. Walker, *Colloidal and bacterial deposition: Role of gravity.* Langmuir, 2009, 26, 314-319.

[160] Z. Steiner, J. Miao and R. Kasher, *Development of an oligoamide coating as a surface mimetic for aromatic polyamide films used in reverse osmosis membranes.* Chemical Communications, 2011, 47, 2384-2386.

[161] F. M. Mirabella, *Internal reflection spectroscopy.* Applied Spectroscopy Reviews, 1985, 21, 45-178.

[162] M. Mänttäri, A. Pihlajamäki, and M. Nyström, *Effect of pH on hydrophilicity and charge and their effect on the filtration efficiency of NF membranes at different pH.* Journal of Membrane Science, 2006, 280, 311-320.

[163] L. Braeken, B. Bettens, K. Boussu, P. Van der Meeren, J. Cocquyt, J. Vermant, and B. Van der Bruggen, *Transport mechanisms of dissolved organic compounds in aqueous solution during nanofiltration.* Journal of Membrane Science, 2006, 279, 311-319.

[164] S.I I. Kuroda, I. Mita, K. Obata, and S. Tanaka, *Degradation of aromatic polymers: Part IV—effect of temperature and light intensity on the photodegradation of polyethersulfone.* Polymer Degradation and Stability, 1990, 27, 257-270.

[165] P. Gijsman, G. Meijers, and G. Vitarelli, *Comparison of the UV-degradation chemistry of polypropylene, polyethylene, polyamide 6 and polybutylene terephthalate.* Polymer Degradation and Stability, 1999, 65, 433-441.

[166] E. M. Vrijenhoek, S. Hong, and M. Elimelech, *Influence of membrane surface properties on initial rate of colloidal fouling of reverse osmosis and nanofiltration membranes.* Journal of Membrane Science, 2001, 188, 115-128.

[167] C. Werner, H. J. Jacobasch, and G. Reichelt, *Surface characterization of hemodialysis membranes based on streaming potential measurements.* Journal of Biomaterials Science, Polymer Edition, 1996, 7, 61-76.

[168] R. Bernstein, S. Belfer, and V. Freger, *Surface modification of dense membranes using radical graft polymerization enhanced by monomer filtration.* Langmuir, 2010, 26, 12358-12365.

[169] W. E. Mickols, *Composite membrane with polyalkylene oxide modified polyamide surface.* United States Patent, 2001, US 6280853 B1.

[170] A. I. Schafer, A. G. Fane, and T. D. Waite, *Nanofiltration - principles and applications.* 2005, UK, Elsevier Advanced technology.

[171] C. Y. Tang, Y. N. Kwon, and J. O. Leckie, *Characterization of humic acid fouled reverse osmosis and nanofiltration membranes by transmission electron microscopy and streaming potential measurements.* Environmental Science & Technology, 2006, 41, 942-949.

[172] Y. N. Wang and C. Y. Tang, *Protein fouling of nanofiltration, reverse osmosis, and ultrafiltration membranes—the role of hydrodynamic conditions, solution chemistry, and membrane properties.* Journal of Membrane Science, 2011, 376, 275-282.

[173] Y. N. Wang and C. Y. Tang, *Fouling of nanofiltration, reverse osmosis, and ultrafiltration membranes by protein mixtures: The role of inter-foulant-species interaction.* Environmental Science & Technology, 2011, 45, 6373-6379.

[174] H. Mo, K. G. Tay, and H. Y. Ng, *Fouling of reverse osmosis membrane by protein (bsa): Effects of pH, calcium, magnesium, ionic strength and temperature.* Journal of Membrane Science, 2008, 315, 28-35.

[175] O. J. Cotterill and A. R. Winter, *Egg white lysozyme.* Poultry Science, 1955, 34, 679-686.

[176] M. D. M. Hossain and G. Fenton, *Concentration of proteins from single component solution using a semibatch foaming process.* Separation Science and Technology, 1998, 33, 1703-1721.

Appendix 1: List of abbreviation

3D	three-dimensional
AFM	atomic force microscopy
AIBN	2, 2'-Azobis (2-methylpropionitrile)
APS	ammonium persulfate
ATR-IR	attenuated total reflection infrared spectrometry
ATRP	atom transfer radical polymerization
$BaSO_4$	barium sulfate
BEE	benzoin ethyl ether
BEE-COBr	4-ethoxy-5-oxo-4,5-diphenylpentanoyl bromide
BEE-COOH	4-ethoxy-5-oxo-4,5-diphenylpentanoic acid
BEE-DH	poly(2-dimethylamino-ethyl methacrylate-*co*-2-methacryloyloxy-ethyl 4-ethoxy-5-oxo-4,5-diphenylpentanoate)
BEE-TH	poly(2-methacryloyloxy-N,N,N-trimethylethanaminium iodide -co-2-methacryloyloxy-ethyl 4-ethoxy-5-oxo-4,5-diphenylpentanoate)
BP	benzophenone
BSA	Bovine serum albumin
$CaCO_3$	calcium carbonate
$CaSO_4$	calcium sulfate
CL	crosslinker
CLSM	confocal laser scanning microscopy
D_2O	deuterium oxide
DC	deposition coefficient
DG	degree of grafting
DH	poly(2-dimethylamino-ethyl methacrylate-*co*-2-hydroxyethyl methacrylate)
DLVO	derjaguin- landau-verwey -overbeek
DMAEMA	2-dimethylamino-ethyl methacrylate

DMSO	dimethyl sulfoxide
EGDMA	ethylene glycol dimethacrylate
EPS	extracellular polymeric substances
Fib	fibrinogen
G’	storage modulus
GPC	gel permeation chromatography
HEMA	2-Hydroxyethyl methacrylate
IEP	isoelectric point
KOH	potassium hydroxide
LB	lysogeny broth
Lys	lysozyme
MBAA	N,N’-methylenebisacrylamide
$MgCl_2$	magnesium chloride
MPS	3-methacryloxypropyl-trimethoxysilane
NaCl	sodium chloride
NaOH	sodium hydroxide
NF	nanofiltration
NMP	N-methyl-2-pyrrolidone
NMR	nuclear magnetic resonance
PEG	poly(ethylene glycol)
PEGMEMA	poly(ethylene glycol) methyl ether methacrylate
RO	reverse osmosis
SAM	self-assembled monolayer
TEMED	N,N,N‘,N‘-tetramethylethylene diamine
TFC	thin film composites

TH	poly(2-methacryloyloxy-N,N,N-trimethylethanaminium iodide-*co*-2-hydroxy ethyl methacrylate)
THF	tetrahydrofuran
TOC	total organic carbon
UV	ultraviolet
ZP	zeta potential

Appendix 2: List of publications and conferences

Publications

1. Inbal Eshet, Viatcheslav Freger, Roni Kasher, Moshe Herzberg, Jing Lei, and Mathias Ulbricht, Chemical and physical factors in design of antibiofouling polymer coatings, Biomacromolecules, 2011, 12, 2681.

2. Jing Lei, Christian Mayer, Viatcheslav Freger and Mathias Ulbricht， Synthesis and characterization of poly(ethylene glycol)-methacrylate based hydrogel networks for anti-biofouling applications，Macromolecular Materials & Engineering, 2012, in press.

3. Jing Lei, Mathias Ulbricht, Grafting antibiofouling polymer hydrogel layer on NF membrane via an electrostatically immobilized photoreactive macroinitiator, Journal of Membrane Science (2012), in preparation.

Invited report

Jing Lei, Viatcheslav Freger, and Mathias Ulbricht, Biofouling-resistant polymer hydrogel coating for desalination membranes, Membrane News, 2011, 85, 13.

Conferences

2010 The 6th Zsigmondy Colloquium, Chemnitz University of Technology, Chemnitz, Germany, 22nd-24th, March.

Biofouling-resistant polymer hydrogel coating for desalination membranes (poster)

2010 NanoMemCourse: Nanostructured materials and membranes for Health and Sustainable Water, Enschede, University of Twente, Netherlands, 7th-16th, April.

Biofouling-resistant polymer hydrogel coating for desalination membranes (poster)

2011 International Congress on Membranes and Membrane Processes (ICOM 2011), Amsterdam, Netherlands, 23rd- 29th, July

Biofouling-resistant polymer hydrogel coating for desalination membranes (Oral presentation)

Visit Experience

2010 Research collaboration, Ben Gurion University, Israel, 10th-28th October

Awards

2010 "Travel Award" from NanoMemCourse. Netherlands.

2011 "Best oral presentation" of ICOM 2011, Netherlands

Appendix 3: Curriculum vitae

Name: Jing Lei

Date of Birth: 28 August 1984

Place of Birth: China

Education

2009 – 2012 (Ph.D): Technical Chemistry II, University of Duisburg-Essen, Germany

2006 – 2008 (M.Sc): Chemical Engineering, Sungkyunkwan University, South Korea

2002 – 2006 (B.Sc): Applied Chemistry, Shandong University, China